

NATIONAL AERONAUTICS
AND SPACE ADMINISTRATION
(NASA Contract NASr-36)

TRANSIENT PRESSURE MEASURING METHODS RESEARCH

DYNAMIC RESPONSE TESTING OF TRANSIENT
PRESSURE TRANSDUCERS FOR LIQUID
PROPELLANT ROCKET COMBUSTION CHAMBERS

(NASA CR 51516; AER 595g) OTS: \$12.00 ph,
5.12 mf

~~(Aeronautical Engineering Report No. 595g)~~

Prepared by:

William C. Bentley
William C. Bentley, Lcdr. USN

and

Joseph J. Walter
Joseph J. Walter, Lt. USN

Approved by:

J. P. Layton
J. P. Layton
Research Leader

Originally published in May 1963 as a joint thesis submitted to the Department of Aeronautical Engineering in partial fulfillment of the requirements for the degree of Master of Science in Engineering

June 1963 164 p 45 refs

Reproduction, translation, publication, use and disposal in whole or in part by or for the United States Government is permitted.

Guggenheim Laboratories for the Aerospace Propulsion Sciences
Department of Aeronautical Engineering
PRINCETON UNIVERSITY
N. J.

7163009

ABSTRACT

21974

An investigation of the dynamic response of transient pressure transducers intended for use in liquid propellant rocket combustion chambers was undertaken. Shock tube testing included optimization of operating techniques especially the tailored interface and the effects of ground shock and other mounting influences. The Kistler 601A quartz transducer was evaluated as a monitor for the Princeton Sinusoidal Pressure Generator (SPG) and a number of water-cooled transient transducers were evaluated for comparison with results from the SPG. An investigation was conducted which satisfactorily demonstrated the practical value of the SPG as a primary test device for transient pressure transducer evaluations to 10,000 cps. During evaluations special consideration was given to developing operating techniques and improving SPG chamber design. The results from shock tube and the SPG show close agreement up to 10,000 cps, the present limit of usable SPG range. Transducers were then tested in experimental liquid propellant rocket motors to compare laboratory measured characteristics with actual transducer performance.

ACKNOWLEDGMENTS

The authors wish to express their gratitude for the continued support and encouragement by many of the people associated with the Guggenheim Laboratories for the Aerospace Propulsion Sciences, Department of Aeronautical Engineering, Princeton University.

Special thanks are extended to J. Preston Layton who suggested the research and whose guidance and assistance were invaluable to its successful completion.

Messrs. Robert C. Knauer and J. David Tregurtha were particularly helpful. For their constructive criticism, advice and patience the authors remain deeply indebted.

Many other members of the staff of the Guggenheim Laboratories contributed their time and effort. Mr. Tony Poli and other members of the design group produced the necessary drawings of the experimental equipment and many of the illustrations appearing in this document. Mr. Jack N. Deeter and members of his computing group aided in programming and in the reduction of data. The authors take this opportunity to thank them all.

The special efforts of Miss Frances Allison who typed the entire manuscript are gratefully appreciated.

Financial support of this research was provided by the National Aeronautics and Space Administration under Contract NASr-36.

TABLE OF CONTENTS

	<u>Page</u>
ABSTRACT	i
ACKNOWLEDGMENTS	i
TABLE OF CONTENTS	ii
FIGURES	iii
SYMBOLS AND NOTATIONS	vii
I. INTRODUCTION	1
II. HISTORICAL BACKGROUND	3
III. SHOCK TUBE	10
A. Purpose and Objectives	10
B. Theory	10
C. Description and Operation of Apparatus	30
D. Experimental Results	38
IV. THE PRINCETON SINUSOIDAL PRESSURE GENERATOR	63
A. Purpose and Objectives	63
B. Theory	64
1. Resonant Modes of the Chamber	64
2. Chamber Pressure	65
a. Average Chamber Pressure	65
b. Peak-to-Peak Pressure Fluctuations	68
C. Description and Operation of Apparatus	73
D. Experimental Results	79
V. ROCKET COMBUSTION CHAMBER TESTS	97
VI. DISCUSSION	101
A. Shock Tube	101
B. Princeton Sinusoidal Pressure Generator	107
1. Resonant Modes of the Chamber	107
2. Chamber Pressure	114
a. Average Chamber Pressure	115
b. Peak-to-Peak Pressure Fluctuations	120
3. Evaluations	122
C. Comparative Testing - Shock Tube and SPG	125
D. Rocket Combustion Chamber Tests	128
VII. CONCLUSIONS AND RECOMMENDATIONS	134
APPENDIX A. References	A-1
B. Development of Miniaturized Thin Film Gauges	B-1
C. Step Function Generation by Balldrop Technique	C-1
D. SPG Chamber Outlet Area Variation	D-1
E. Design Recommendations for Improved Sinusoidal Pressure Generator	E-1

LIST OF FIGURES

<u>Figure No.</u>	<u>Title</u>	<u>Page</u>
1	Methods of Transduction	4
2	Shock Tube and Associate Instrumentation	11
3	Shock Tube Pressure Profiles	13
4	Wave Diagram for Nonreflecting Interface	14
5	Compression Chamber Pressure Ratio Versus Shock Strength	17
6	Reflected Shock Amplitude Versus Incident Shock Amplitude	19
7	Reflected Shock Amplitude Versus Shock Front Velocity	20
8	Variations in Flow Parameters Behind a Normal Reflected Shock Wave Versus Incident Shock Wave Mach Number for Variable Specific Heat	23
9	Tailored Interface Condition	28
10	Photograph Shock Tube Test Section	31
11	Photograph, New Miniaturized Thin Film Gauge Compared with Conventional Thin Film Gauge	33
12	Miniaturized Thin Film Gauge Waveform	35
13	Photograph, Benson-Lehner Optical Scanner and IBM Card Punch	37
14	Shock Tube Speed Calibration	39
15	Shock Wave Mach Number Versus Diaphragm Pressure Ratio	40
16	Transducer Evaluation Test - Kistler 601A (Shock tube end)	42
17	Transducer Evaluation Test - Kistler 603 (Shock tube end)	43
18	Transducer Evaluation Test - Kistler 601 (Shock tube end)	44
19	Transducer Evaluation Test - Kistler 601 (Shock tube end)	45

LIST OF FIGURES (Continued)

<u>Figure No.</u>	<u>Title</u>	<u>Page</u>
20	Transducer Evaluation Test - Dynisco PT-49 AF-IM (Shock tube end)	46
21	Transducer Evaluation Test - Elastronics EBL 6009 (Shock tube end)	47
22	Transducer Evaluation Test - Dynisco PT-76-IM (Shock tube end)	48
23	Transducer Evaluation Test - Photocon Model 755 (Shock tube end)	49
24	Transducer Evaluation Test - Kistler 601A (Shock tube end)	50
25	Transducer Evaluation Test - Kistler 603A (Shock tube end)	51
26	Transducer Evaluation Test - Dynisco PT-49 AF-IM (Shock tube end)	52
27	Transducer Evaluation Test - Kistler 601A (Ground shock)	53
28	Transducer Evaluation Test - Kistler 603A (Ground Shock)	54
29	Transducer Evaluation Test - Kistler 601A (Ball drop)	55
30	Transducer Evaluation Test - Kistler 601A (Ball drop)	56
31	Transducer Evaluation Test - Elastronics EBL 6009 (Ball drop)	57
32	Transducer Evaluation Test - Photocon Model 755 (Ball drop)	58
33	Kistler 601 Transducer Evaluation by National Bureau of Standards	59
34	Kistler 601A Side Mount Tests Comparison of Copper and Plastic Seals	62
35	Transverse Modes of Pressure Oscillation in a Cylindrical Chamber	66
36	Phase Relationships	72

LIST OF FIGURES (Continued)

<u>Figure No.</u>	<u>Title</u>	<u>Page</u>
37	Sinusoidal Pressure Generator	74
38	Photograph, Sinusoidal Pressure Generator	75
39	Typical Instrumentation Schematic	83
40	Peak-to-Peak Pressure Fluctuations Versus Frequency for Side Mounted Kistler 601 with Nitrogen at Supply Pressure of 132 psia	84
41	Peak-to-Peak Pressure Fluctuations Versus Frequency for Monitor Kistler 601 with Nitrogen at Supply Pressure of 132 psia	85
42	Peak-to-Peak Pressure Fluctuations Versus Frequency with Helium at Supply Pressure of 121 psia	86
43a	SPG Chamber Response with Helium at 120 psia Supply Pressure	87
43b	SPG Chamber Response with Helium at 360 psia Supply Pressure	88
44	Comparison of Theoretical and Experimental Peak-to-Peak Pressure Fluctuations Versus Frequency in SPG Chamber with Helium at Reservoir Pressure of 115 psia	89
45	Same as Figure 44, except for 221 psia	90
46	Same as Figure 44, except for 345 psia	91
47	Comparison of Filtered SPG Output and Generated Sine Wave of Same Frequency	93
48	Response Ratio Versus Frequency for Kistler 603	95
49	Response Ratio Versus Frequency for Kistler 601A	95
50	Response Ratio Versus Frequency for Dynisco PT-49 AF-IM	96
51	Response Ratio Versus Frequency for Photocon Model 755	96
54	Chamber Response with Nitrogen	109

LIST OF FIGURES (Continued)

<u>Figure No.</u>	<u>Title</u>	<u>Page</u>
55	Transducer Evaluation Comparison for Kistler 603	126
56	Transducer Evaluation Comparison for Kistler 601A	126
57	Transducer Evaluation Comparison for Dynisco PT-49 AF-IM	127
58	Transducer Evaluation Comparison for Photocon Model 755	127
61	Cylindrical Rocket Chamber Cold Runs	98
62	Hot Runs of Rocket Combustion Chambers	99
63	Square Rocket Combustion Chamber Test Runs	100
B-1	Engineering Drawing of Thin Film Gauge	B-2
D-1	Outlet Area Variation	D-2
D-2	Theoretical Outlet Area Variation	D-5

SYMBOLS AND NOTATIONS

a	=	chamber radius
A	=	area
c	=	speed of wave propagation
C_p	=	specific heat at constant pressure
C_v	=	specific heat at constant volume
D	=	diameter of shock tube
f	=	frequency (cps)
q	=	gravitational constant
J	=	Bessel function
K	=	constant
L	=	chamber length
\dot{m}	=	mass flow rate
m	=	running index 0, 1, 2, 3 ...
M	=	mass
M_s	=	shock front velocity
n	=	running index 0, 1, 2, 3 ...
n_z	=	running index 0, 1, 2, 3 ...
P	=	instantaneous pressure
r	=	radial cylindrical coordinate
R	=	gas constant
S	=	diaphragm thickness
S_{ult}	=	ultimate tensile strength
t	=	time
T	=	absolute temperature
v	=	volume

SYMBOLS AND NOTATIONS (Continued)

- V = velocity
 X = Cartesian coordinate
 y = Cartesian coordinate
 z = longitudinal cylindrical coordinate
 \mathcal{L}_{mn} = solution of $J_m(\pi \mathcal{L}_{mn})/d\mathcal{L} = 0$
 γ = specific heat ratio
 δ = damping factor
 \emptyset = angular cylindrical coordinate
 γ = resonant frequency
 π = 3.14159
 ρ = density - mass per unit volume

Subscripts

- 0 = reservoir conditions
1, 2, ... 5 = quasi-steady uniform states of basic shock
tube flow
avg = average
dy = dynamic component
eff = effective
in = inlet of chamber
max = maximum
out = outlet of chamber
* = peak to peak

I. INTRODUCTION

An important part of many research programs involves the requirement for accurate measurement of pressures. Such measurements are usually of a static nature and present no particular difficulty. Sometimes, however, rapidly oscillating pressures must be measured, and the devices used to measure static pressure are not capable of the fast response necessary to measure rapid changes. Special transducers and systems for these transient measurements must be developed and evaluated.

Rocket motor research, especially that concerned with combustion instability in liquid rocket engines, requires a transient pressure measurement system including a transducer capable of accurate sensing of oscillating pressures under the very severe operating conditions associated with the intense heat of rocket thrust chamber combustion. As rocket technology advances, these pressure oscillations exhibit marked effects on motor performance and influence such factors as heat transfer rates and design tolerances of material strengths. Consequently, it is important that pressure records be exact representations of the actual pressure variations.

The requirements for an optimal pressure measuring system stipulate that the relationship between input and output be defined over the entire range of intended use and that the output or response be readily interpreted. The goal of testing is to determine this relationship between input and output and to provide an evaluation or calibration of the overall system. Generally transient pressure measuring systems are tested by applying a known step function or

sinusoidal input and accurately measuring the output. This report discusses both shock tube testing, which utilizes the step input generated by a shock wave and testing utilizing the Princeton Sinusoidal Pressure Generator, which generates a sinusoidal pressure variation over a range of frequencies as the input. Comparison of the test results of these devices in the laboratory with the requirements for rocket thrust chamber pressure measurements is discussed and conclusions and recommendations for further work are presented.

II. HISTORICAL BACKGROUND

Since James Watt began experimentation with the steam engine, an expanding interest has been placed in transient pressure measuring systems. The simple piston and spring pressure measurement device of this era proved satisfactory only so long as the speed and rate of change of pressure were both low. The combined effect seldom gave components higher than 50 cps. With the development of the internal combustion engine a response 1000 times faster was required of a pickup in order to resolve details of phenomena such as detonation (Ref. 1).^{*} The evolution of high frequency pressure measurement techniques particularly those applicable to combustion, explosion, and shock wave investigations are of comparatively recent origin. Progress in this area was accelerated by the advent of even higher energy release devices such as rockets, nuclear reactors, and exotic propulsive devices (Ref. 2).

As the need for improved transient pressure measuring systems grew, so grew the need for testing and calibrating these systems. Since Lord Rayleigh's first attempts at calibration of transient pressure systems during the advent of steam power, many investigators have endeavored to develop means to test these devices so that an exact relationship between the output of a system and its input function may be determined (Ref. 3). Devices for measuring transient pressures are usually small flush-diaphragm pickups employing the strain-gage, variable capacitance, variable inductance or piezoelectric principle. Figure 1 is a reproduction from Reference 4 which illustrates the various basic methods of transduction.

^{*}The list of references is included as Appendix A.

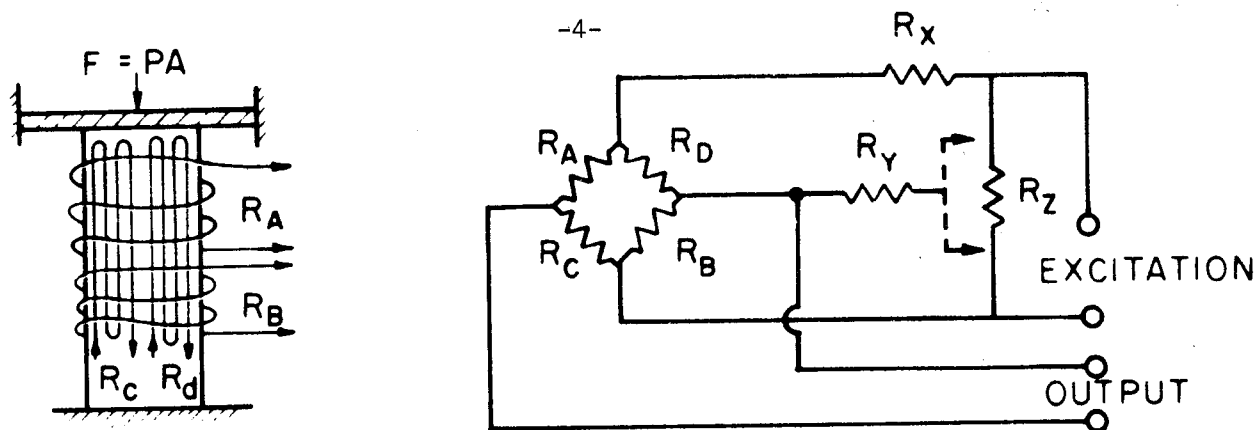


FIGURE 1a - STRAIN GAGE

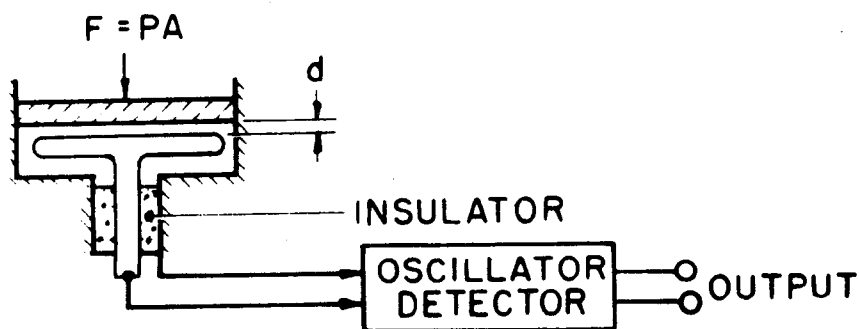


FIGURE 1b - CAPACITIVE

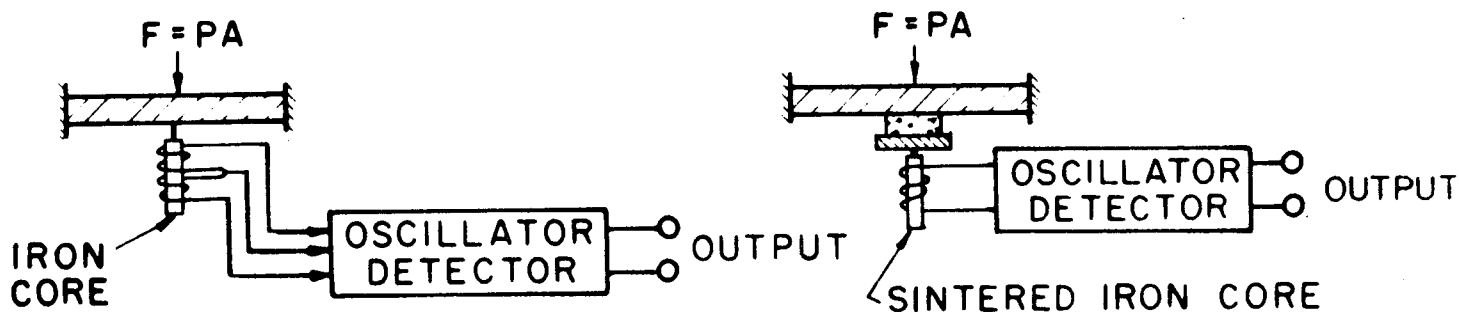


FIGURE 1c - VARIABLE RELUCTANCE

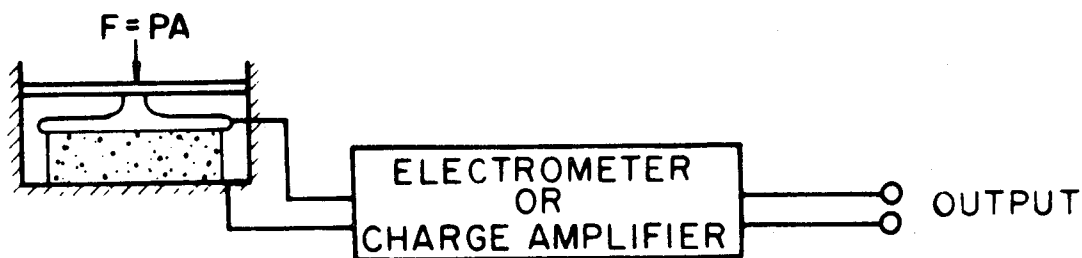


FIGURE 1d - PIEZOELECTRIC

METHODS OF TRANSDUCTION

Determination of the dynamic characteristics of a transient pressure transducer requires a pressure input of a predictable shape and pressure level, which must be obtained for a sufficient time to obtain a steady record of transducer response. Either a sinusoidal input function or a step function input may be used to obtain frequency response data.

The most desirable method of testing the frequency response of a transient pressure measuring system is to excite the system directly with a number of sinusoidal oscillating pressures in frequencies over the range of interest. The Jet Propulsion Laboratory at the California Institute of Technology developed a sinusoidal oscillating pressure device, a siren-driven resonant chamber, but discontinued its use after achieving only limited success. The device was restricted to frequencies from 200 to 4000 cps and generated a maximum oscillating pressure of only 5 psi at a 600 psia static level (Ref. 5). The Princeton Sinusoidal Pressure Generator (hereinafter SPG), developed by H. B. Jones, considerably expanded the range of frequencies and pressures available for testing (Ref. 4,6). Briefly, the Princeton Sinusoidal Pressure Generator is a flow throttling device utilizing a gas as the flowing medium. For transducer testing, a device of this type is superior to a liquid-coupled type. Devices utilizing a liquid coupling exhibit a large interdependence between the transducer acoustic input impedance and the operation of the device. There is also a large and unpredictable effect upon transducer damping (Ref. 4). The present range of operation of the Princeton Sinusoidal Pressure Generator extends to 10 kcps, and it is expected that this range of operation will be extended in the near future.

The choice of the present design was based on frequency requirements and transducer dimensions. In general, the chamber should be as small as practical since the lowest resonant frequency of the chamber will vary inversely with the chamber diameter. Therefore, small chambers will have high resonant frequencies, which is desirable. The limit of chamber diameter is thus determined by the diameter of the largest transducer to be tested.

Carwile (Ref. 6) investigated the response of the chamber to forced pressure oscillations. The work concluded that the pressure in the chamber was uniform throughout and generally was sinusoidal in variation up to 10 kcps, if helium is the test gas. This device, in its improved version, will be thoroughly discussed in the next section of this report.

Step function changes in pressure have been more widely used to test transient pressure measuring systems. Step changes have been produced by breaking a bottle, quickly opening a valve, and by burst diaphragm devices (Ref. 3,5,7,8,9). A considerable variety of approaches have been attempted; these have found only limited success in certain restricted applications. Some devices which show considerable promise are of the quick opening, large pressure release class. A fast opening valve capable of generating selected pressure steps to 5000 psi, similar to a high pressure version developed by the National Bureau of Standards, has been employed by the Ballistics Research Laboratories at the Aberdeen Proving Ground in Maryland (Ref. 9). This device provides an accurate positive step with a rise time of about 200 micro-seconds. The rate of pressure change or rise time of such devices is inherently long in comparison with the period of the

natural frequency of modern transducers, so that response to such comparatively slow pressure changes cannot accurately be investigated. Dynamic calibration with these devices is generally more applicable to transducers with predominant modes of oscillation at frequencies below 10,000 cps.

For transient pressure measuring systems having a fast response, that is, well-damped gauges having natural frequency in excess of 50,000 cps, the step function generator must be capable of changing pressure from one known level to another in an extremely short time. Of equipment presently in use the shock tube best meets these requirements, since it can provide a step increase in pressure on the order of 10^{-9} seconds.

During the past twenty years, the shock tube has gained singular pre-eminence as the basic instrument for the study of non-stationary problems in fluid mechanics. Recently, the apparatus has been employed in a seemingly unending and extensive variety of studies. These include magnetohydrodynamics, combustion and flame propagation, relaxation phenomena in gases, ionization, dissociation, wave interactions, transonic and supersonic flow, shock loading of structures, atomic physics of the states behind strong shock waves, gage performance, and many others. Literature on this tool has grown quite extensively; however, since most does not apply to the present endeavor, merely a handful of classic and current pieces of literature are cited as background material (Ref. 10-16).

Quite interesting is the first demonstration by Paul Vieille at the turn of the century that a compression wave produced by breaking a diaphragm separating regions of different pressure travels faster

than sound (Ref. 17). As early as 1910, Kobes (Ref. 18) developed the theory of the ideal shock tube in a paper discussing the hydrodynamic theory of vacuum and pressure air brakes for railroad rolling stock. In 1932 Schardin (Ref. 19) utilized the theory of Kobes in a treatise on the noise generated when a diaphragm separating regions of different pressure in a pipe ruptured.

Unfortunately, the device was forgotten until the early 1940's when Payman and Shepherd (Ref. 20) contributed significantly with their experimental studies of shock tube flow processes. The early papers of Kobes and Schardin were unknown to several scientists who derived the shock tube theory independently in the 1940-1950 period. The fundamental theory of the shock waves produced in the shock tube was formulated by Stokes, Riemann, Rankine and others (Ref. 21). The basic theory of the shock tube was subsequently developed by a number of investigators (Ref. 18, 19, 22). The shock tube work of G. T. Reynolds (Ref. 23) at Princeton in 1943 laid the ground work for subsequent transient pressure system testing.

The methods of data interpretation for frequency response testing are quite diverse. The sinusoidal pressure generating devices covering the frequencies of interest offer simple direct measurement of frequency response. Step function pressure generating devices are considerably more difficult to analyze. A transformation must be made to amplitude versus frequency since the usual record is response to a step function, that is, amplitude versus time. A solution to this limitation of transforming response from the time to frequency domain can be found through the use of computers, but there is considerable drudgery in translating the step function record into a usable form for

the computer. The transient may be obtained from an oscilloscope using a Polaroid camera. This photograph, usually enlarged to aid in picking off the coordinates, may then be analyzed either manually or by an optical scanning device. The data so received can then be fed to an IBM card punch for the computer program. Another method is to generate the transient response periodically and then determine the frequencies present in the periodic waveform with a harmonic wave analyzer. Since this periodic waveform represents the system response to a square wave, it is the response to an input which contains all harmonics of the frequency of repetition, with the amplitude of each harmonic inversely proportional to the harmonic number. The "flying spot scanner" used by the Jet Propulsion Laboratory obtains transducer system response by multiplying the wave analyzer output at each harmonic by the number of the harmonic (Ref. 2,5). This system has great advantage in its simplicity and rapid speed of operation. Many other instrumented aids are available for the analysis of data. Included among these are overlay grids as an aid in numerical integration, mechanical integration devices such as Henderson's mechanical harmonic analyzer and Montgomery's optical harmonic analyzer, and magnetic wave drum analyzers (Ref. 7,24, 25,26).

III. SHOCK TUBE

A. Purpose

The primary purpose of the shock tube work presented in this report are:

1. to determine the possibilities of shock tube testing of transient pressure measuring systems, including investigation of the characteristics of the step function, ground shock and related shock tube phenomena.
2. to develop more rapid, precise and convenient methods of evaluating shock tube data and obtaining frequency response for transient pressure measuring systems.
3. to find a transducer capable of high frequency response which has a response ratio of unity to frequencies in excess of 15,000 cps and can be used as a monitor in the Princeton Sinusoidal Pressure Generator.
4. to investigate shock tube end mounting versus side mounting techniques which more closely duplicate rocket motor testing.

B. Theory

Determination of the dynamic characteristics of the transient pressure measuring system requires a step function input of a predictable shape and pressure level in a time sufficiently short to shock-excite the system under test. The pressure level must be maintained for a sufficient time to obtain a steady record of the transducer response. Until the present time, the shock tube has been the most satisfactory apparatus for meeting these requirements.

1. Shock Tube Performance

A typical shock tube used for transient pressure testing (Figure 2) consists essentially of a straight, constant cross-section

SHOCK TUBE AND ASSOCIATED INSTRUMENTATION

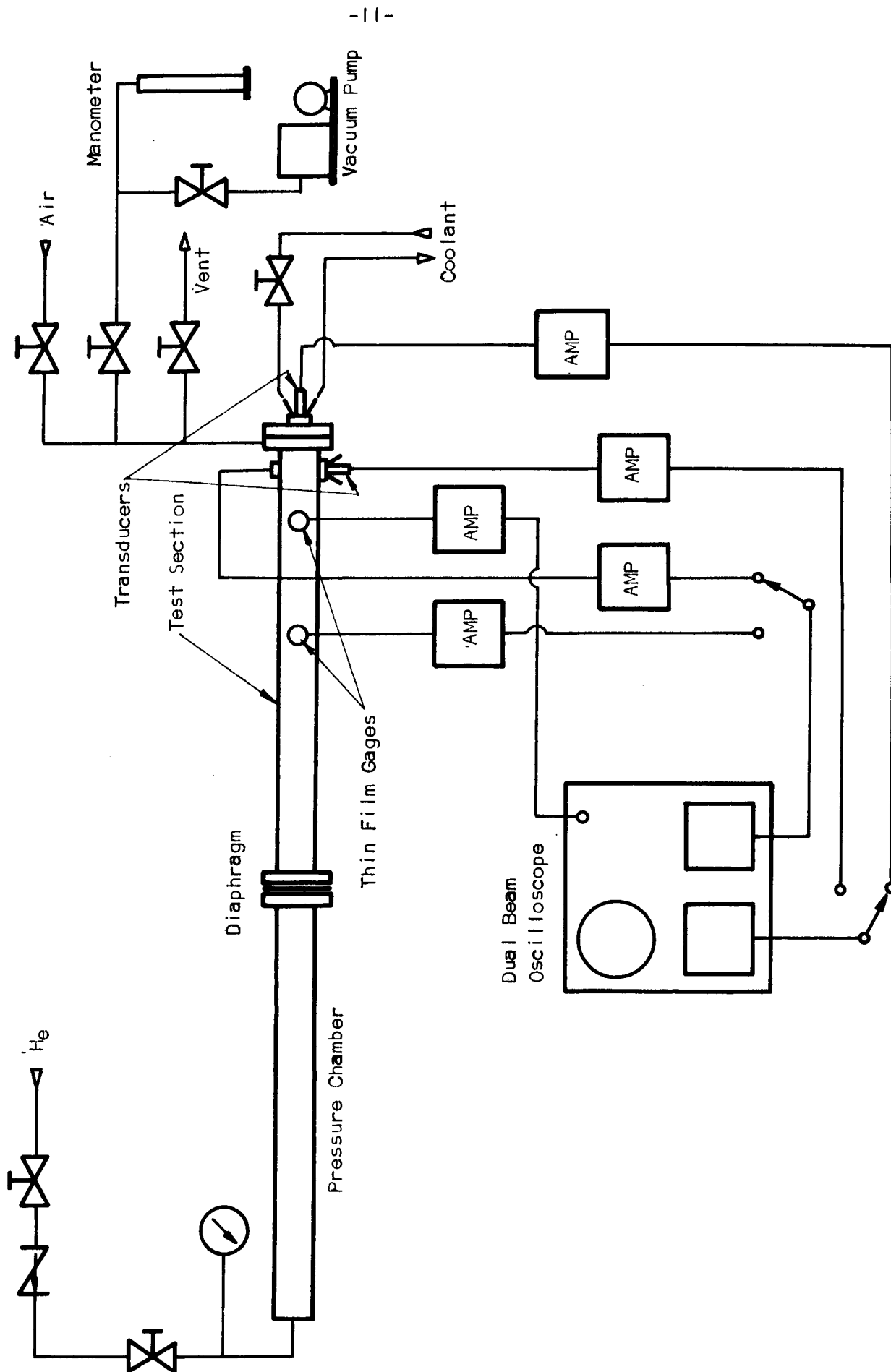


FIGURE 2

pipe closed at both ends and divided into two compartments by a thin burst diaphragm. The upstream compartment contains the driving gas at a higher pressure P_4 ; the downstream or test section portion contains the test gas at a lower pressure P_1 . The diaphragm separates the two gases until it is burst either manually or by the pressure of the driving gas. Upon rupture the driving gas compresses and produces a shock wave in the test gas which travels at supersonic speed with a rise time of about 10^{-9} seconds (Ref. 14). Simultaneously a rarefaction or expansion wave moves back into the driving gas chamber. The shock wave system is not fully developed until it travels at least 10 times the diameter beyond the diaphragm (Ref. 27). Theoretically the diaphragm is completely and instantaneously removed. As a result, a plane shock wave is instantly propagated into the test section and a centered rarefaction wave into the upstream high pressure compartment.

A pressure profile and wave diagram is depicted in Figures 3 and 4. The pressure profiles are represented for three successive times. At $t = t_0$ prior to rupture of the diaphragm the equilibrium pressure difference P_4 and P_1 is shown. At $t = t_1$ after rupture the shock wave produces a step-function increase in pressure and temperature in the test gas, while imparting to it a certain velocity. The high pressure driving gas expands through the rarefaction wave to match this pressure and velocity condition at the contact surface. At $t = t_2$ the shock wave meets the closed end of the test section and reflects back upstream in still another sharp increase in pressure. Subsequently, more complicated interactions occur between the reflected shock waves, contact surface, and rarefaction waves. These are not of interest in this report, since only the shock wave and its reflection

SHOCK TUBE PRESSURE PROFILES AT
INTERVALS AFTER DIAPHRAGM BURST

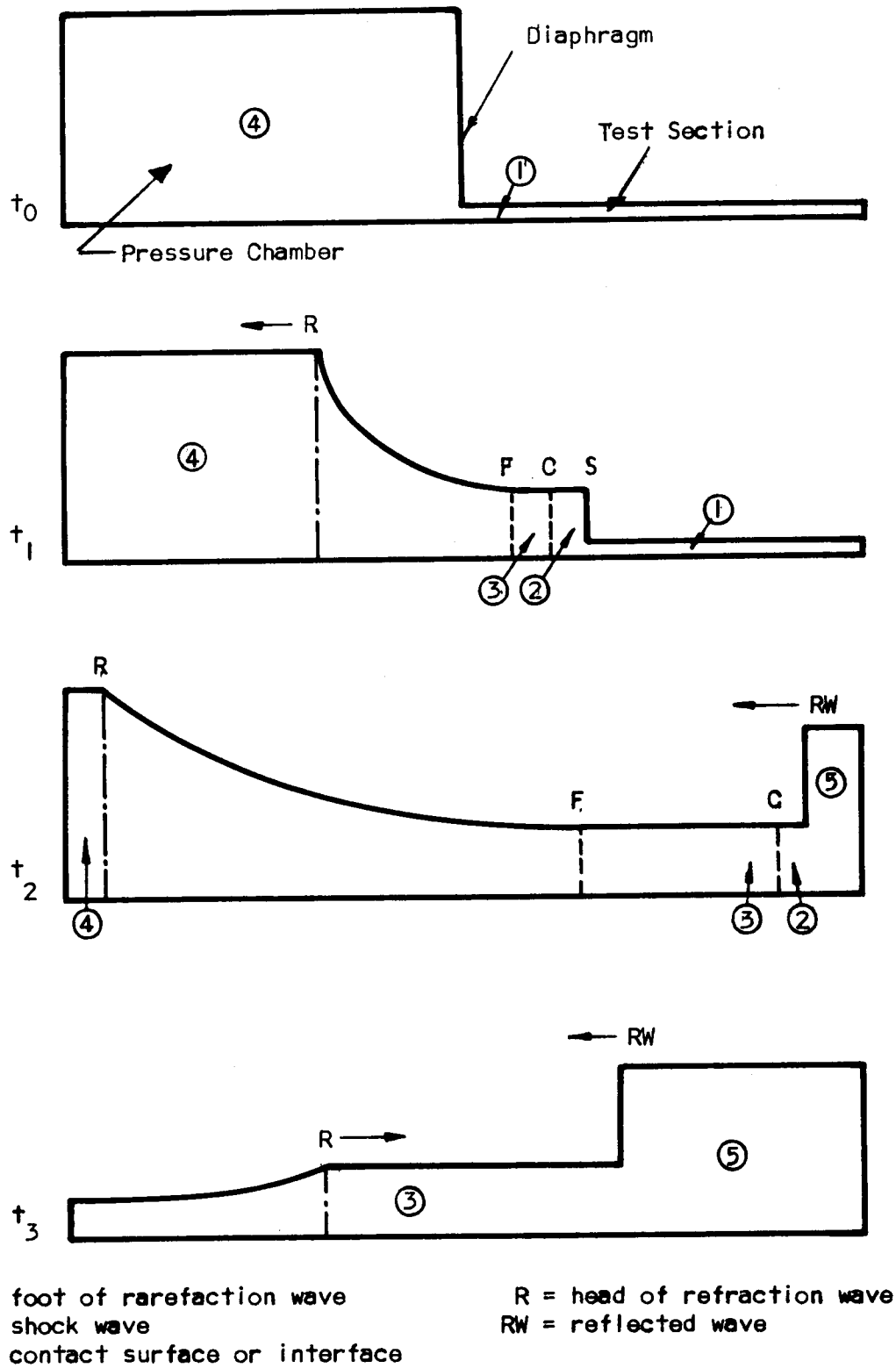


FIGURE 3

WAVE DIAGRAM FOR NONREFLECTING
INTERFACE FOR HELIUM TO AIR

AT $M_s = 3.2$

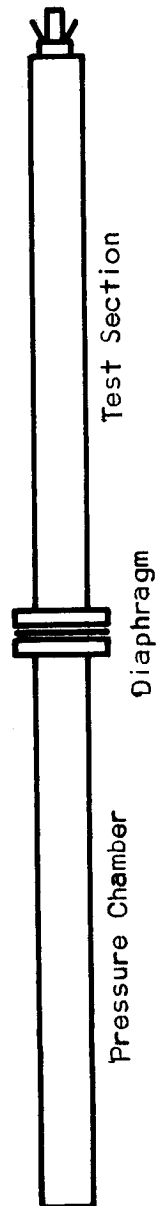
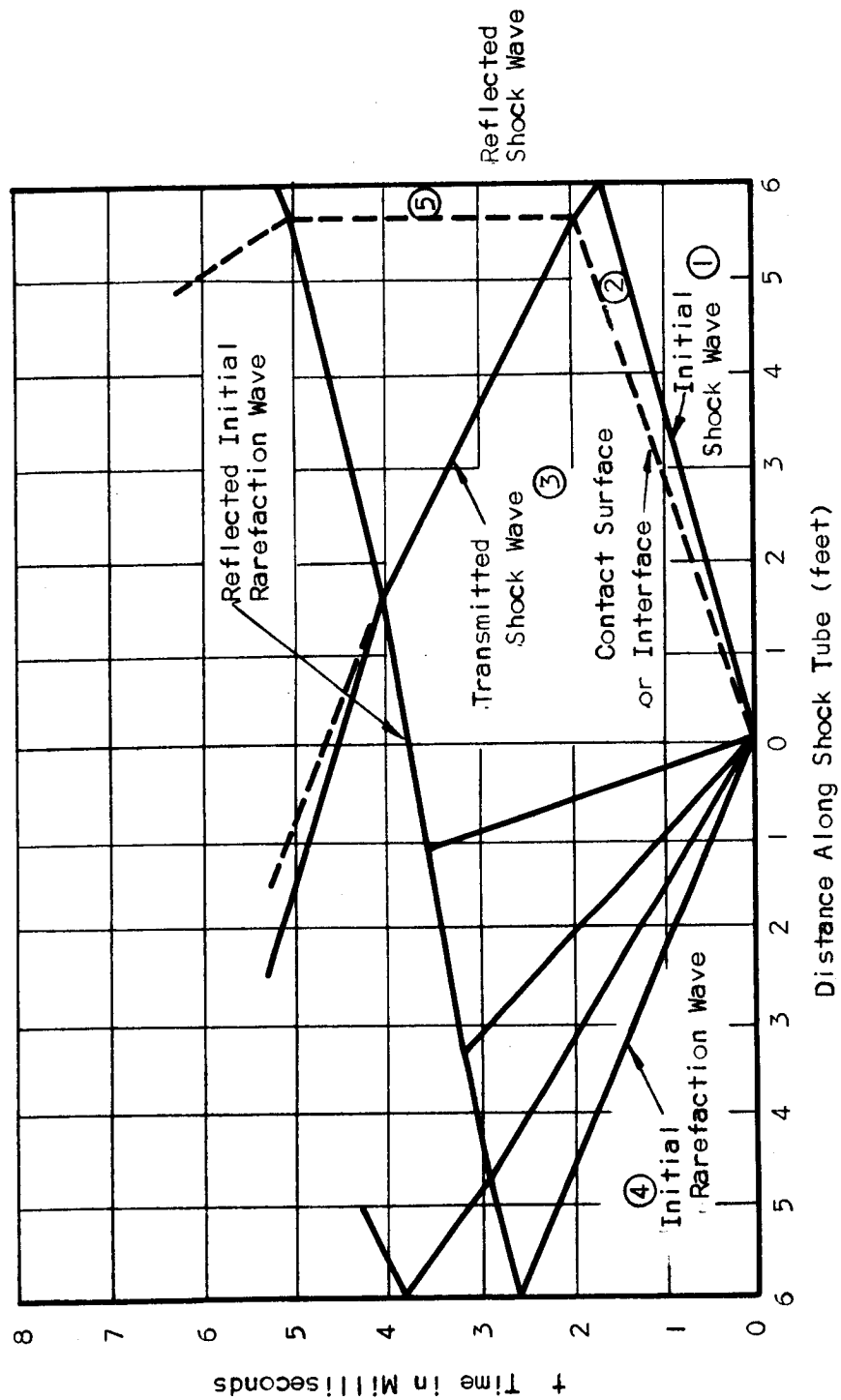


FIGURE 4

from the closed end are used to produce the step function for the transducer evaluation. The theoretical and practical aspects of these interactions are, however, well covered in literature previously referenced.

The wave diagram of Figure 4 represents a concise picture of the flow situation in the shock tube. The abscissa represents distance along the tube while the ordinate is the time after start of the shock. The wave phenomena appear as straight lines of constant propagation velocity. The line separating region ① and ② is the shock wave, S . The dot-dash lines between regions ③ and ④ represent the expansion fan of the centered rarefaction wave. The line separating the shocked test gas ② and the fully-expanded driving gas ③ is called the contact surface or interface which can support no pressure or velocity discontinuity. When the initial shock wave reaches the end of the tube, it reflects and propagates back up the tube, recompressing the once-compressed gas of region ② to a still higher level of temperature and pressure, region ⑤.

2. Ideal Shock Tube Theory

The theory of supersonic flow and shock tubes is covered in many textbooks and reports (Ref. 10,13,19,21,22,28,29, etc.). Much of the research has been accomplished using air in both chambers of the tube, assuming that the gas is ideal, and at constant values of specific heat. Using these assumptions, relationships have been obtained between the initial upstream and test section pressure ratios and the flow quantities after diaphragm rupture. Yoler (Ref. 30) developed a convenient relationship by matching pressure and velocity at the contact surface or as in Figure 3 that pressures, $P_2 = P_3$, and velocities, $V_2 = V_3$. Using an isentropic expansion from region ④, the state of region ③ may

be found and region ② may be calculated from the conditions in region ① by the Rankine-Hugoniot shock relations. This relationship in Reference 30 where it is referred to as 1.66 is

$$\frac{P_1}{P_2} = \frac{P_1}{P_2} \left[1 - \left(\frac{P_2}{P_1} - 1 \right) \sqrt{\frac{\left(\frac{\gamma_4 - 1}{2\gamma_4} \right) \frac{\rho_1}{P_4}}{\left(\frac{\gamma_1 + 1}{\gamma_1 - 1} \right) \frac{P_2}{P_1} + 1}} \right]^{\frac{2\gamma_4}{\gamma_4 - 1}} \quad (1)$$

An analysis of this equation by Yoler shows that an increase in shock strength will be obtained for a given value of the pressure ratio across the diaphragm (P_4/P_1) if the driving gas contains a higher internal energy per unit mass than the driven gas. This analysis concludes that the lightest gas, hydrogen, would produce the strongest shocks. Helium to air was used in this study because of the inherent risk of explosion when using a hydrogen-to-air shock. Glass (Ref. 13) points out the advantages of using helium as driving gas and covers thoroughly many other theoretical developments regarding helium-to-air shock tube operation similar to that employed in this study. The pressure ratio across the diaphragm for the helium-to-air shock tube is:

$$\frac{P_4}{P_1} = (P_2 + P_1) / P_1 \left[1 - P_2/P_1 (128.7 P_2/P_1 + 150.4)^{-\frac{1}{2}} \right]^5 \quad (2)$$

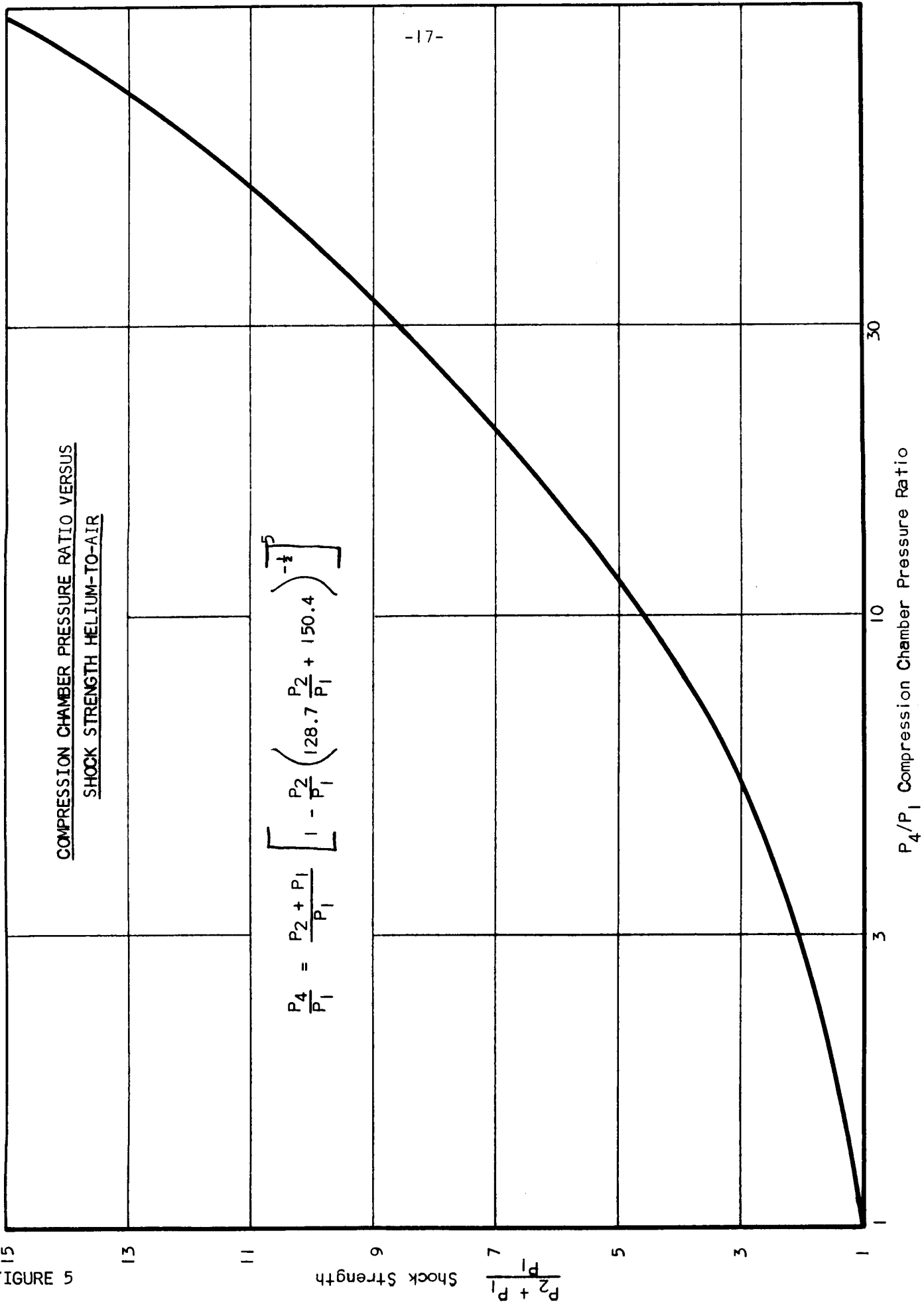
This relationship is plotted in Figure 5 (Ref. 14).

The relation between incident shock wave Mach number, M_s , and amplitude is:

$$\frac{P_2}{P_1} = \frac{7}{6} \left[M_s^2 - 1 \right] \quad (3)$$

This assumes that $P = \rho (C_p - C_v) T$, adiabatic flow, and constant

FIGURE 5



specific heat (Ref. 31). Shock front velocity can easily be measured in the shock tube by measuring the time it takes for the shock front to travel between two points in the tube. This will be described in the discussion of thin film gauges.

The relation between incident and reflected shock amplitudes upon reflection from a rigid wall is

$$P_2 = 2P_1 \left[\frac{7P_1 + 4P_2}{7P_1 + P_2} \right] \quad (4)$$

Combining Equation (4) with Equation (3) provides a more useful relation between the reflected shock amplitude, undisturbed expansion chamber pressure and incident shock front velocity.

$$\frac{P_2}{P_1} = \frac{7}{3} \left(M_s^2 - 1 \right) \left(\frac{2 + 4M_s^2}{5 + M_s^2} \right) \quad (5)$$

Figures 6 and 7 show these relationships are of significant use in shock tube design and initial experimentation.

The velocity of the contact surface or the translational particle velocity of the gas in the constant pressure region of the wave is:

$$V_3 = \frac{5}{6} a_0 \left[\frac{M_s^2 - 1}{M_s} \right] = \frac{5}{7} a_0 \left(\frac{P_2}{P_1} + \frac{6}{7} \frac{P_2}{P_1} + 1 \right)^{-\frac{1}{2}}$$

where a_0 = speed of sound in the undisturbed expansion chamber air.

The velocity of the hot gas of the incident wave of the shock wave reflected from the rigid end wall is:

$$V_5 = V_3 \frac{\gamma + 1 + (\gamma - 1) \left(\frac{P_5 + P_1}{P_2 + P_1} \right)}{2 \left(\frac{P_5 + P_1}{P_2 + P_1} - 1 \right)}$$

REFLECTED SHOCK AMPLITUDE
VERSUS
INCIDENT SHOCK AMPLITUDE

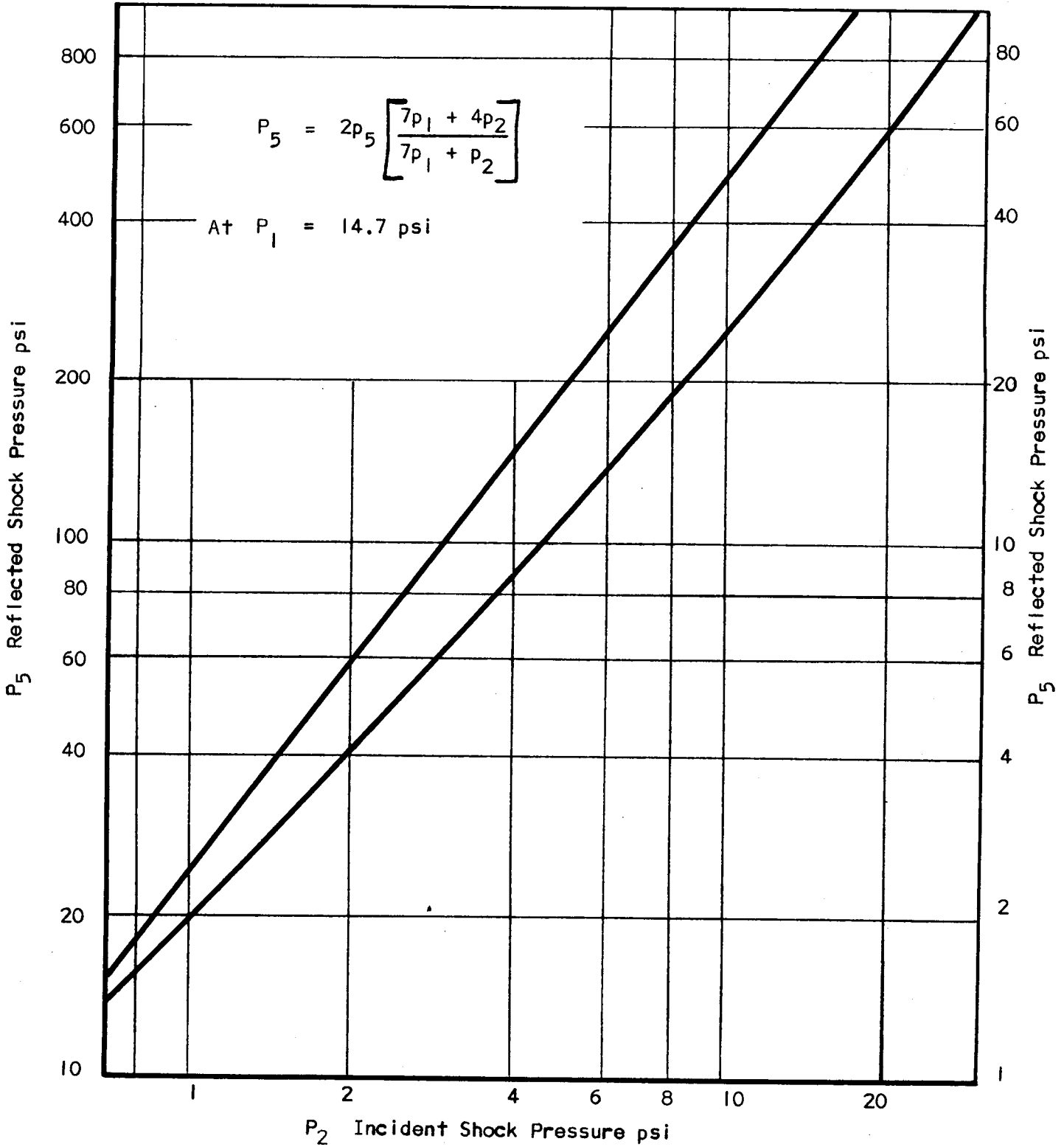


FIGURE 6

REFLECTED SHOCK AMPLITUDE VS SHOCK FRONT VELOCITY

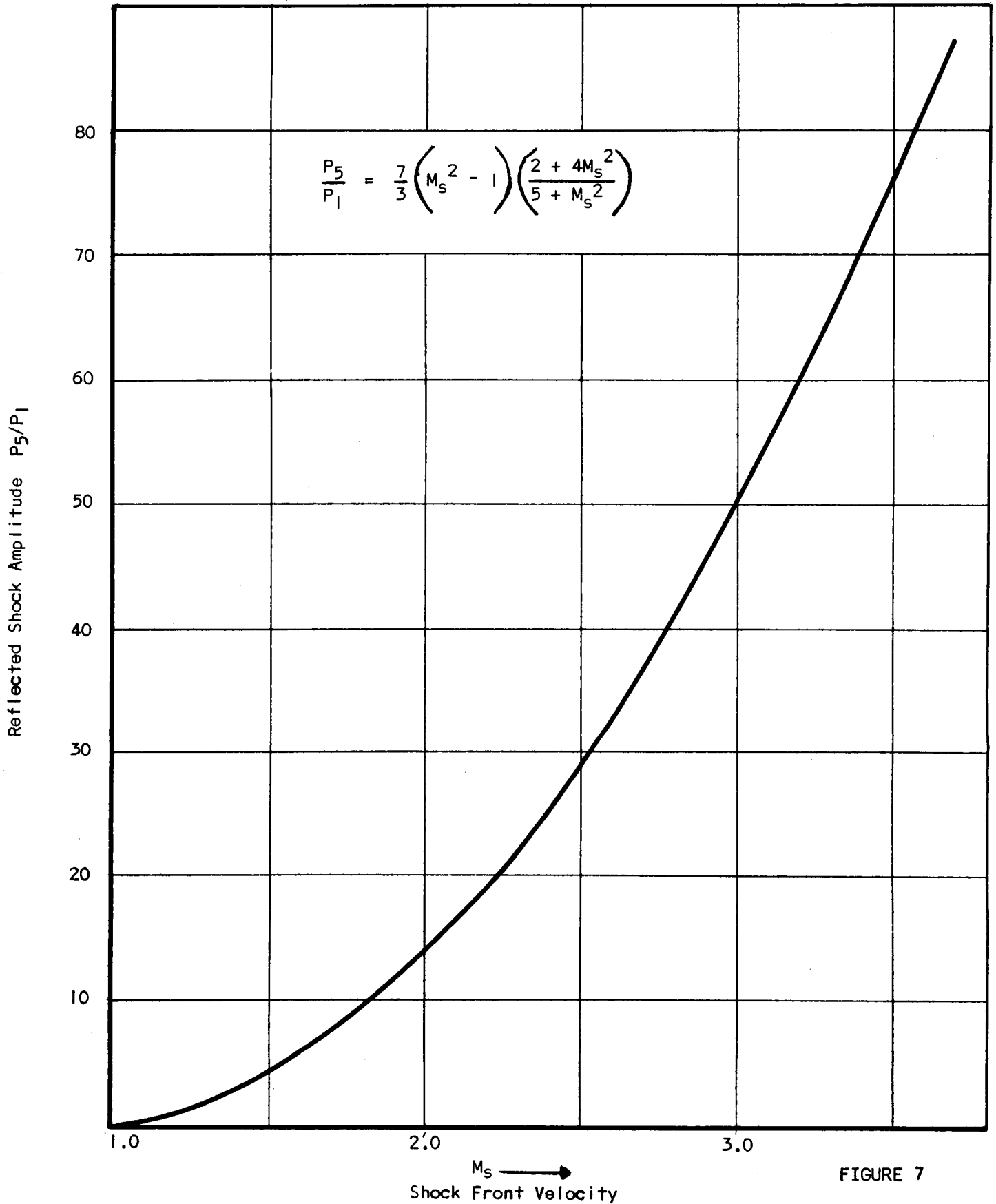


FIGURE 7

JPR 1689

This relation applies only prior to the passing of the reflected wave through the contact surface. The specific heat ratio, γ , changes as the gases are mixed and the equation is no longer valid.

In the helium-to-air shock tube employed at $P_4 = 515$ psia and $P_1 = 6.6$ psia, $P_2 \approx 75$ psia and $P_5 \approx 400$ psia.

3. Behavior of a Real Shock Tube

The ideal shock tube theory assumes that the perfect gas law applies, that specific heats are constant, and that the flow is adiabatic. This is, of course, not true for the real shock tube. The specific heats of the gases become temperature dependent at Mach numbers greater than two or three and the algebraic relationships previously mentioned, which were developed on the basic assumptions, are no longer valid (Ref. 13). Many complex numerical methods have been developed in this area and may be applied for precise solution of pressure and velocity problems. Table I, derived from Table 4, Ref. 13, lists the flow quantities on the high pressure side of the shock waves in air computed for temperature dependent specific heats. Figure 8 shows variations of the flow parameters in air behind a normal reflected shock wave versus the incident shock wave Mach number for a variable specific heat (Ref. 10). At Mach numbers above five ionization and dissociation effects become pronounced, however, since all experimentation was conducted below $M_s = 5$ these effects were ignored.

The ideal shock tube assumed that the diaphragm burst instantaneously and did not interfere with the flow and the shock waveform. This is hardly the real case. The diaphragm must be pierced or ruptured by pressure. It must then fold back to allow the helium to flow into the test section. The shock wave actually forms after it passes over

Table I

Flow Quantities on the High Pressure Side of
Shock Waves in Air with Temperature
Dependent Specific Heat

M_s	ρ_2 / ρ_1	T_2	P_2 / P_1
1.523	1.907	400	2.54
1.984	2.659	500	4.43
2.377	3.225	600	6.45
2.725	3.663	700	8.55
3.041	4.015	800	10.71
3.331	4.314	900	12.94
3.611	4.540	1000	15.23
4.235	5.069	1250	21.12
4.797	5.454	1500	27.27
5.307	5.746	1750	33.52

VARIATIONS IN FLOW PARAMETERS BEHIND A NORMAL
REFLECTED SHOCK WAVE VS INCIDENT SHOCK WAVE
MACH NUMBER FOR VARIABLE SPECIFIC HEAT

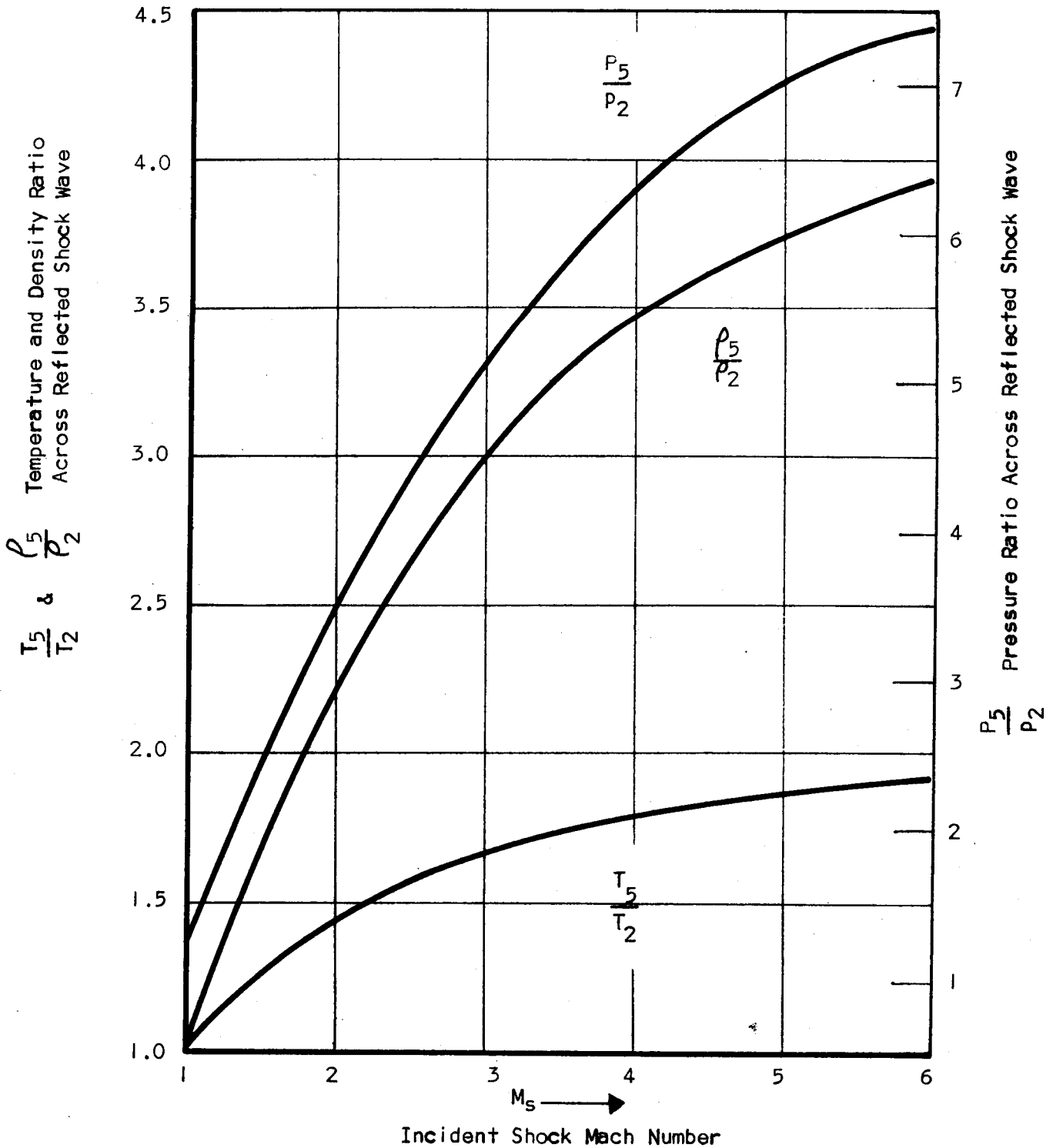


FIGURE 8

a finite length of tube. Both maximum amplitude and velocity are less than predicted by ideal theory (Ref. 13). The formation distance increases with initial pressure ratio, P_4/P_1 , and the decrement of both front amplitude and velocity increase with formation distance. Thereafter, the shock front is continuously attenuated, both amplitude and velocity decreasing with distance traveled (Ref. 32).

McAlevy (Ref. 33) developed and evaluated a self-bursting disc made of commercially available aluminum sheet. Experimentation with this disc corresponded closely to the theoretical which he predicted by assuming that the diaphragm distorts to a hemispherical shape. Applying the stress analysis of a spherical shell smoothly supported at the rim, McAlevy obtained the following relationship which correlated the experimental data quite well.

$$P_4 = 4 S/D S_{ult}$$

where P_4 is burst pressure

S is diaphragm thickness

D is diameter of tube

S_{ult} is ultimate tensile strength

Deviation with pressure was of the order of ± 10 psi when burst at pressures up to 600 psia. No material was lost from these burst diaphragms, an important consideration when evaluating highly expensive thin-diaphragm transducers. A similar self-burst .020 inch thick, aluminum diaphragm was utilized in this program, found to be highly satisfactory, and, very inexpensive to use. Commercially available aluminum sheet was simply cut into 2.5 inch squares and inserted between the flanges at the center of the shock tube. Care had to be exercised

when tightening the four bolts joining these flanges to insure that the aluminum diaphragm was evenly supported at the rim. During velocity calibration runs the quantities affecting shock strength formation, such as burst pressure, diaphragm opening time, did not vary more than a few percent of the measured shock velocity. This confirmed the reproducibility and persistent petal formation pattern of the diaphragm rupture process.

Although the mechanism of the formation and growth of the shock wave is still being actively investigated. McChesney in Reference 34 has propounded an excellent study on the subject. Riemann assumed the gas to be a continuum or structureless fluid. The gas in the tube is, however, composed of atoms or molecules and considerable empty space - it is far from being a continuum. In a container of gas the molecules tirelessly rush about colliding with one another, the sides of the wall, and then travel freely to collide again. At the moment of rupture of the diaphragm the molecules of gas in the test section are moving over relatively long molecular mean free paths, because of the low density of the gas. These molecules travel about 1000 feet per second. Compression of the gas in the first small segment just ahead of the driver gas shortens the mean free path of the molecules and increases the rate of collision among them, increasing the velocity and temperature of the test section gas. The first minute disturbance passes forward at the speed of sound into the next segment, compressing and preheating it for the arrival of the next wave. As the waves overtake one another, building up into a large pressure pulse, and as the pulse grows into a shock wave, the mean free path of the molecules in the wave grows still shorter and the temperature rises.

It is not possible for the shock wave to become an infinite discontinuity, or to have zero thickness, precisely because it is

formed from molecules of gas. The shock wave must always have some finite thickness usually on the order of a few mean free paths. Across this finite distance the pressure, temperature, density, and velocity all change. As the shock wave forms and these gradients grow steeper, energy in the form of heat and also momentum flows more swiftly from high temperature regions and the velocity to the regions in the wake of the wave where these quantities are low. Ultimately these opposing mechanisms of steepening and spreading balance and the shock wave profile becomes stable. Glass (Ref. 13) has found experimentally that a fast burst for a 3" x 3" tube requires about 33" of travel beyond the diaphragm before the shock front is fully developed and maximum shock velocity and strength are obtained.

The Rankine-Hugoniot shock wave relations predict quite accurately the pressure level immediately following reflection of the shock wave. Unfortunately, as the shock wave propagates back up the tube it overtakes an attenuated, non-uniform slug of once-shocked test gas, the contact surface, expansion wave, etc., and its interactions produce reflected waves which propagate to the end wall to produce pressure fluctuations. As a result of these interactions, the pressure history at the end wall or test section is very difficult to predict theoretically. Therefore, in order to know the pressure of the gas during transient pressure transducer testing, an experimental determination of the pressure history over a range of incident shock velocities ($2 < M_s < 5$) had to be made.

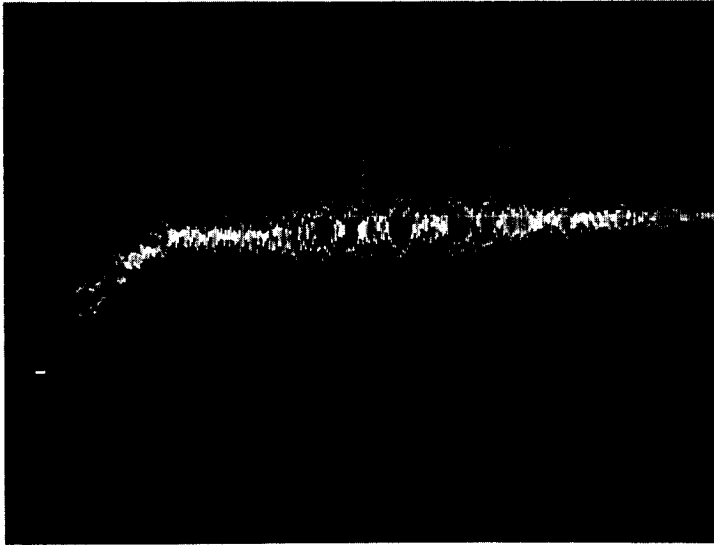
It is particularly advantageous to conduct the transducer shock tube test at a constant test gas pressure level. Such a situation can be realized if the reflected shock wave passes smoothly through the

contact surface without creating a reflected wave. Both the driving and test gases must be brought to equal pressure and velocity by the passage of the reflected shock wave for this to occur.

This condition is referred to as the "tailored interface" or the non-reflecting contact surface (Ref. 35). By imposing this matching condition on the shock tube equations, it is possible to calculate, for any reflected shock in a testing gas, the initial temperature and pressure of driving gas necessary to produce this desired condition. It has been found that a unique relation between the desired shock Mach number and the composition of the driving gas will produce this condition. For helium-to-air, at constant specific heat and at room temperature, the calculated shock Mach number is $M_s = 3.8$ (Ref. 35). Several other authors have experimentally found that the non-reflecting condition is quite insensitive to the actual M_s , so long as it is close to the critical value (Ref. 33,36). During the present program the pressure histories obtained showed this to be true for values of $3.3 < M_s < 3.8$. Using an end-mounted Kistler 601A pressure transducer records were obtained of the pressure history of the shock reflection process. See Figure 9. At Mach numbers less than critical, Figure 9c, the shock wave seemed to be absorbed as it was refracted at the interface, a situation which resulted in reflected rarefaction waves which decreased the end wall pressure. At Mach numbers greater than critical, Figure 9a, the shock waves were amplified when refracted at the interface and compression waves were reflected, producing a gradual pressure rise.

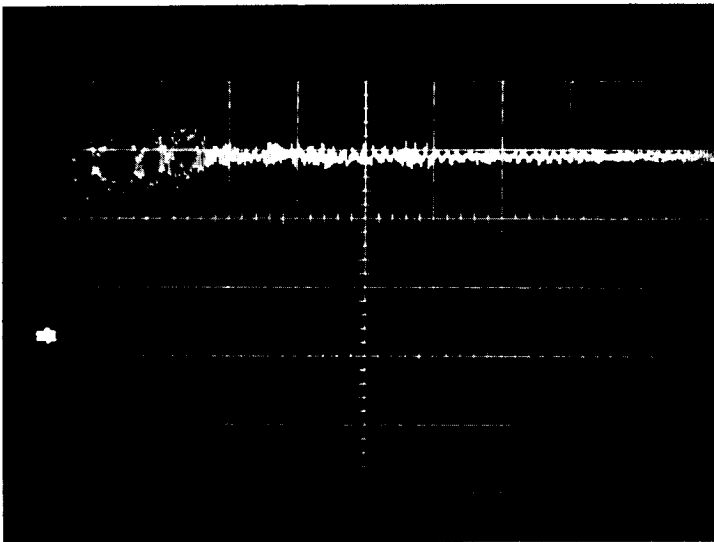
The duration of the constant test gas pressure level at the end wall is also contingent upon the length of the shock tube (Ref. 15, 16,28). It is necessary to select a design length dependent upon the

TAILORED INTERFACE CONDITION



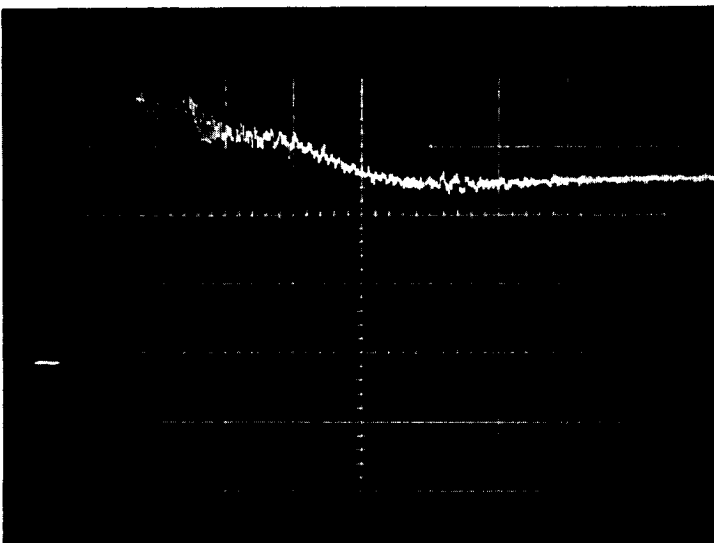
Kistler 601A end mounted
in shock tube $M_s = 4.8$
Sweep at 200 μ sec/cm

FIGURE 9a



Kistler 601A end mounted
in shock tube $M_s = 3.6$
Sweep at 200 μ sec/cm
Shows constant pressure
level which is obtained
by operation at tailored
interface.

FIGURE 9b



Kistler 601A end mounted
in shock tube $M_s = 2.8$
Sweep at 200 μ sec/cm

FIGURE 9c

characteristics of the transducers to be tested, so that damped oscillations resulting from the pressure step can die down appreciably. To obtain this limiting time it is important to choose values of P_4 , P_1 , and shock tube design length to optimize the advantage of the tailored interface and the desired transducer steady pressure testing duration. It has been experimentally determined during this program that for the particular design of shock tube employed the optimum operating conditions were $P_4/P_1 = 120$, which with a 72-inch test section, produced an $M_s = 3.60$ (See Fig. 9b). These conditions were therefore selected for the majority of all system testing and provided the sharpest pressure rise and more than four milliseconds of steady pressure after shock wave impingement on the transducer diaphragm.

A factor detracting from the sharpness of the shock-induced step function, a factor which reduces the rise time of the initial normal shock front, is the irregularity in certain transducer diaphragms. These irregularities caused by the particular design of cooling passages, cause a broadening of the impingement of the shock front. This effect causes an undesirable increase in wave rise time. Despite this factor the rise time does not exceed one microsecond.

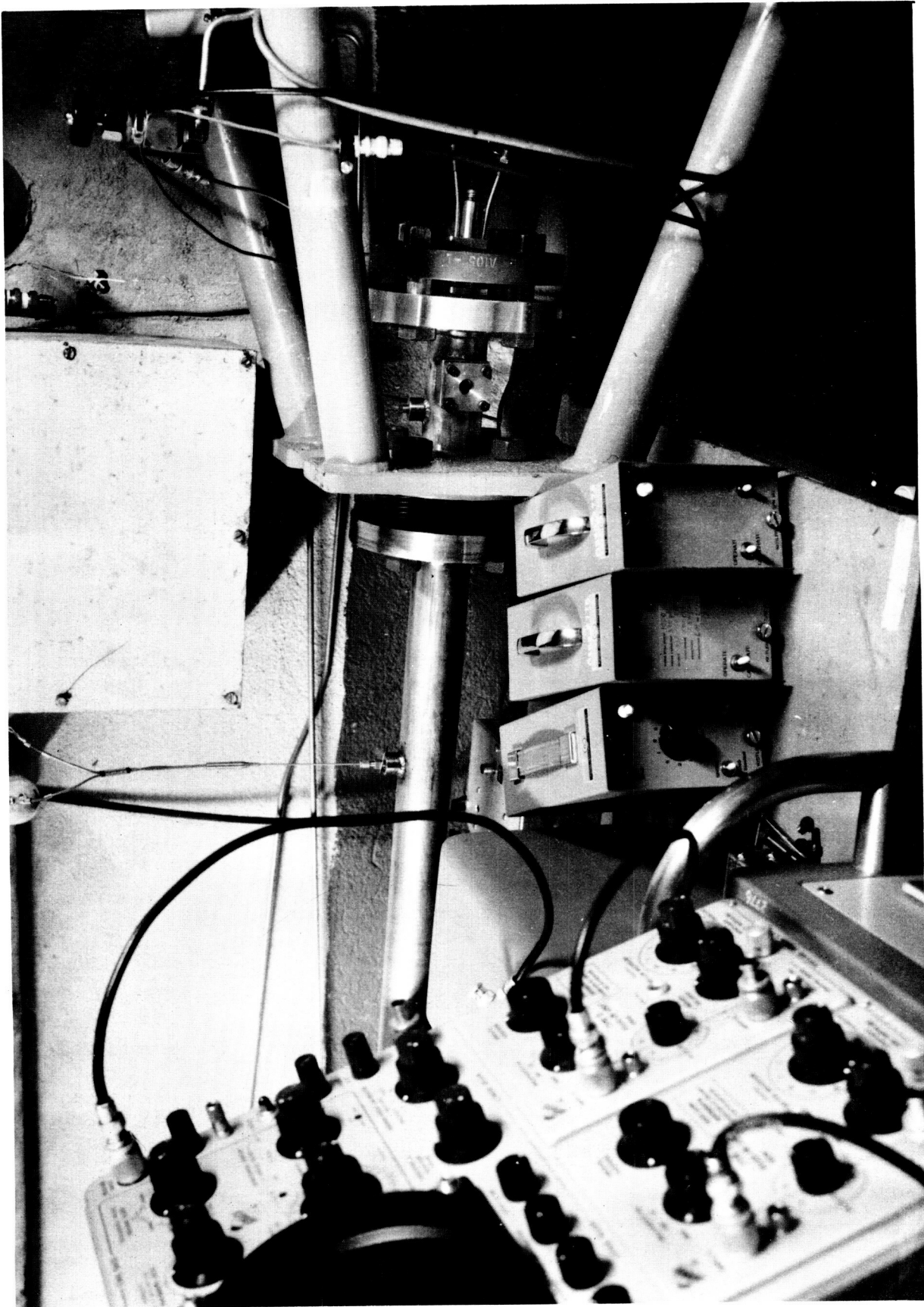
Several experimenters (Ref. 13,14,32) have determined that roughness of the tube wall contributes significantly to attenuation. Any irregularities of the wall surface also result in shock reflections and complex interactions. These then cause a certain amount of "noise" to be superimposed upon the tread of the step in the transducer photographs obtained in testing. It is important therefore to machine the inner walls of the tube to minimize irregularities and to keep the walls as free of protuberances as possible. In an attempt to keep the inner walls

clean and to reduce this form of interference, a miniaturized thin film gauge with a .218 inch diameter was devised for temperature surveys and to act as trigger for the oscilloscope. This new device will be described later in the report and in Appendix B.

Ground shock is another interference factor which is undesirable in system testing. This effect is caused by the shock being transmitted through metal of the tube. Since the speed of sound in the metal is several times the speed of the shock in the test section, the ground wave through the metal arrives at the test station some time ahead of the shock front. The vibration due to this ground shock results in the generation of a spurious electrical signal which is superimposed on the response of the transducer. Smith and Lederer (Ref. 14) concluded that the tube was set into vibration upon rupture of the diaphragm and again, at a higher amplitude, upon the arrival of the shock at the closed end. This vibration was predominantly longitudinal and since the tube is not a simple structure more than one resonant frequency could be expected. Normally, increasing the rigidity of the mounting of the shock tube decreases the vibration magnitude. Jones (Ref. 4) found that by using springs to suspend the shock tube in the axial plane, it was possible to lower the frequency of the vibration sufficiently to essentially eliminate interference from this source.

C. Description and Operation of the Apparatus

A photograph of the 1.6 inch diameter shock tube is found in Figure 10. The appropriate valving and a pressure gauge for the helium gas supply are connected to the pressure inlet on the driving end of the tube (See Figure 2). A vacuum pump, manometer, and valving to the atmosphere complete the test section connections. Various connections

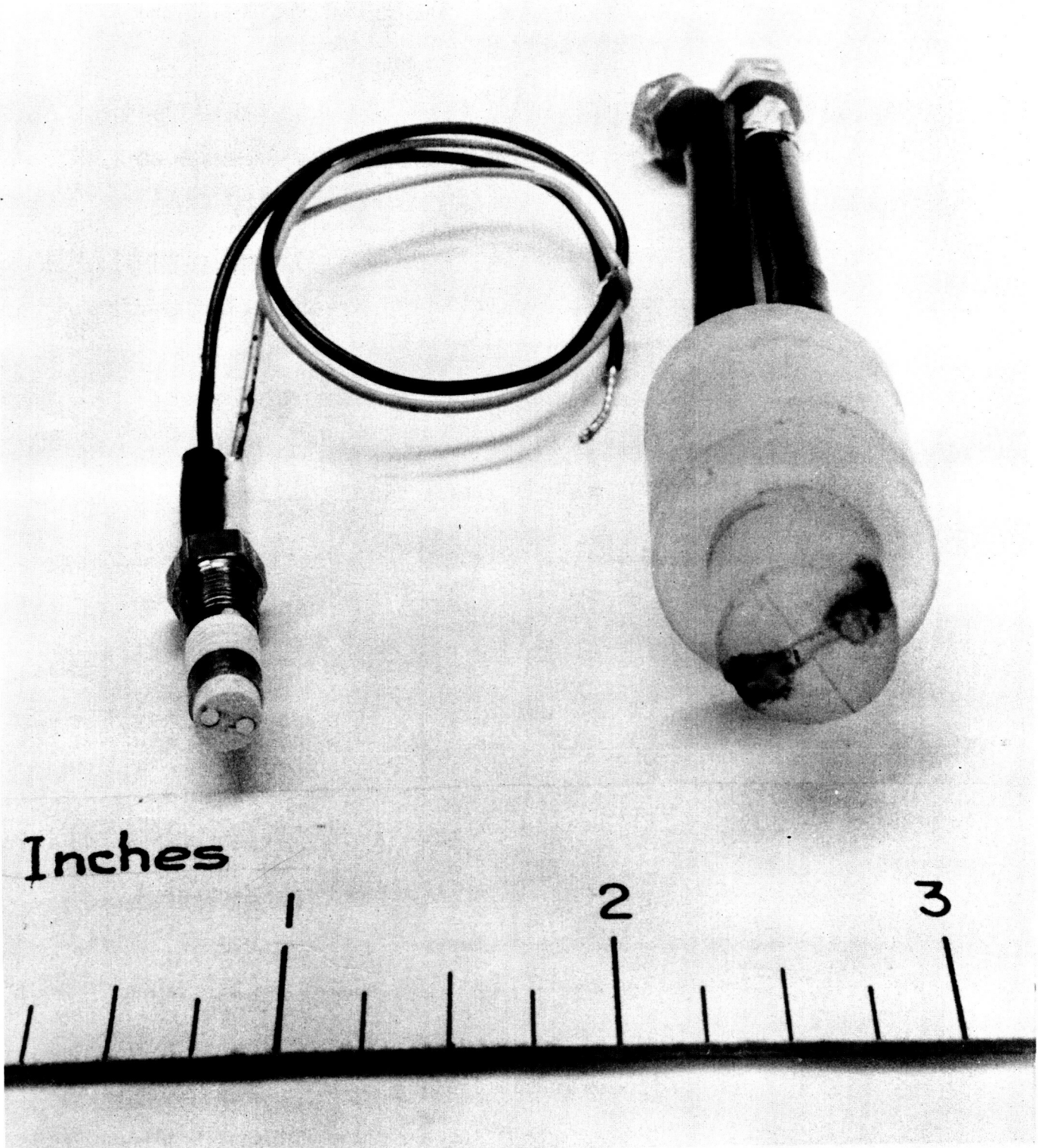


Shock Tube Test Section

and valving for transducer coolant flow are also available. Adapters for the installation of various types and sizes of transient pressure measuring pickups are located in the side and in the replaceable end flanges. The housings for the thin film gauges which are used for velocity measurement and to act as triggers for the initiation of the oscilloscope sweep are seen on the test section. The diaphragm holder flanges separate the upstream and downstream portions of the tube. The shock tube is free to move axially under the compression of four springs which shock mount the tube to the bulkhead.

A record of the transducer response to the step input is obtained by photographing the trace on a Tektronix (type 551 Dual Beam) Oscilloscope using a Polaroid Hewlett-Packard Model 196A Oscilloscope camera. The high-impedance charge signal of the transient pressure transducer tested was converted to a low-impedance voltage or current signal through its own amplifier.

A unique miniaturized thin film gauge was developed to serve the twofold purpose of measuring the velocity of the shock wave and sensing the arrival of the wave early enough to permit initiation of the oscilloscope sweep (See Figure 11). The thin film gauge signal is fed into its own specially designed amplifier which is equipped with a gain control so that gain may be adjusted when required to reduce its sensitivity to stray electrical transients. The aluminized thin film (about 1/10 micron) of the gauge senses the impulsive passage of the hot gas of the shock wave. This causes a jump in the electrical resistance of the film providing a small, but precise, step voltage rise across the element. The rise time of the thin film gauge is less than one microsecond and the output about three millivolts when



New Miniaturized Thin Film Gauge
Compared with Conventional Thin Film Gauge

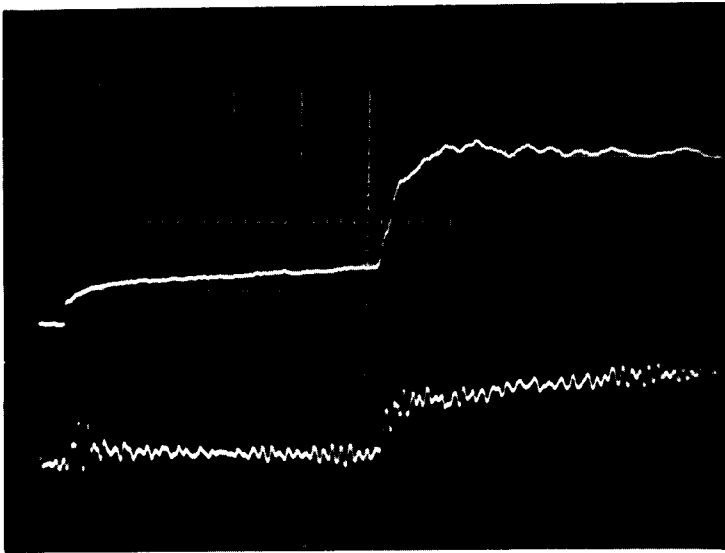
FIGURE 11

used in the circuit as shown in Figure 2. Figure 12 shows typical waveforms of the film gauge output and Appendix B describes the design and construction of the new miniaturized thin film gauges.

The transducer to be tested is mounted either in the end flange or in the side of the tube. Another transducer, normally a Kistler 601A, is mounted alongside in the end flange or opposite in the side configuration as in Figure 2. This transducer then acts as monitor and enables an accurate comparison and a means of cross checking previous tests. In this manner it is possible to verify the operating conditions in both the shock tube and sinusoidal pressure generator. The water-coolant flow is then connected and adjusted to the manufacturer's recommended flow rates and/or pressures. An aluminum diaphragm is inserted between the holding flanges and the flanges bolted together. The vacuum pump is actuated and the test section of the tube is evacuated to the desired pressure. After connection of all electrical leads to transducers, thin film gauges, amplifiers, oscilloscope, etc., helium is introduced into the upstream portion of the tube; pressure is increased until the diaphragm bursts. Immediately after the burst the helium pressure valve is turned off and the shock tube vented to the atmosphere.

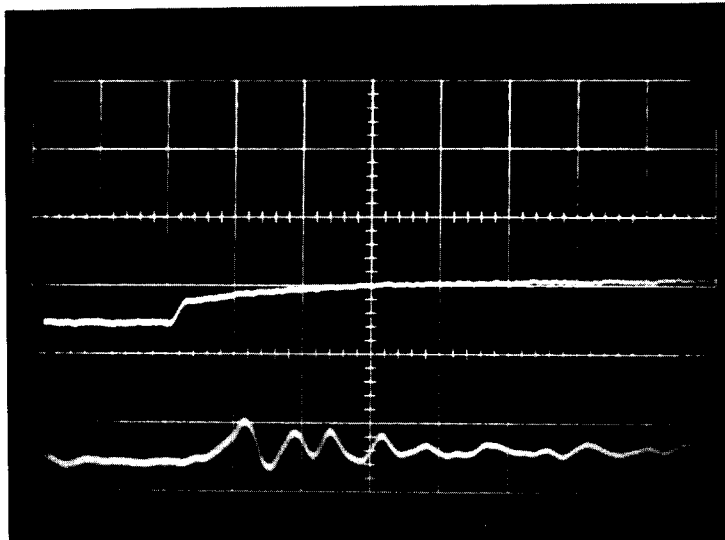
In addition to operating in the manner just described, temperature surveys and shock wave velocity checks were performed using extra thin film gauges mounted in the transducer test stations. The output of the thin film gauges were then recorded on the oscilloscope. When conducting shock wave velocity measurements the amplitude output of the thin film gauges (which for this purpose are spaced exactly 12.0 inches apart) was used to actuate a Hewlett-Packard Model 521

MINIATURIZED THIN FILM GAUGE WAVEFORM



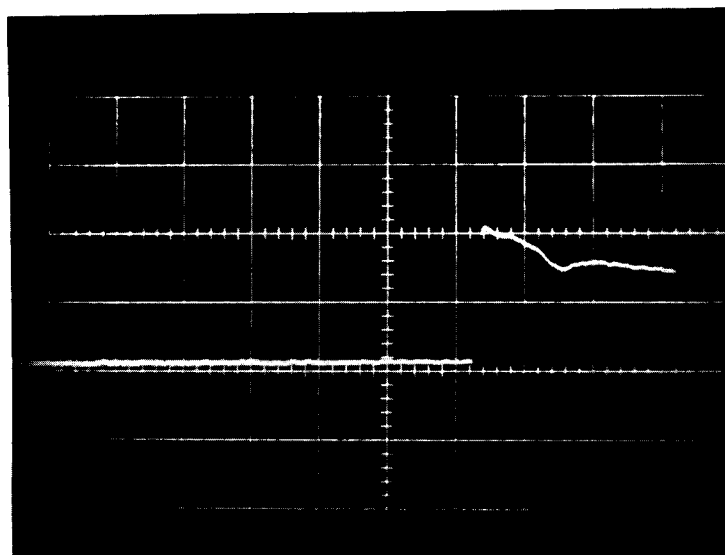
Thin film gauge output waveform compared with Kistler 601A, both side mounted in shock tube at $M_s = 3.6$
Sweep 50 μ sec/cm

FIGURE 12a



Thin film gauge output waveform compared with Kistler 601A, both side mounted in shock tube at $M_s = 3.6$
Sweep 10 μ sec/cm

FIGURE 12b



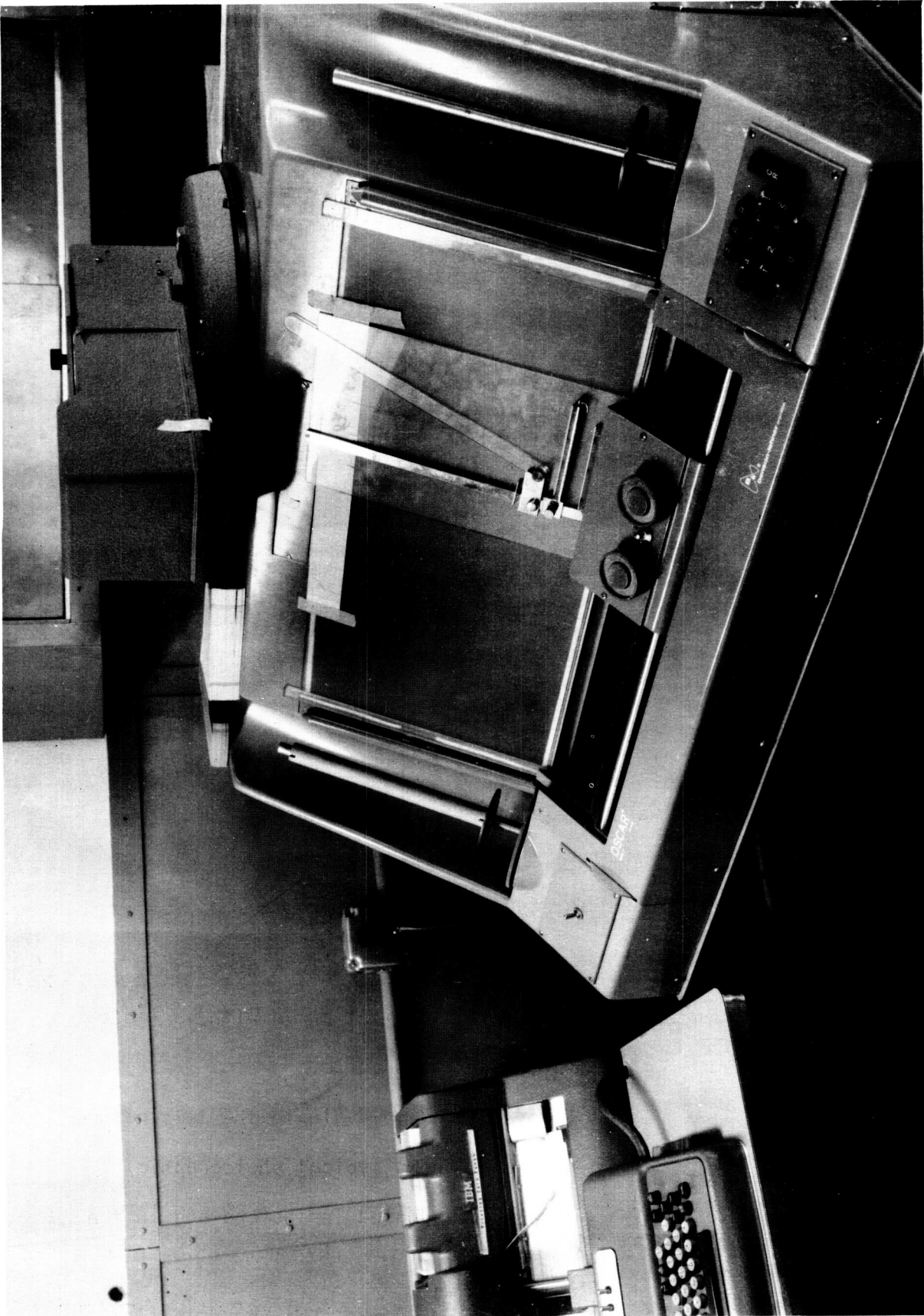
Thin film gauge output waveform mounted in end of shock tube at $M_s = 3.6$
Sweep 10 μ sec/cm
Rise time $\approx 1 \mu$ sec

FIGURE 12c

Electronic Interval Counter to verify the time between traces on the oscilloscope record.

Once a photograph on measurement of the dynamic physical phenomena is obtained, the task becomes one of evaluating and analyzing the obtained data. The characteristically high speed, complex, waveform does not easily lend itself to interpretation, and may not divulge its intrinsic volume of information unless a convenient, rapid analytical evaluation process is available to the research program. Each slope, amplitude, turn and wiggle of a complex waveform may have its significance in the system's dynamic behavior; and must not be neglected in the evaluation process.

Although the Princeton Group does not have available a high speed flying spot-scanner of the JPL type of analog-to-digital converter (Ref. 2,5), considerable use was made of a Benson-Lehner Optical Scanner which was coupled to an IBM card punch unit (See Figure 13). This device enabled a competent operator to reduce the waveform to x and y coordinates where readout is effected as a "signal magnitude versus time" function in coded punch cards. This device reduced the tedious hand reduction of data to a matter of minutes (less than an hour). The punch cards are then fed into an IBM 7090 computer program in which the frequency response of a transient pressure measuring system may be obtained by comparing its output as a function of time to a known input function. When the shock tube is operated at the tailored interface condition the shock wave produced closely approximates a step function input and is of sufficient constant pressure level duration to obtain a steady record of the transducer response. The computer program then evaluates the Fourier transform of the output function



Benson-Lehner Optical Scanner and IBM Card Punch

FIGURE 13

to the Fourier transform of a step input function. This, when calculated, is printed out as frequency versus response and quantitatively represents the dynamic response of the system under test. Knowing the dynamic response enables the obtaining of a true recording of the instantaneous pressures, regardless of the rapidity of the oscillations. This information is especially vital in attacking such problems as combustion instability in liquid propellant rocket engines.

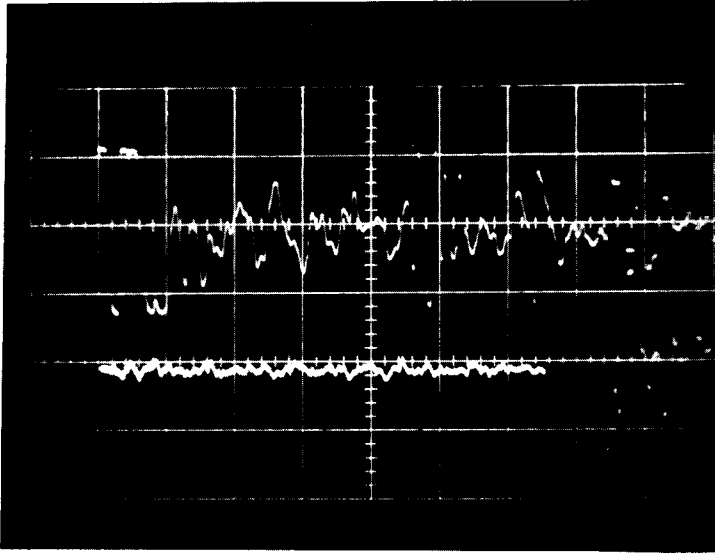
D. Experimental Results

An evaluation of the actual shock wave Mach number versus diaphragm pressure ratio was completed using the thin film gauge to detect the arrival and time of passage of the shock wave across a known distance. The time interval between voltage pulses was measured with 1 microsecond accuracy by means of a Hewlett Packard Model 521 Electronic Interval Counter. The accuracy of the time interval was checked simultaneously by displaying the output of the two gauges, which were spaced 12 inches apart, on the Tektronix Oscilloscope and photographing the trace (See Figure 14). From the measured pressures, P_4 , P_1 , the temperature in test section, and hence knowing the speed of sound in air the speed of the shock wave can be determined. The experimental points which were found are plotted in Figure 15, showing a very close agreement with the theoretical curve with variable specific heat obtained from Figure 24 of Reference 30.

The thin film gauges were also used to evaluate the temperature profile within the shock tube. Figure 12 shows typical photographic traces of the thin film gauge output while mounted in the end and in the sides of the shock tube.

To investigate the characteristics of the shock tube in its

SHOCK TUBE SPEED CALIBRATION
THIN FILM GAUGES USED TO MEASURE TIME OF SHOCK PASSAGE



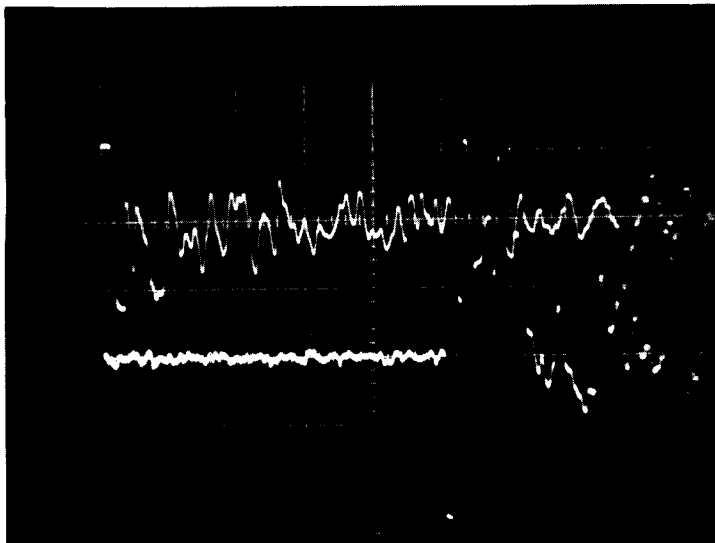
Sweep 50 μ sec/cm

$$p_4/p_1 = 35.5$$

$$V = 1/328 = 3050 \text{ fps}$$

$$M_s = 2.70$$

FIGURE 14a



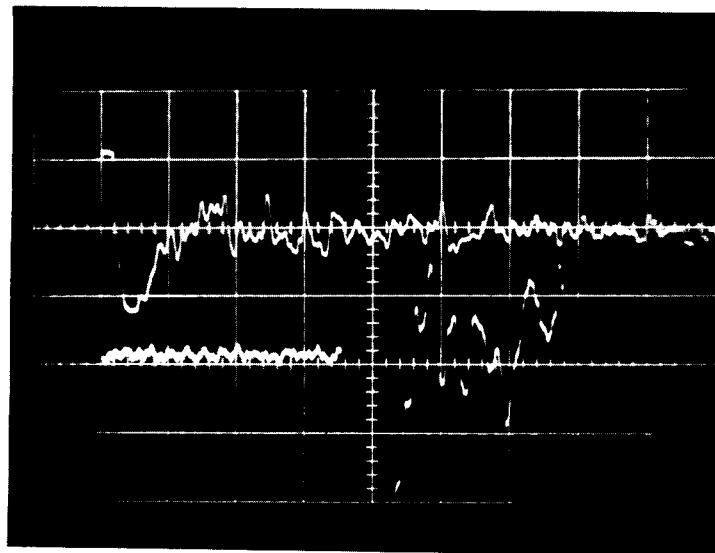
Sweep 50 μ sec/cm

$$p_4/p_1 = 103.3$$

$$V = 1/252 = 3970 \text{ fps}$$

$$M_s = 3.50$$

FIGURE 14b



Sweep 50 μ sec/cm

$$p_4/p_1 = 525$$

$$V = 1/177 = 5650 \text{ fps}$$

$$M_s = 4.97$$

FIGURE 14c

SHOCK WAVE MACH NUMBER
VERSUS
DIAPHRAGM PRESSURE RATIO
HELIUM-TO-AIR

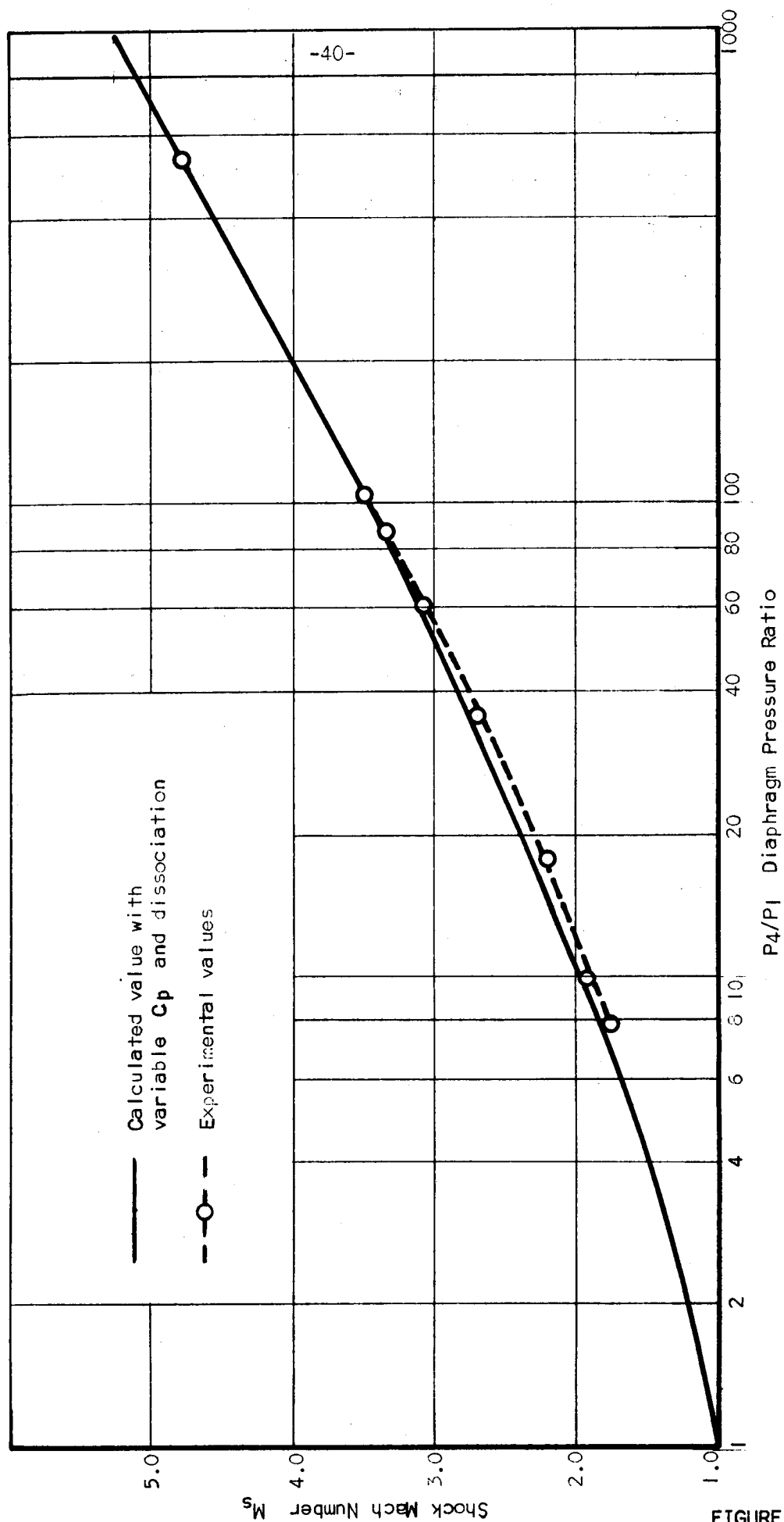


FIGURE 15

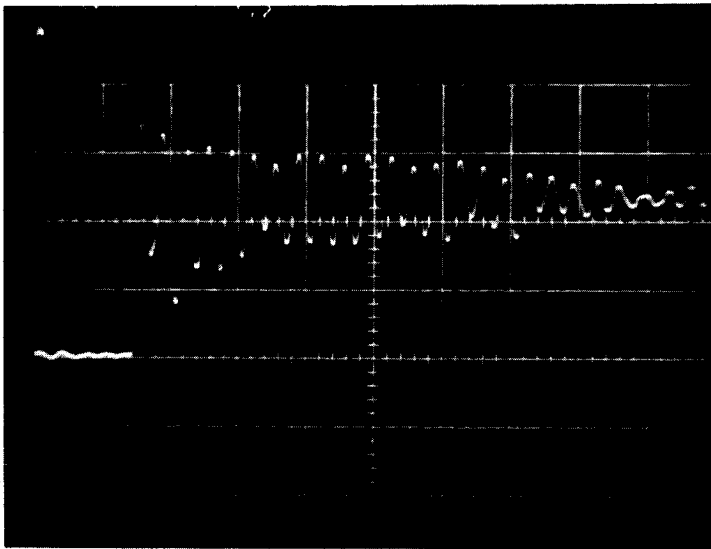
application to the testing of transient pressure measuring systems, several different test applications were utilized. These consisted of end-mounted, side-mounted, ground shock, and ball drop technique evaluations. Comparisons when possible were also made with the results of the sinusoidal pressure generator, rocket motors, and other test devices such as the Bureau of Standards pneumatic step function generator and the Bureau's large shock tube installation. The majority of testing was done with such transducers as the Kistler 601, 601A, 603A and to a lesser extent with the Dynisco PT-49, PT-76, Elastronic EBL 6009 and Photocon Model 755.

Figure 16 through Figure 33 are transducer evaluation tests showing the oscilloscope photograph obtained, the pertinent test conditions, natural frequency, rise time, damping, and the frequency-response curve.

The end mounted tests were conducted by installing the transducer in an appropriately sized end plate or adaptor, and operating the shock tube as previously described (See Figures 16 through 23). The side mounted tests were similarly conducted (See Figures 24 through 26).

The investigation of the effect of ground shock on the transducer was conducted by mounting the transducer as in the end-mounted position, described above. However, a one-quarter inch thick steel plate was inserted immediately forward of the end mounting flange. The average maximum amplitude of the Kistler 601A and 603A transducers tested in this manner was about one-fortieth as strong as that average maximum amplitude felt when the shock wave impinged directly on an end-mounted transducer diaphragm while operating at $M_s = 3.25$ and

TRANSDUCER EVALUATION TEST

Model Kistler 601A		Serial 3037	Date 3 March 1963
Type of Evaluation Shock Tube		Mounting End	Run No. 4
Test Conditions			
Test Sect. Press. $P_1 = 17$ in. HG (VAC) air			
Driver Sect. Press. $P_4 = 530$ PSI Helium			
Shock Wave Velocity $M_s = 3.32$	Sweep Speed $20 \mu\text{sec/cm}$		
Sensitivity			
Upper 2000 mv/cm	Lower mv/cm		
Natural Frequency 149,000 cps	Damping Factor $\delta = .012$		
Rise Time $2 \mu\text{sec}$	Type Analysis OSCAR-7090		
Remarks/Comments 566 Charge Amplifier 10 mv/pcb			

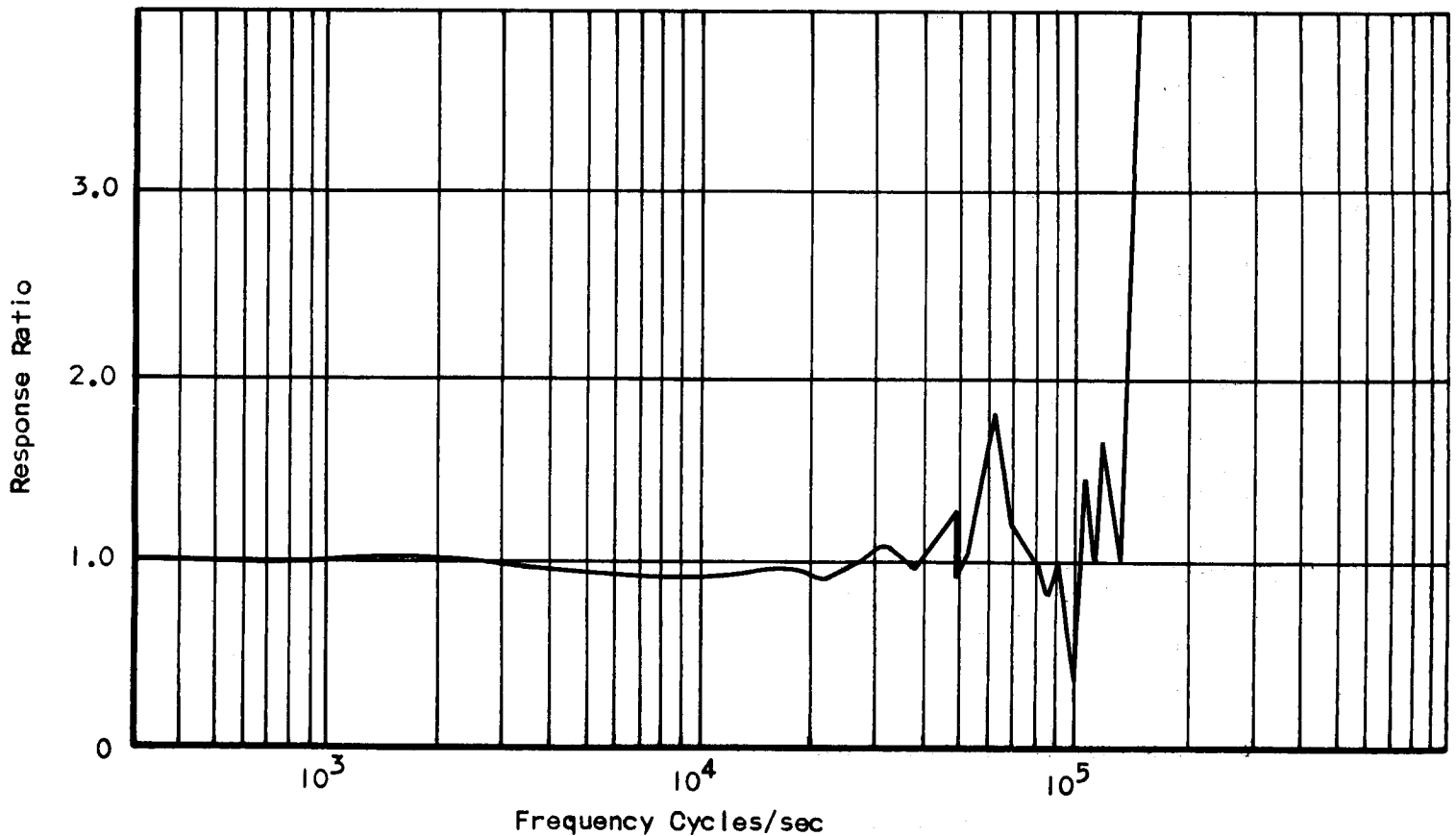


FIGURE 16

TRANSDUCER EVALUATION TEST

Model Kistler 603A	Serial 3484	Date 10 April 1963
Type of Evaluation Shock Tube	Mounting End	Run No. 13
Test Conditions		
Test Sect. Press. $P_1 = 17$ in. HG (VAC) air		
Driver Sect. Press. $P_4 = 530$ PSIG Helium		
Shock Wave Velocity $M_s = 3.32$	Sweep Speed $20 \mu\text{sec/cm}$	
Sensitivity		
Upper 500mv/cm	Lower mv/cm	
Natural Frequency 171,000cps	Damping Factor $\delta = .03$	
Rise Time $1.5 \mu\text{sec}$	Type Analysis OSCAR-7090	
Remarks/Comments 566 Charge Amplifier 10 mv/pcb		

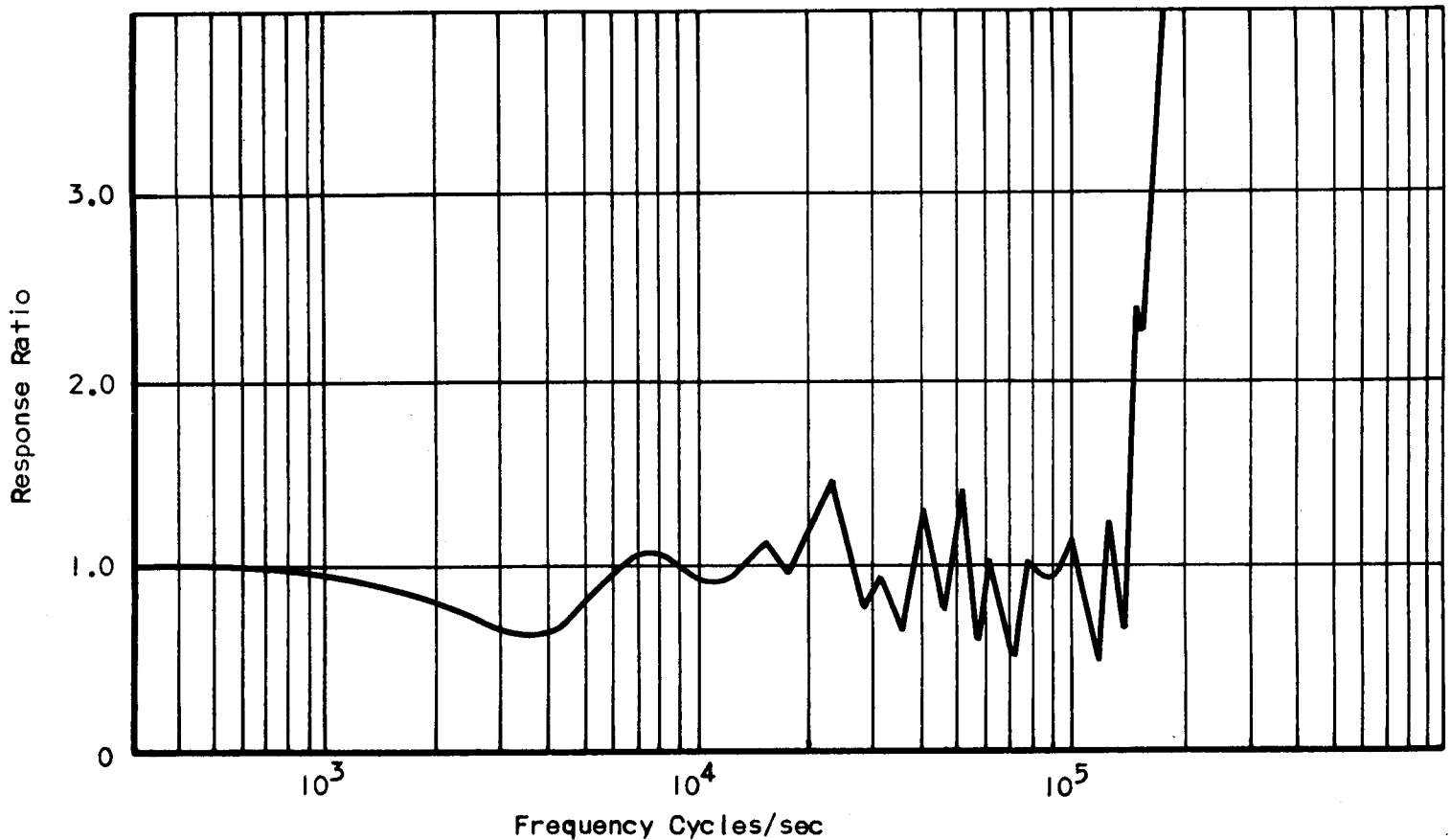
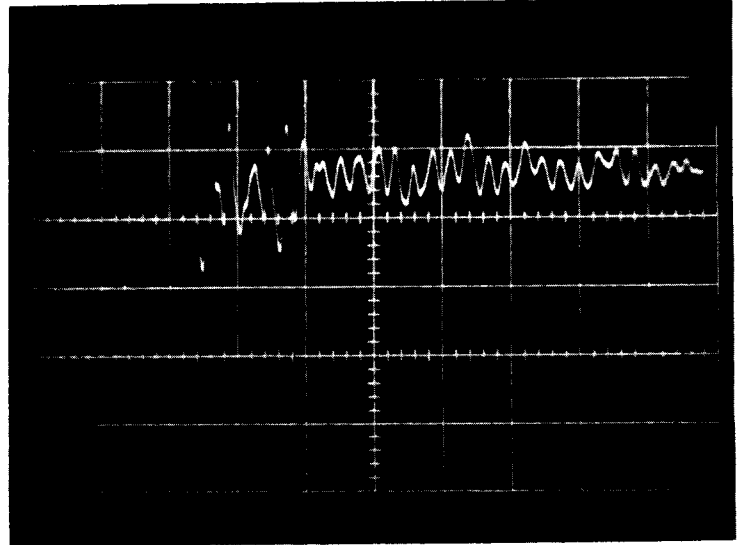


FIGURE 17

TRANSDUCER EVALUATION TEST

Model Kistler 601	Serial 1886	Date 3 March 1963
Type of Evaluation Shock Tube	Mounting End	Run No. 16(5A)
Test Conditions		
Test Sect. Press. $P_1 = 17$ in. HG (VAC) air		
Driver Sect. Press. $P_4 = 500$ PSIG Helium		
Shock Wave Velocity $M_s = 3.30$	Sweep Speed 20 μ sec/cm	
Sensitivity		
Upper 1000mv/cm	Lower mv/cm	
Natural Frequency 132,000 cps	Damping Factor $\delta = .10$	
Rise Time 2 μ sec	Type Analysis OSCAR-7090	
Remarks/Comments 566 Charge Amplifier 10 mv/pcb		

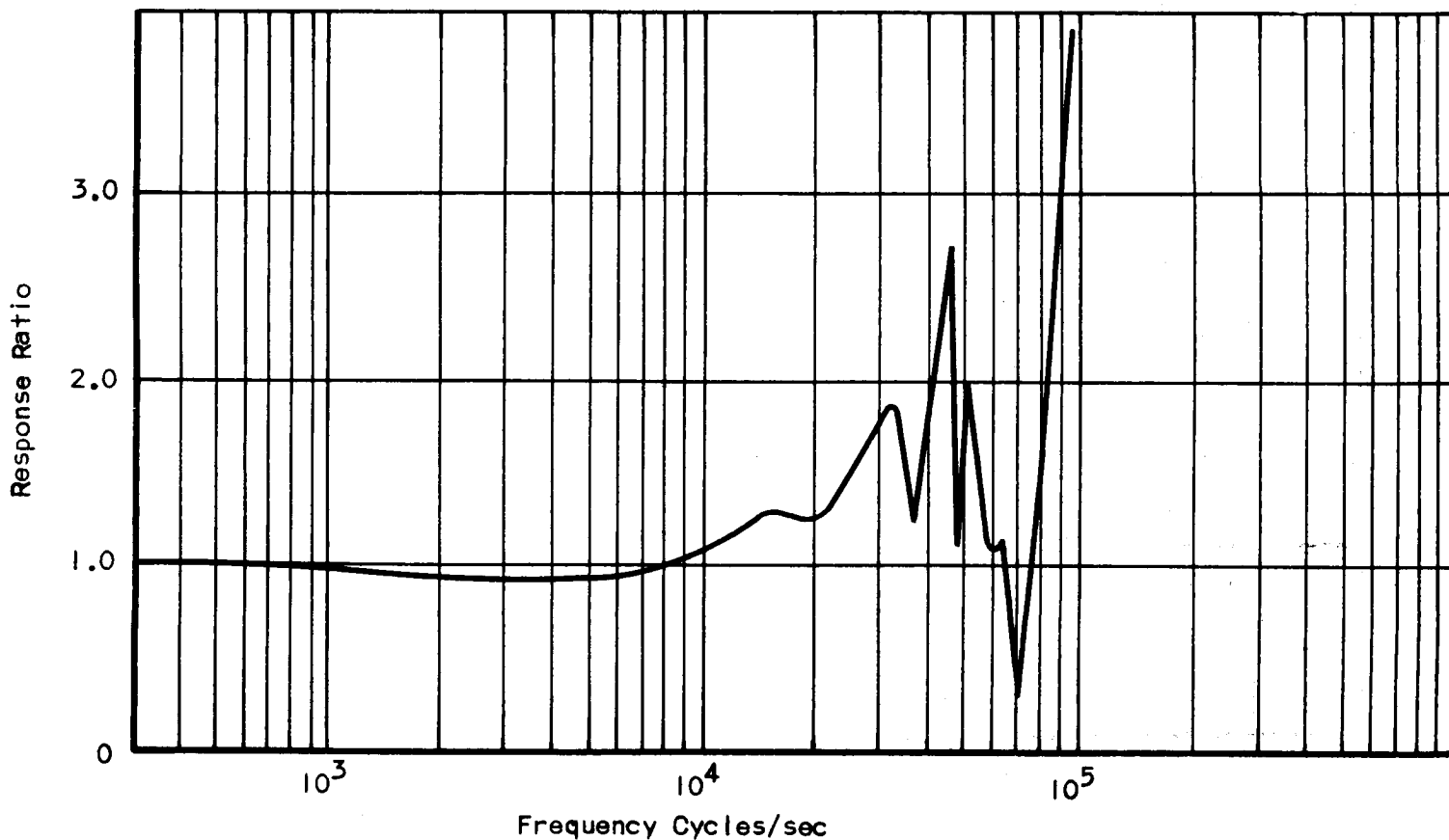
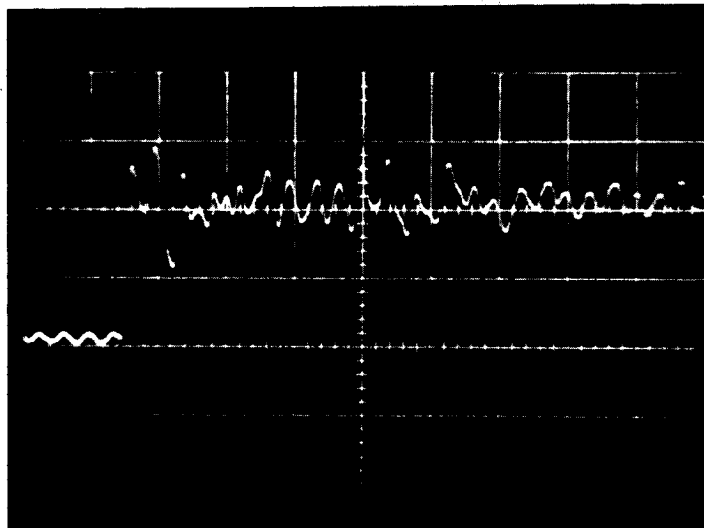
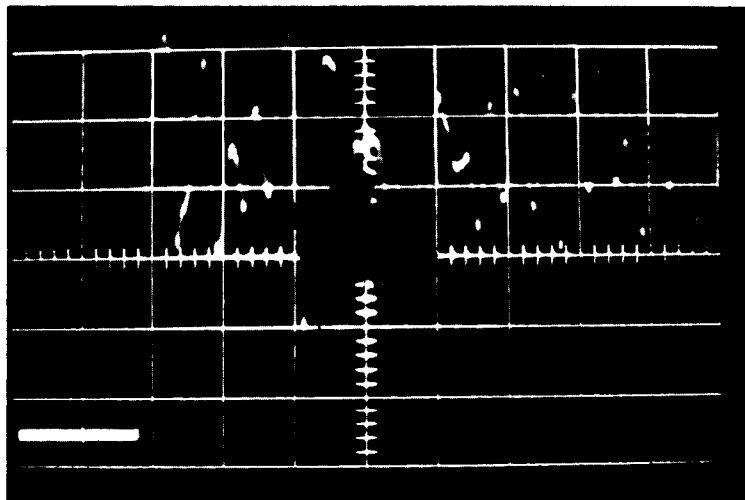


FIGURE 18

TRANSDUCER EVALUATION TEST

Model Kistler 601		Serial	Date October 1962
Type of Evaluation Shock Tube		Mounting End	Run No. 6
Test Conditions			
Test Sect. Press. $P_1 =$ in. HG (VAC) air			
Driver Sect. Press. $P_4 =$ PSI Helium			
Shock Wave Velocity $M_s =$	Sweep Speed 20/sec/cm		
Sensitivity			
Upper mv/cm	Lower mv/cm		
Natural Frequency 130,000cps	Damping Factor =		
Rise Time 3 μ sec	Type Analysis OSCAR-7090		
Remarks/Comments National Bureau of Standards. Shock Tube photograph for comparison with magnetic drum wave analyzer.			

Marks at bottom of graph indicate resonances found by magnetic drum

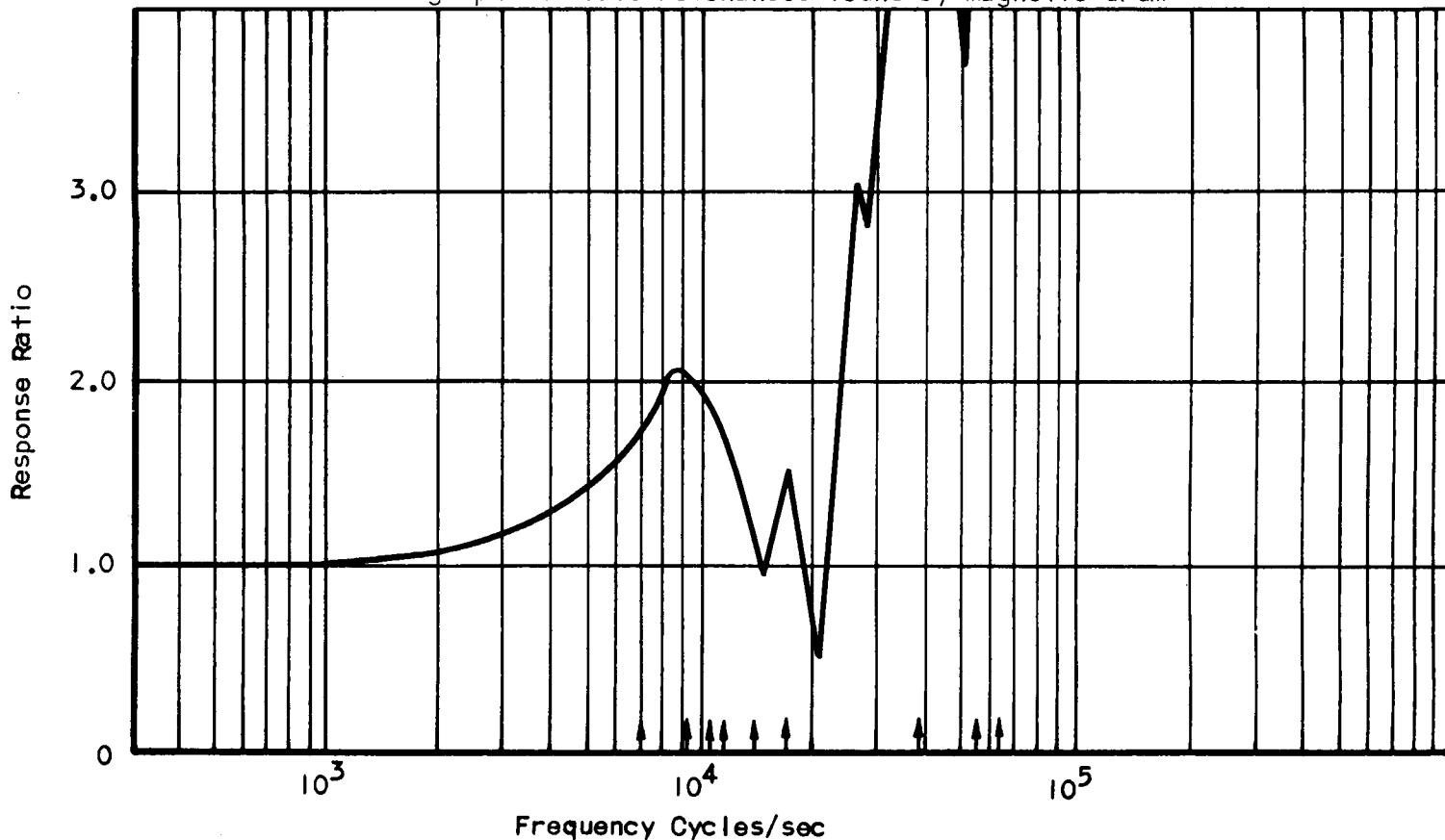
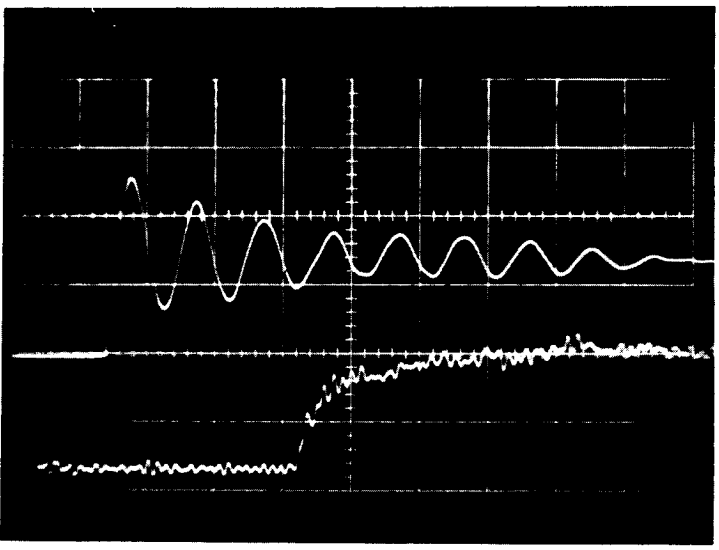


FIGURE 19

TRANSDUCER EVALUATION TEST

Model Dynisco PT49 AF-IM		Serial 10970	Date 13 March 1963
Type of Evaluation Shock Tube		Mounting End	Run No. 14
Test Conditions			
Test Sect. Press. $P_1 = 17$ in. HG (VAC) air			
Driver Sect. Press. $P_4 = 500$ PSIG Helium			
Shock Wave Velocity $M_s = 3.30$	Sweep Speed $50 \mu\text{sec/cm}$		
Sensitivity			
Upper 10 mv/cm	Lower 2000 mv/cm		
Natural Frequency 20,000 cps	Damping Factor $\delta = .040$		
Rise Time 11 μ sec	Type Analysis OSCAR-7090		
Remarks/Comments Lower trace is Kistler 601 monitor used in side			

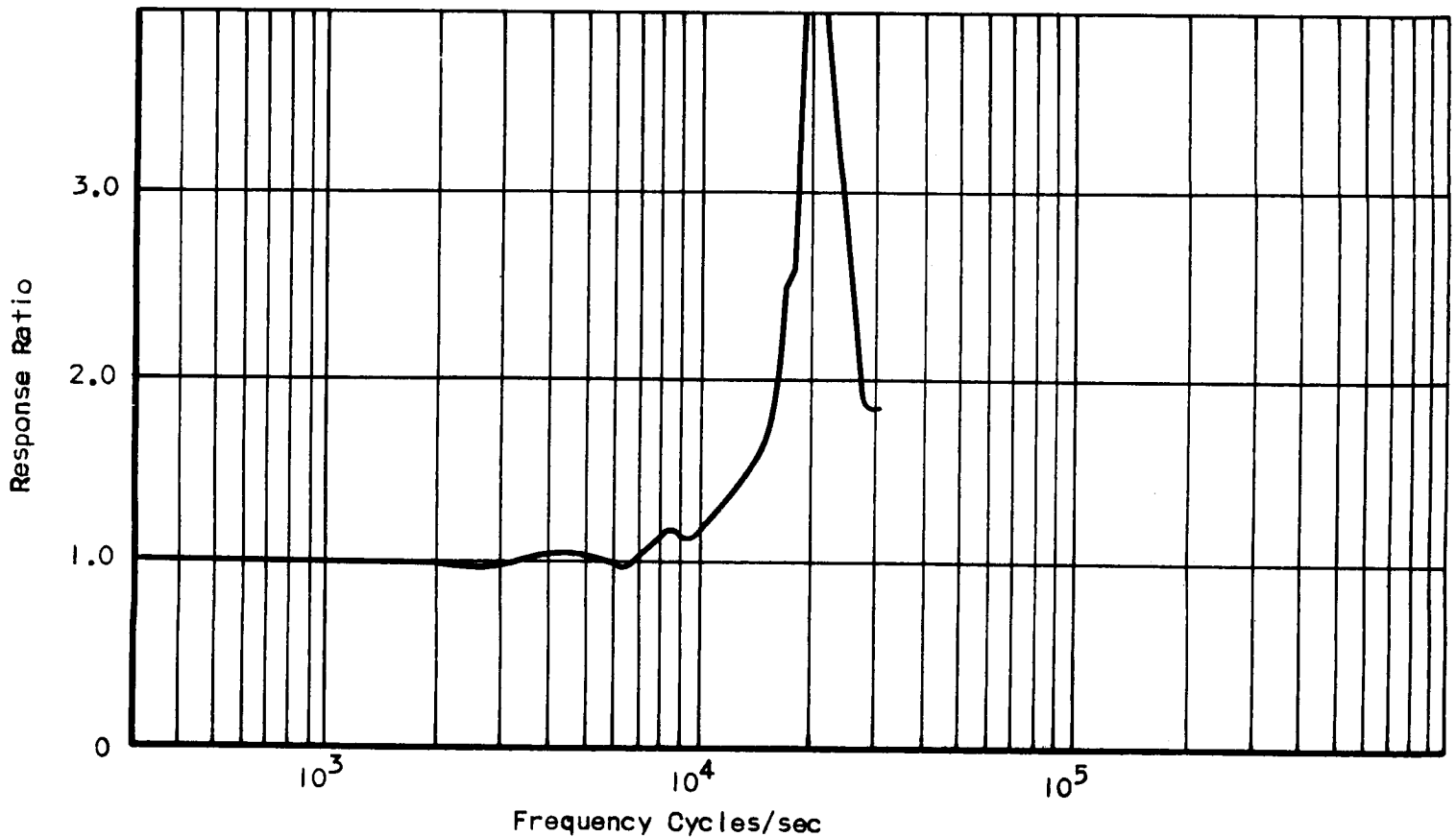


FIGURE 20

TRANSDUCER EVALUATION TEST

Model Elastronics EBL 6009	Serial 259	Date 17 April 1963
Type of Evaluation Shock Tube	Mounting End	Run No. 18
Test Conditions		
Test Sect. Press. $P_1 = 17$ in. HG (VAC) air		
Driver Sect. Press. $P_4 = 542$ PSIG Helium		
Shock Wave Velocity $M_s = 3.33$	Sweep Speed 20 μ sec/cm	
Sensitivity		
Upper 1000 mv/cm	Lower mv/cm	
Natural Frequency 57,000cps	Damping Factor $\delta = .031$	
Rise Time 4 μ sec	Type Analysis OSCAR-7090	
Remarks/Comments Type 21 Wide Band D.C. Dynaelectrometer		

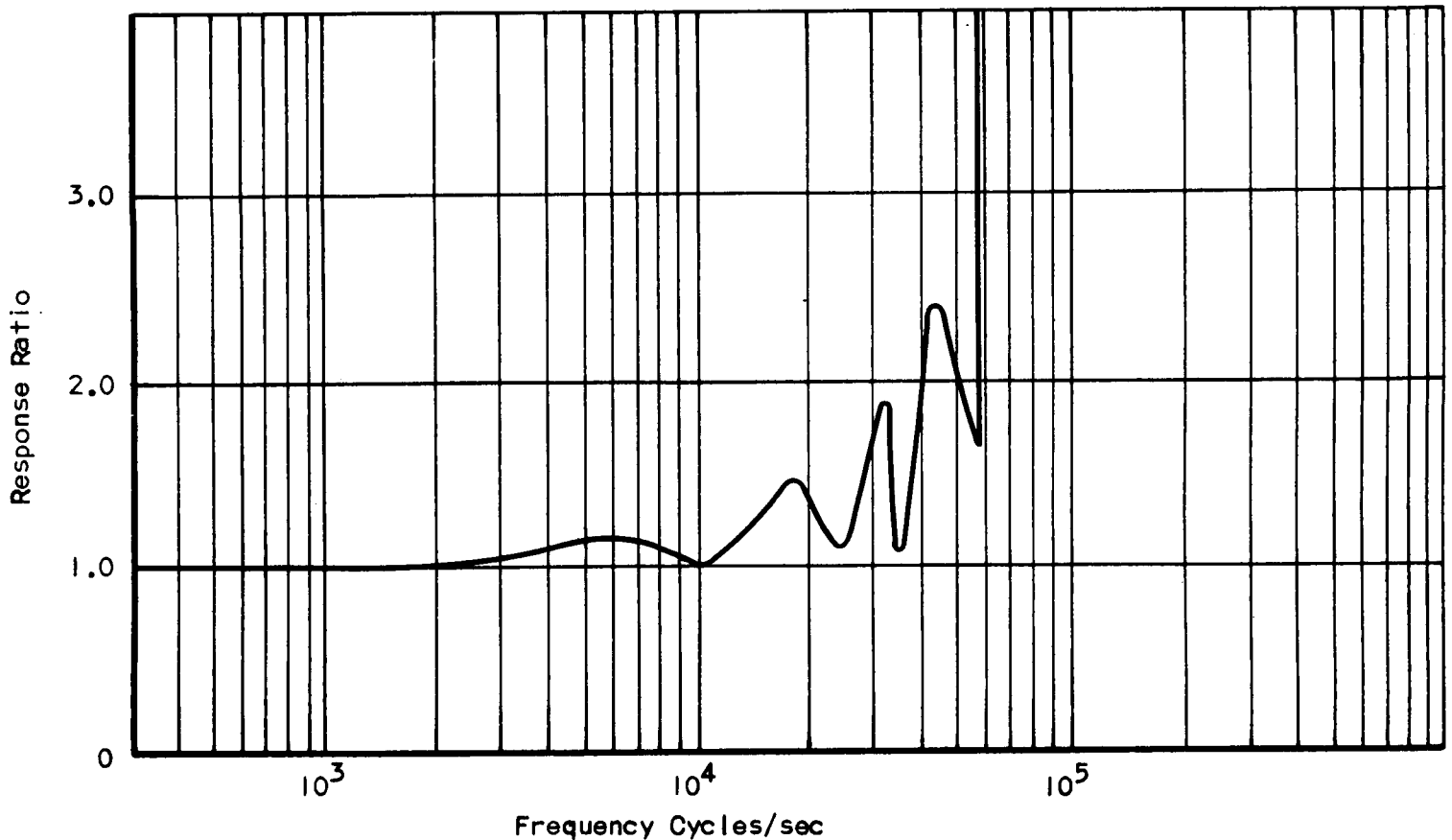
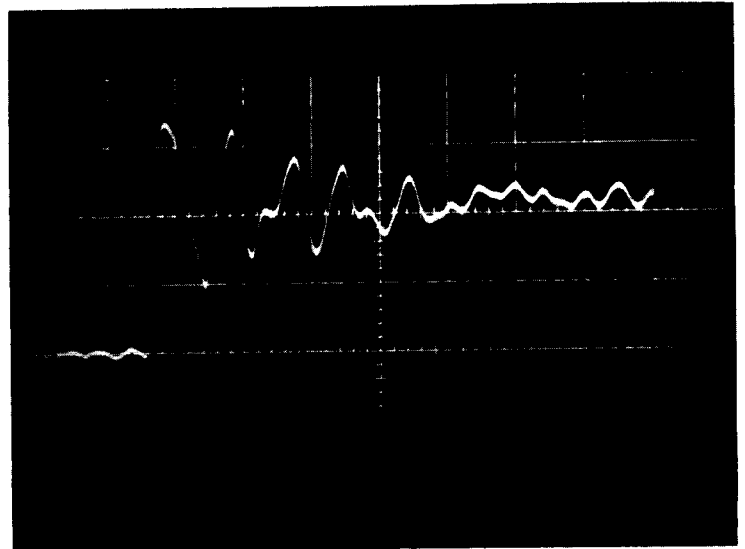
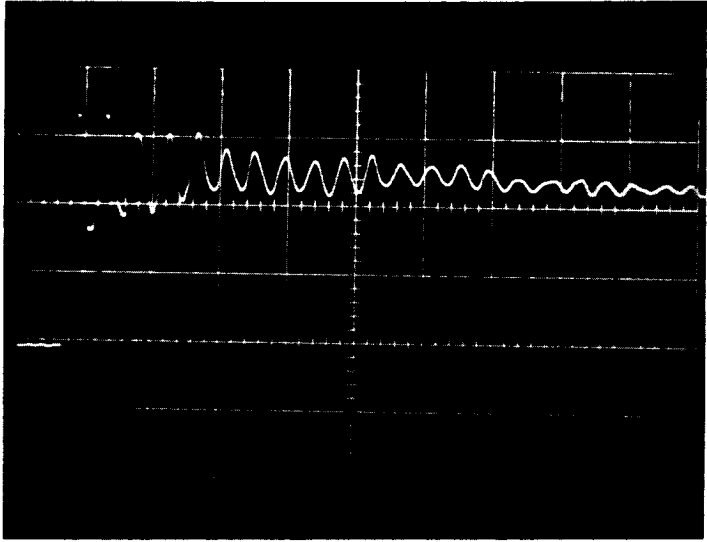


FIGURE 21

TRANSDUCER EVALUATION TEST

Model Dynisco PT76-1M		Serial 9375	Date 11 April 1963
Type of Evaluation Shock Tube		Mounting End	Run No. 23
Test Conditions			
Test Sect. Press. $P_1 = 17$ in. HG (VAC) air			
Driver Sect. Press. $P_4 = 540$ PSIG Helium			
Shock Wave Velocity $M_s = 3.37$	Sweep Speed $100 \mu \text{ sec/cm}$		
Sensitivity			
Upper 5 mv/cm	Lower mv/cm		
Natural Frequency 23,000 cps	Damping Factor $\zeta = .03$		
Rise Time 12 μ sec	Type Analysis OSCAR-7090		
Remarks/Comments			

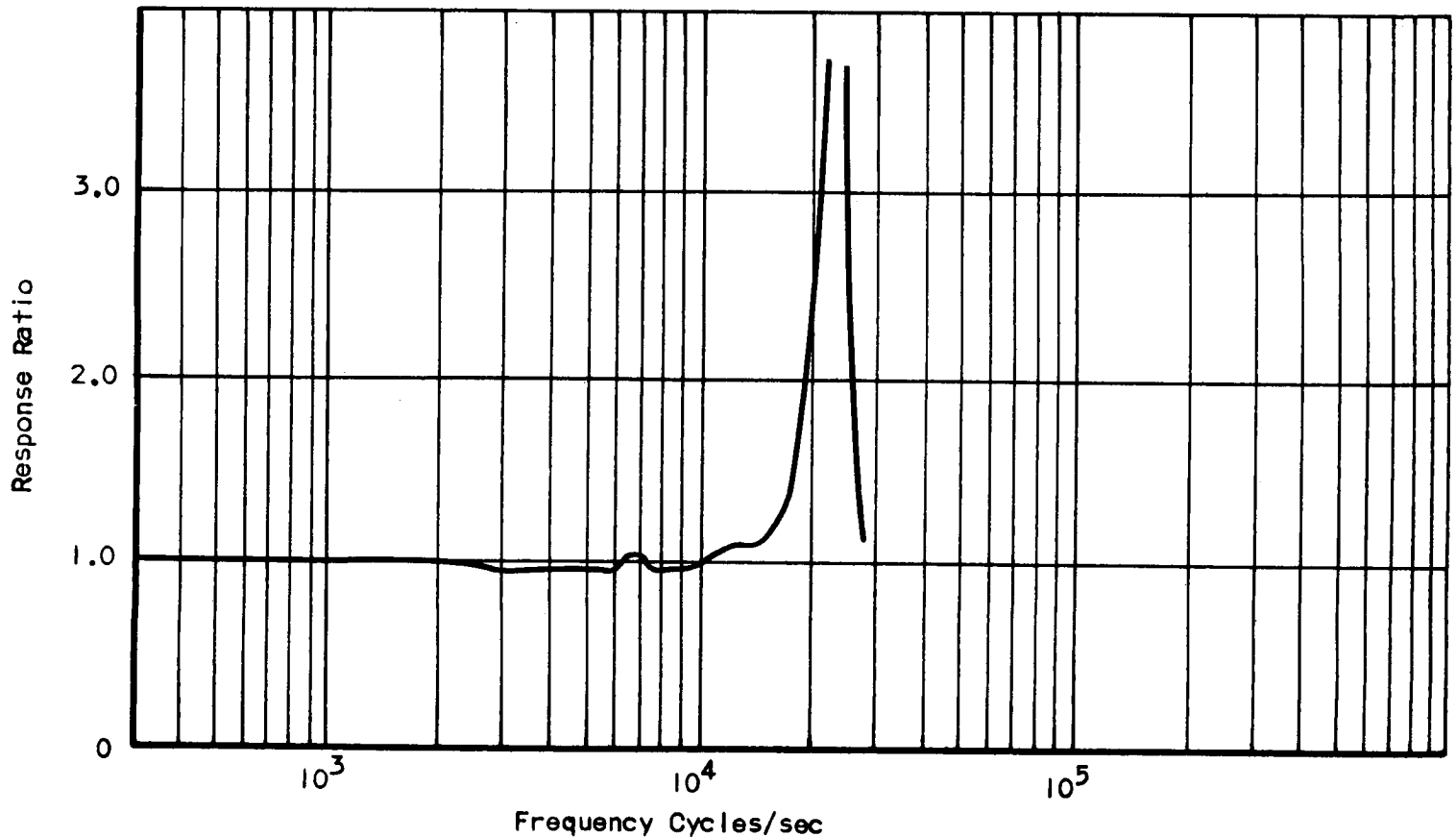
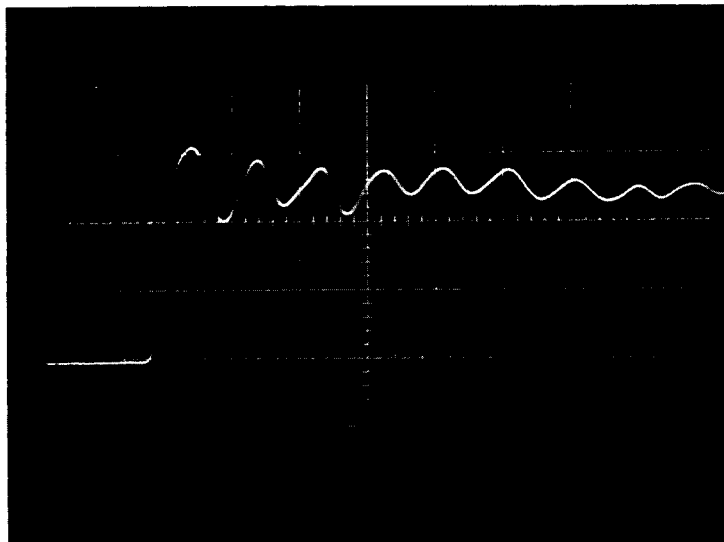


FIGURE 22

TRANSDUCER EVALUATION TEST

Model Photocon Model 755	Serial PRP6202	Date 17 April 1963
Type of Evaluation Shock Tube	Mounting End	Run No. 25
Test Conditions		
Test Sect. Press. $P_1 = 17$ in. HG (VAC) air		
Driver Sect. Press. $P_d = 512$ PSIG Helium		
Shock Wave Velocity $M_s = 3.22$	Sweep Speed 50 μ sec/cm	
Sensitivity		
Upper 1000 mv/cm	Lower mv/cm	
Natural Frequency 20,500 cps	Damping Factor $\delta = .028$	
Rise Time 15 μ sec	Type Analysis OSCAR-7090	
Remarks/Comments Dynagage D.G. 605 Amplifier used		

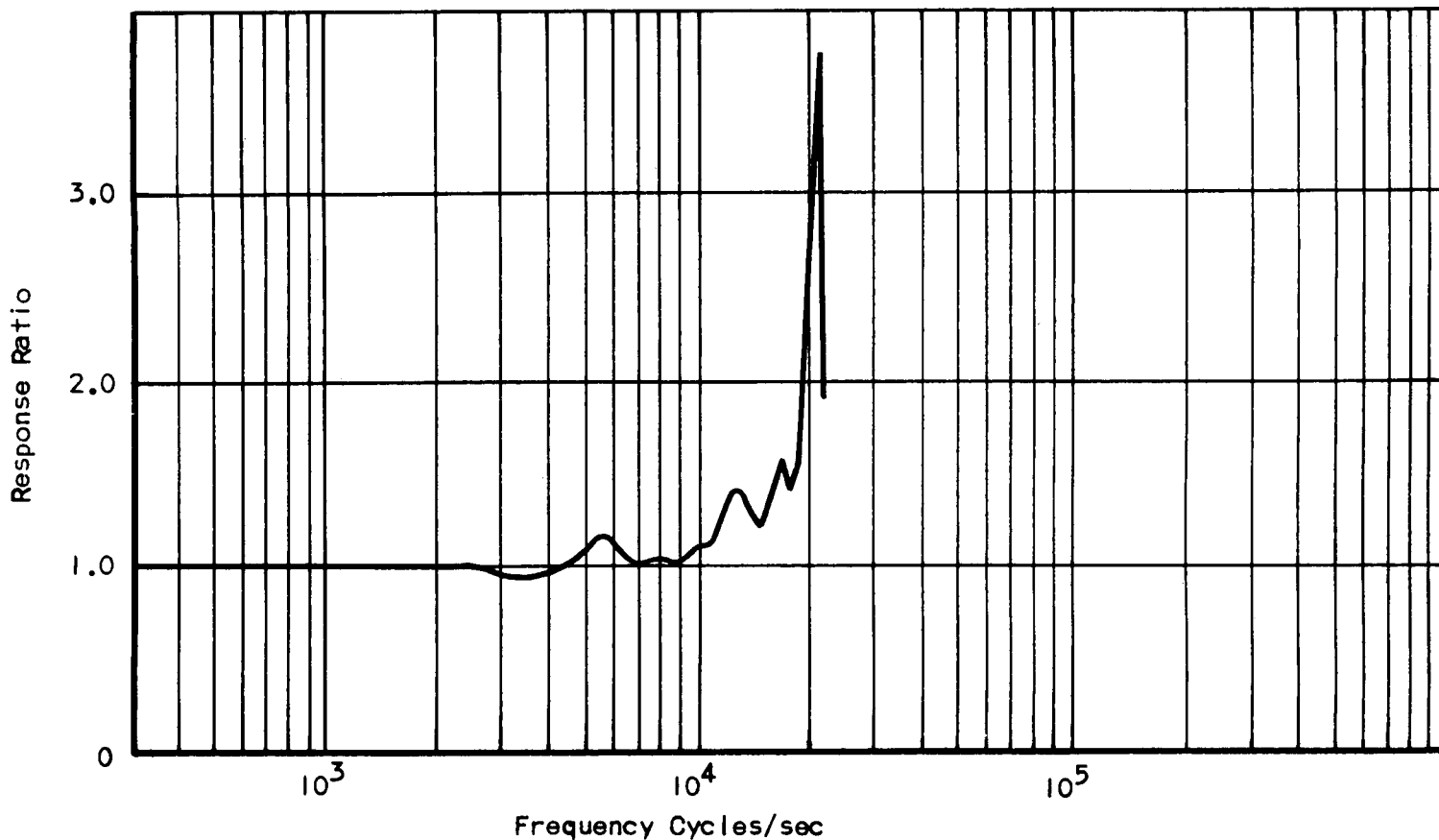
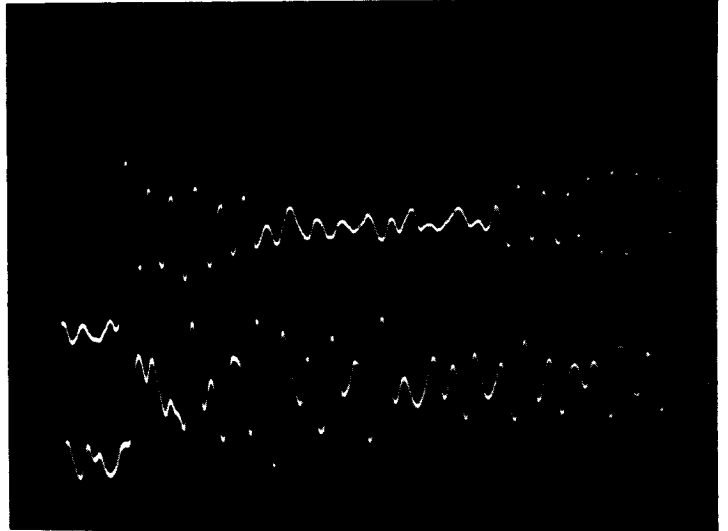


FIGURE 23

TRANSDUCER EVALUATION TEST

Model Kistler 601A		Serial 3467	Date 4 May 1963
Type of Evaluation Shock Tube		Mounting Side	Run No. 33/34
Test Conditions			
Test Sect. Press. $P_1 = 20.5 \text{ in. HG (VAC) air}$			
Driver Sect. Press. $P_4 = 530 \text{ PSIG Helium}$			
Shock Wave Velocity $M_s = 3.60$	Sweep Speed $20 \mu \text{ sec/cm}$		
Sensitivity			
Upper 500 mv/cm	Lower 500 mv/cm		
Natural Frequency 143,000 cps	Damping Factor $\zeta = .024$		
Rise Time $3 \mu \text{ sec}$	Type Analysis OSCAR-7090		
Remarks/Comments Kistler 601A used as monitor mounted diametrically opposite the test transducer.			

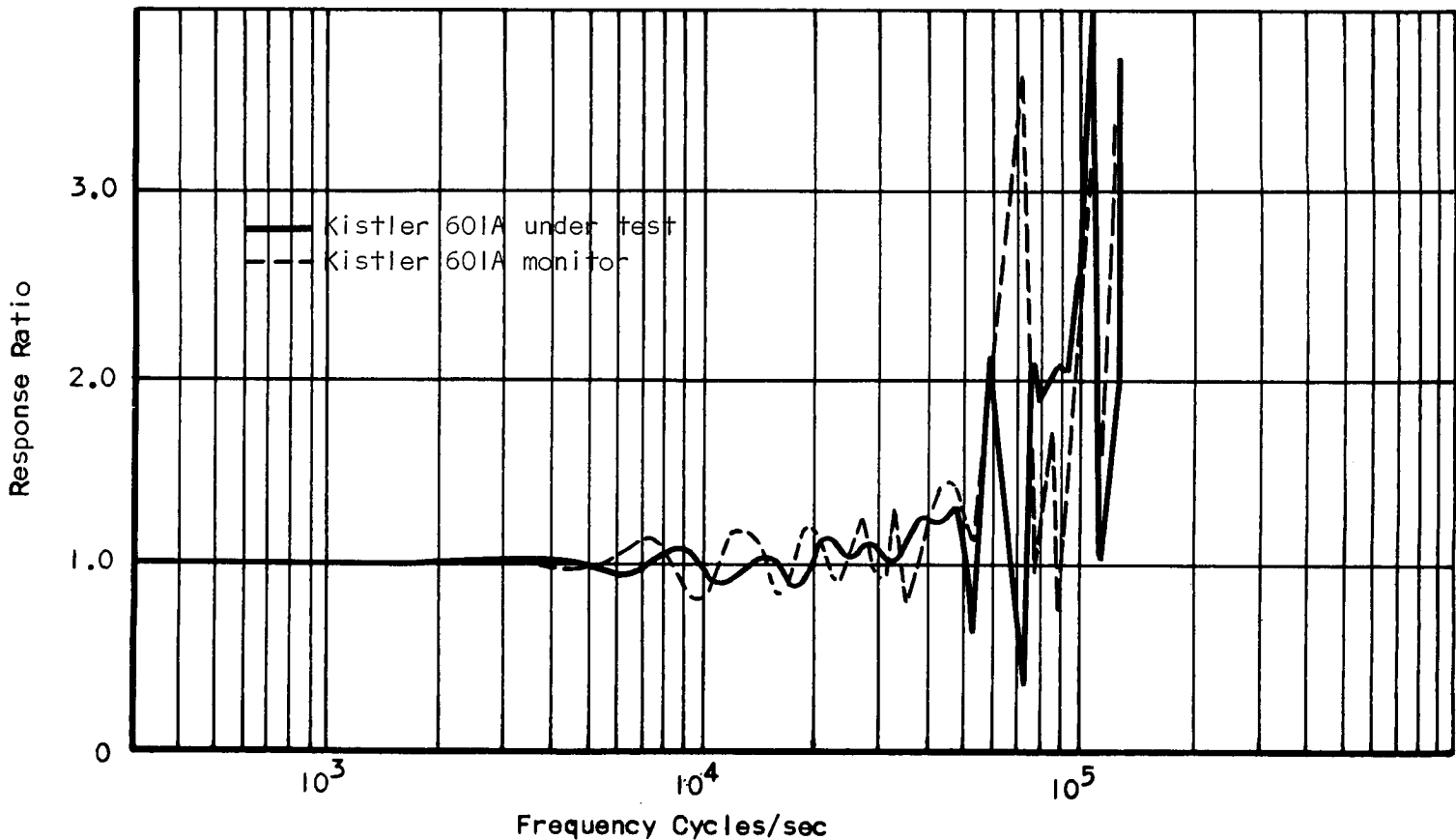


FIGURE 24

TRANSDUCER EVALUATION TEST

Model Kistler 603A	Serial 3484	Date 18 April 1963
Type of Evaluation Shock Tube	Mounting Side	Run No. 10
Test Conditions		
Test Sect. Press. $P_1 = 17$ in. HG (VAC) air		
Driver Sect. Press. $P_4 = 542$ PSIG Helium		
Shock Wave Velocity $M_s = 3.33$	Sweep Speed $20 \mu\text{sec/cm}$	
Sensitivity		
Upper 100 mv/cm	Lower mv/cm	
Natural Frequency 171,000 cps	Damping Factor $\delta = .009$	
Rise Time $2 \mu\text{sec}$	Type Analysis OSCAR-7090	
Remarks/Comments 566 Charge AMPL 10 mv/pcb		

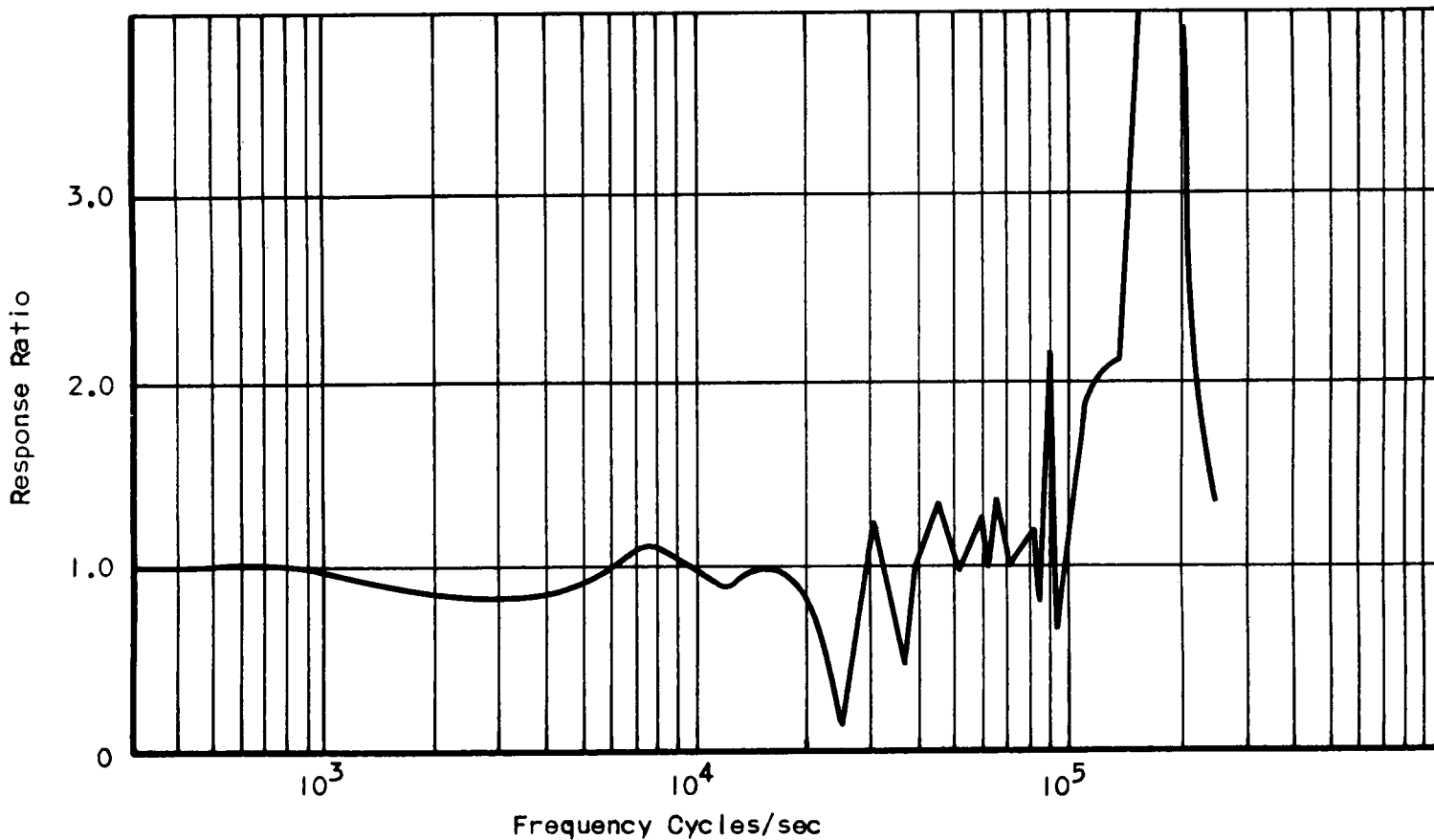
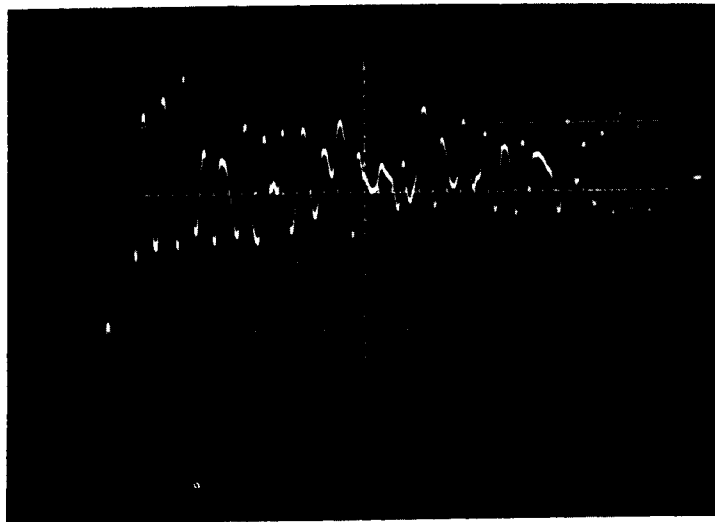
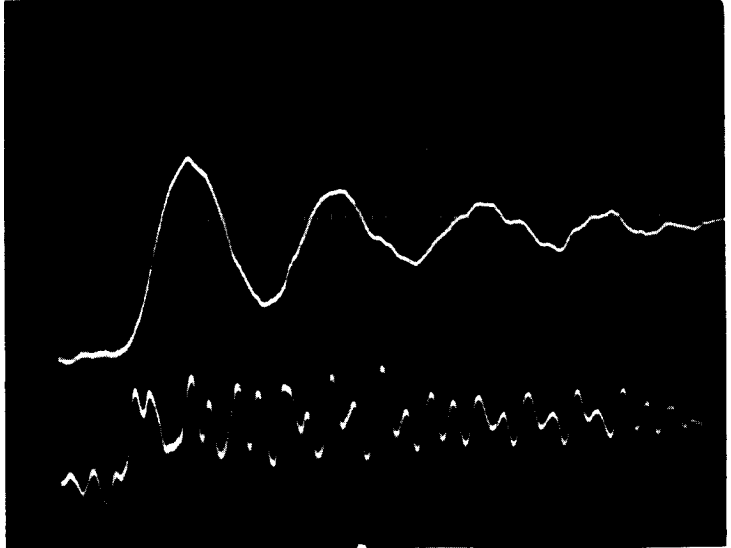


FIGURE 25

TRANSDUCER EVALUATION TEST

Model Dynisco PT49 AF-IM		Serial 9625	Date 4 May 1963
Type of Evaluation Shock Tube		Mounting Side	Run No. 31/32
Test Conditions			
Test Sect. Press. $P_1 = 20.5 \text{ in. HG (VAC) air}$			
Driver Sect. Press. $P_4 = 530 \text{ PSIG Helium}$			
Shock Wave Velocity $M_s = 3.60$	Sweep Speed 20.4 sec/cm		
Sensitivity			
Upper 1 mv/cm	Lower 500 mv/cm		
Natural Frequency 22,800cps	Damping Factor $\delta = .075$		
Rise Time 10.4 sec	Type Analysis OSCAR-7090		
Remarks/Comments Kistler 601A used as monitor, mounted in side diametrically opposite Dynisco			

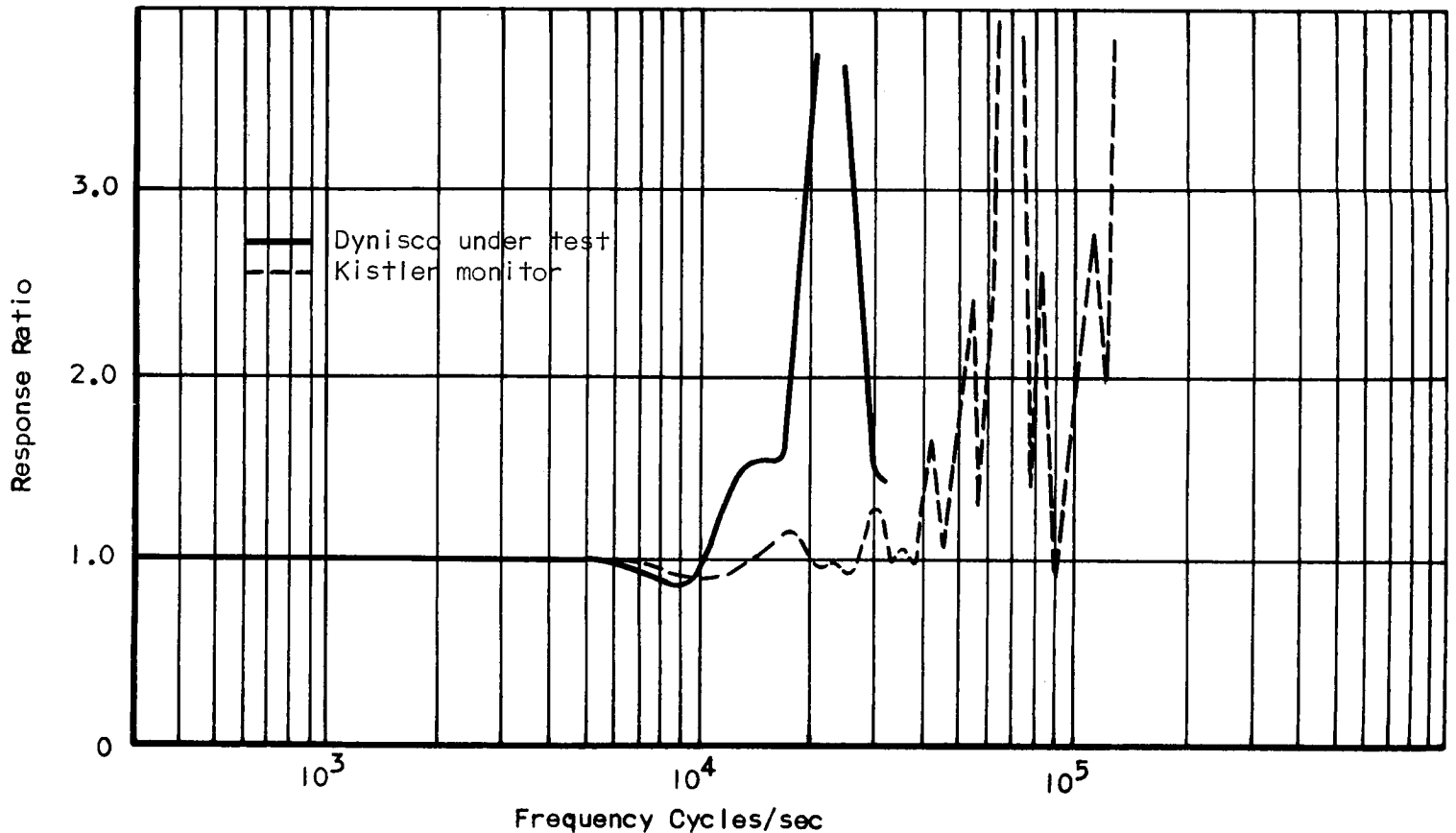
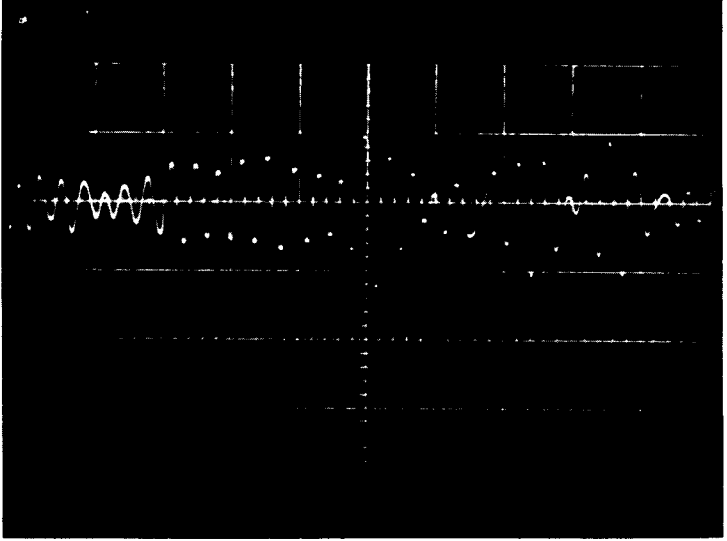


FIGURE 26

TRANSDUCER EVALUATION TEST

Model Kistler 601A		Serial 3037	Date 4 March 1963
Type of Evaluation Shock Tube Ground Shock		Mounting End - Behind 1/4" Plate	Run No. 7
Test Conditions			
Test Sect. Press. $P_1 = 17$ in. HG (VAC) air			
Driver Sect. Press. $P_4 = 518$ PSIG Helium			
Shock Wave Velocity $M_5 = 3.33$	Sweep Speed 20 sec/cm		
Sensitivity			
Upper 50 mv/cm	Lower mv/cm		
Natural Frequency 147,000 cps	Damping Factor =		
Rise Time sec	Type Analysis OSCAR-7090		
Remarks/Comments Shock Wave Impacts at 2 cm			

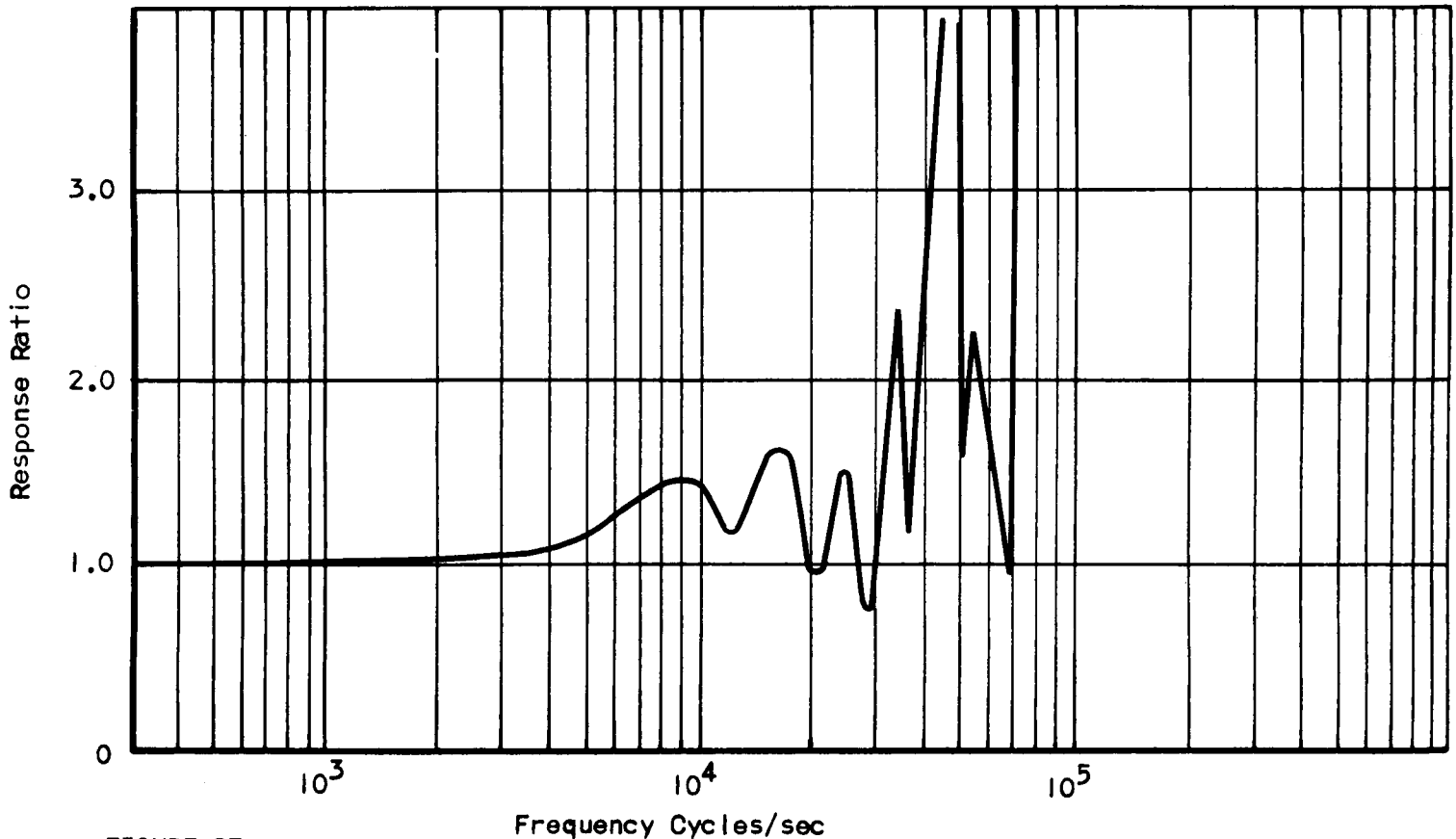
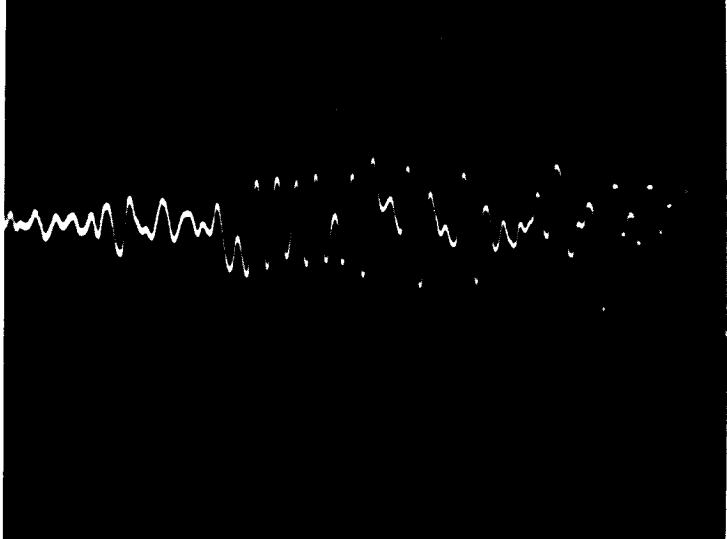


FIGURE 27

TRANSDUCER EVALUATION TEST

Model Kistler 603A		Serial 3484	Date 10 April 1963
Type of Evaluation Shock Tube Ground Shock		Mounting End - Behind 1/4" Plate	Run No. 11
Test Conditions			
Test Sect. Press. $P_1 = 17$ in. HG (VAC) air			
Driver Sect. Press. $P_4 = 520$ PSIG Helium			
Shock Wave Velocity $M_s = 3.34$	Sweep Speed $20 \mu\text{sec/cm}$		
Sensitivity			
Upper 50 mv/cm	Lower mv/cm		
Natural Frequency 183,000 cps	Damping Factor =		
Rise Time sec	Type Analysis OSCAR-7090		
Remarks/Comments Shock Wave Impacts at 3 cm			

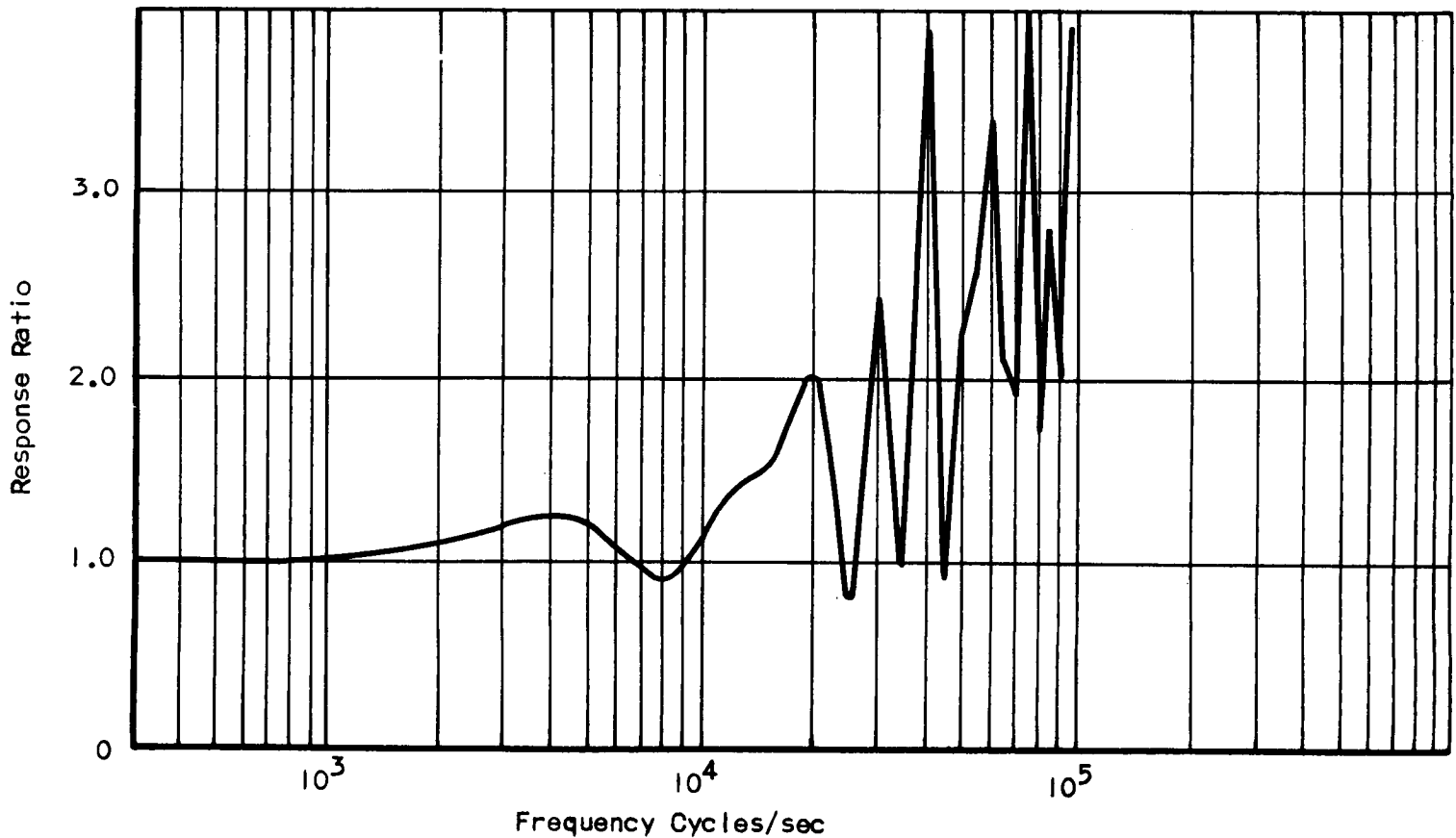
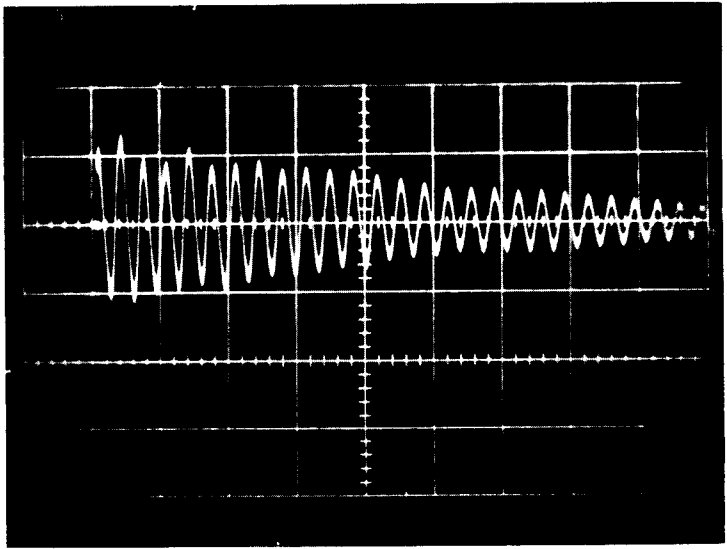


FIGURE 28

TRANSDUCER EVALUATION TEST

Model Kistler 601A		Serial 3037	Date 1 March 1963
Type of Evaluation Ball Drop		Mounting	Run No. 3
Test Conditions			
Test Sect. Press. $P_1 =$ in. HG (VAC) air			
Driver Sect. Press. $P_4 =$ PSI Helium			
Shock Wave Velocity $M_s =$	Sweep Speed 20 μ sec/cm		
Sensitivity			
Upper 500 mv/cm	Lower mv/cm		
Natural Frequency 145,000 cps	Damping Factor $\delta = .0085$		
Rise Time sec	Type Analysis Graphical-7090		
Remarks/Comments 566 Charge Amplifier 10 mv/pcb			

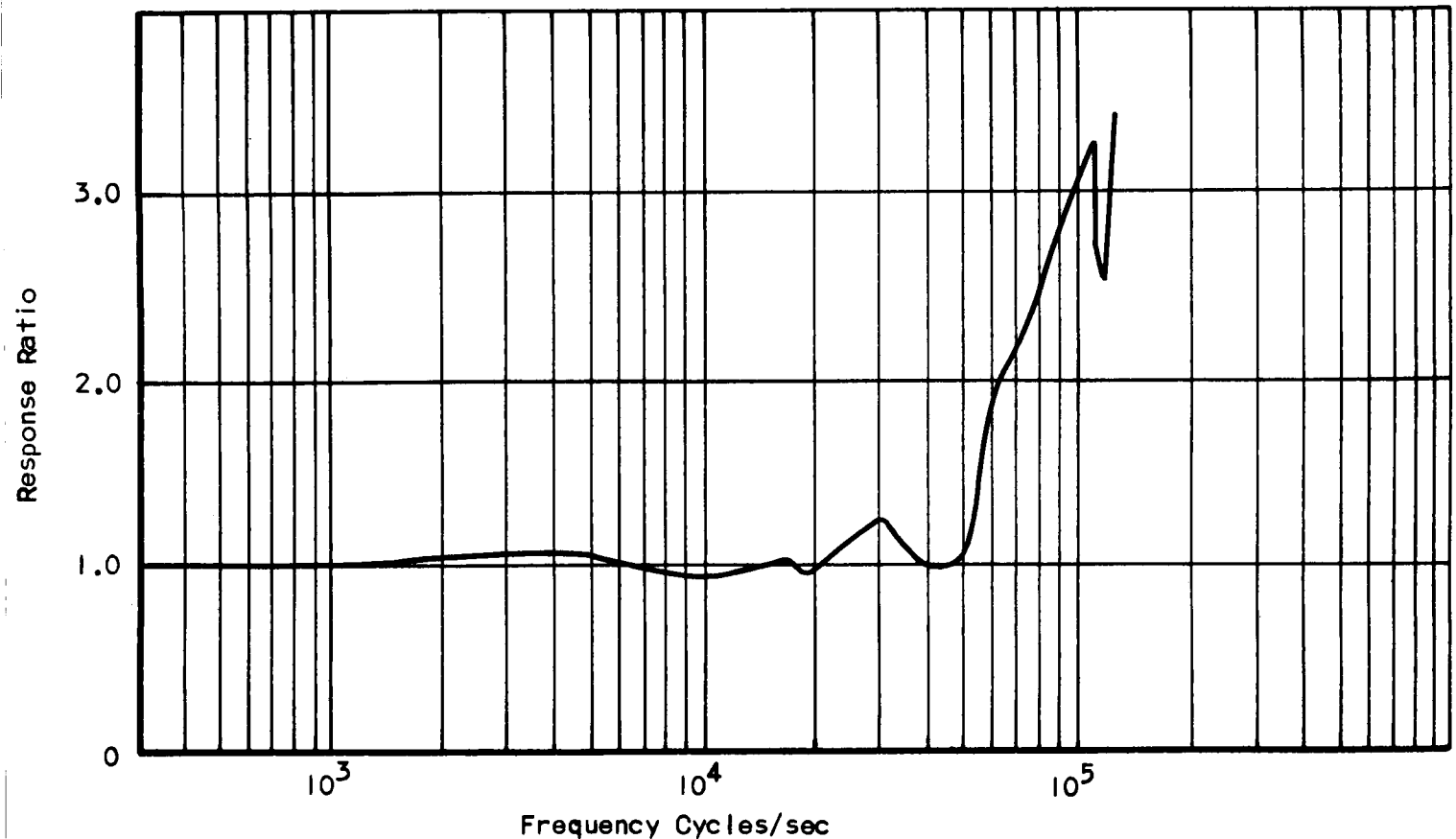
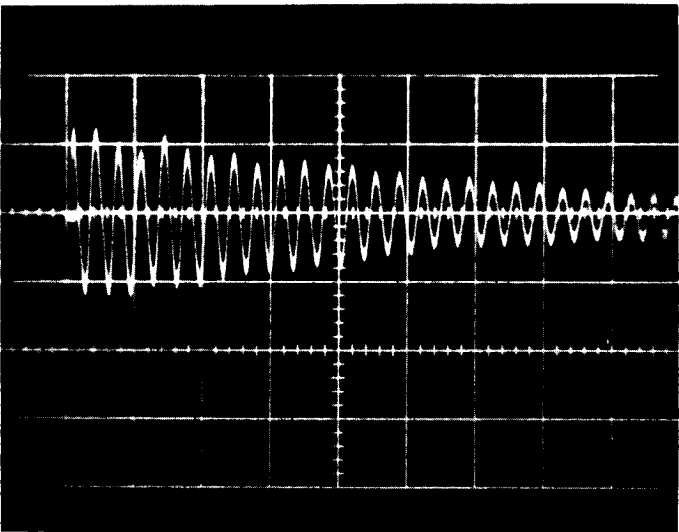


FIGURE 29

TRANSDUCER EVALUATION TEST

Model Kistler 601A		Serial 3037	Date 1 March 1963
Type of Evaluation Ball Drop		Mounting	Run No. 15
Test Conditions			
Test Sect. Press. $P_1 =$ in. HG (VAC) air			
Driver Sect. Press. $P_4 =$ PSI Helium			
Shock Wave Velocity $M_s =$	Sweep Speed 200 μ sec/cm		
Sensitivity			
Upper 500 mv/cm	Lower mv/cm		
Natural Frequency 145,000 cps	Damping Factor $\delta = .0078$		
Rise Time sec	Type Analysis OSCAR-7090		
Remarks/Comments 566 Charge Amplifier 10 mv/pcb			

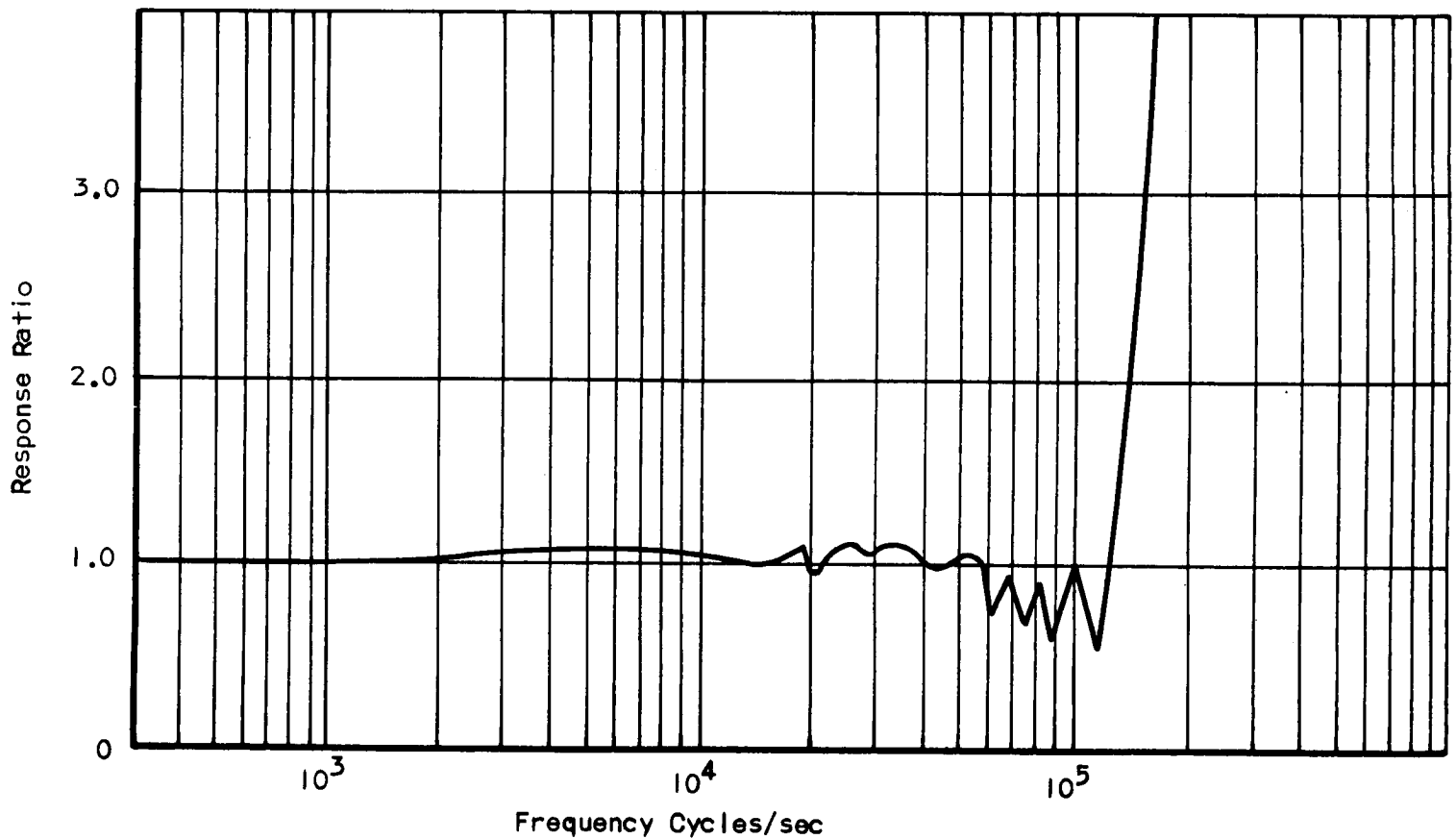


FIGURE 30

TRANSDUCER EVALUATION TEST

Model Elastronics EBL 6009	Serial 259	Date 17 April 1963
Type of Evaluation Ball Drop	Mounting	Run No. 19
Test Conditions		
Test Sect. Press. $P_1 =$ in. HG (VAC) air		
Driver Sect. Press. $P_4 =$ PSI Helium		
Shock Wave Velocity $M_s =$		Sweep Speed 20 μ sec/cm
Sensitivity		
Upper 100 mv/cm	Lower mv/cm	
Natural Frequency 63,000 cps	Damping Factor $\delta = .027$	
Rise Time sec	Type Analysis OSCAR-7090	
Remarks/Comments		

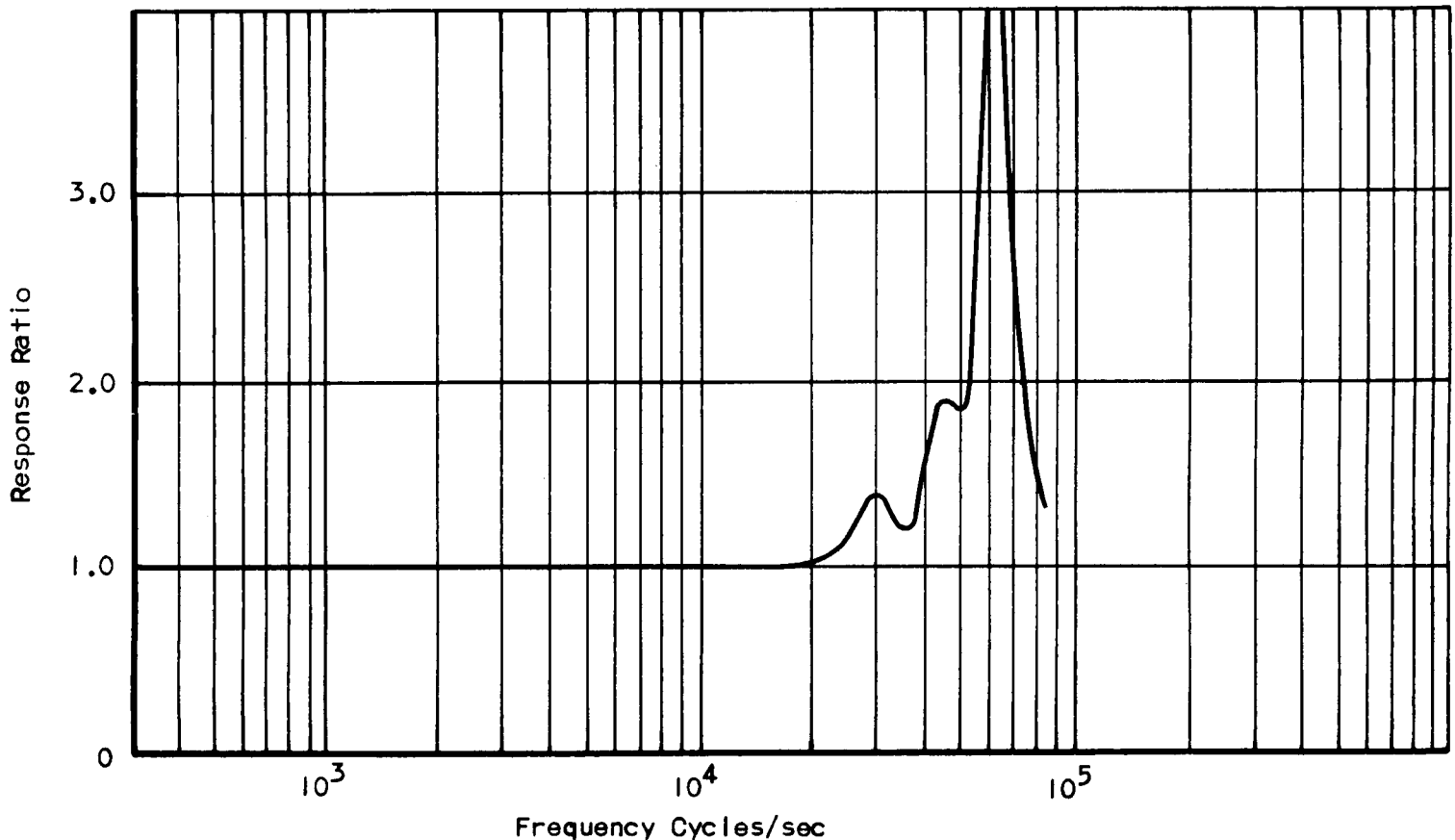
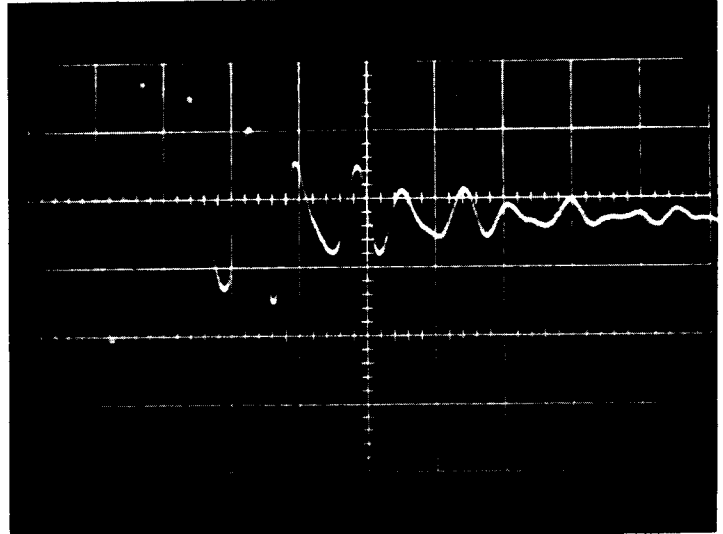
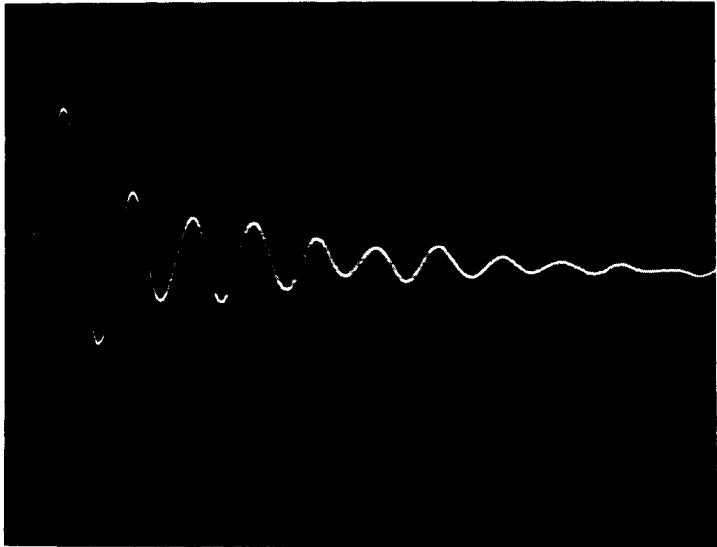


FIGURE 31

TRANSDUCER EVALUATION TEST

Model Photocon PRP 6202		Serial Mod. 755	Date 7 April 1963
Type of Evaluation Ball Drop		Mounting	Run No. 29
Test Conditions			
Test Sect. Press. $P_1 =$ in. HG (VAC) air			
Driver Sect. Press. $P_4 =$ PSI Helium			
Shock Wave Velocity $M_s =$	Sweep Speed 50 μ sec/cm		
Sensitivity			
Upper 200mv/cm	Lower mv/cm		
Natural Frequency 22,000 cps	Damping Factor $\delta = .087$		
Rise Time sec	Type Analysis OSCAR-7090		
Remarks/Comments			

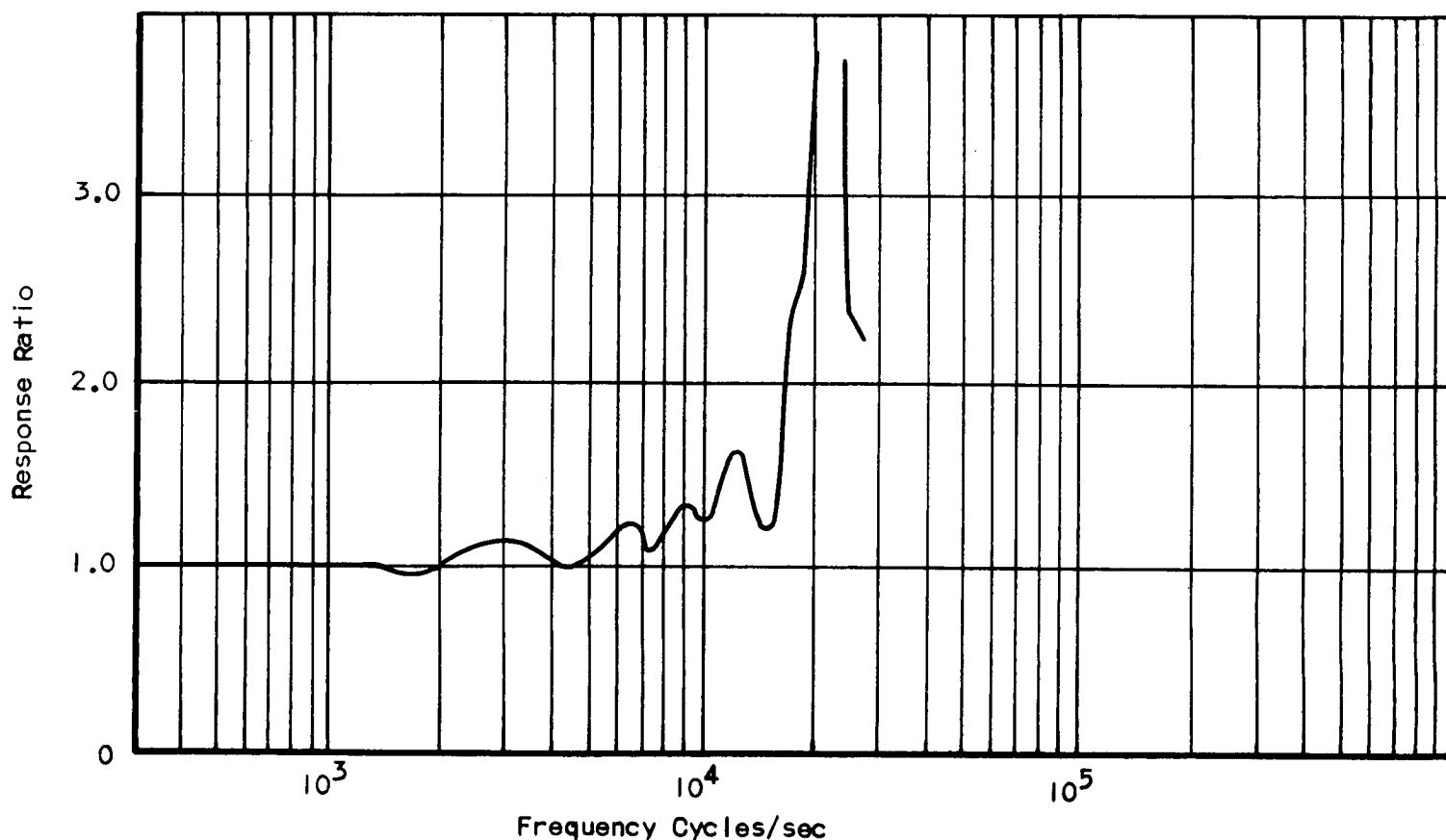
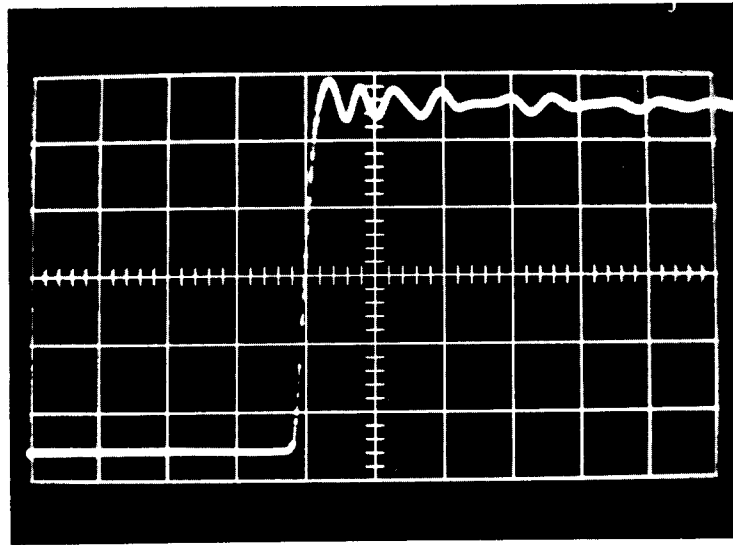
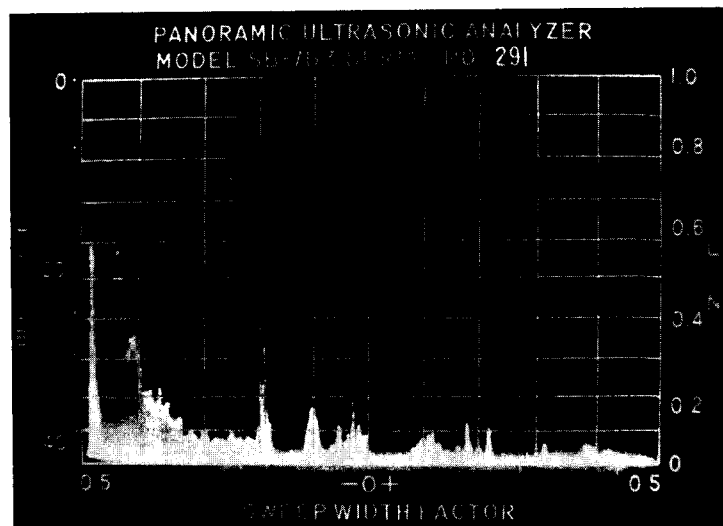


FIGURE 32

KISTLER 601 TRANSDUCER EVALUATION
BY NATIONAL BUREAU OF STANDARDS



Pneumatic step function generator test of Kistler 601 transducer (sweep 2 msec/cm, step is 49.7 psi)



Magnetic wave drum recorder analysis of Kistler 601 transducer

FIGURE 33a

FIGURE 33b

$M_s = 3.60$. The average maximum amplitude of the ground shock was one-tenth as strong as the average maximum amplitude of a side-mounted transducer (See Figures 27 and 28).

The ball drop technique of transducer excitation, which is explained in detail in Appendix C was utilized to verify the shock tube results and to aid in selecting a transducer suitable for use as monitor in the sinusoidal pressure generator. An evaluation of the transducers tested in this manner is included in Figures 29 through 32 which show the natural frequency, damping, and frequency response curves.

Figures 19 and 33 include evaluations of a Kistler 601 transducer obtained for this program by the National Bureau of Standards. This transducer was tested in the Bureau of Standards pneumatic pressure function generator and shock tube. The shock tube run was analyzed by magnetic drum wave analyzer. Analysis of this same shock tube run was also performed by the optical scanner and IBM 7090 computer. These results are depicted in Figure 19.

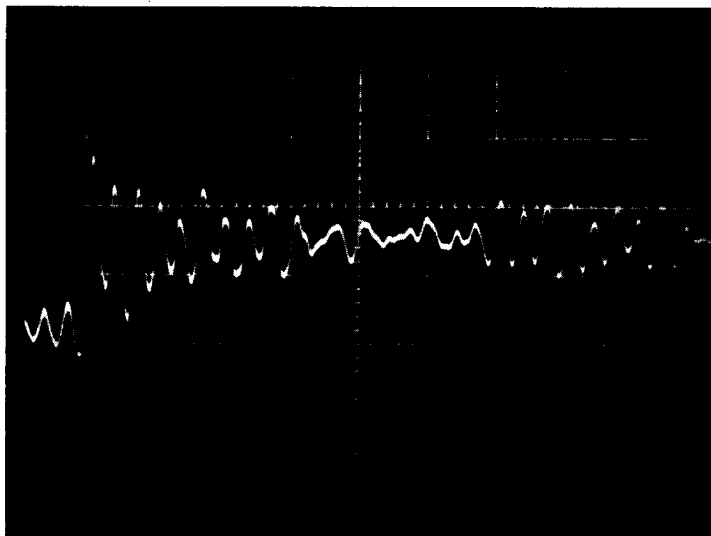
Dual end-mounted and dual side-mounted shock tube tests were conducted. A flange was constructed which enabled the side-by-side end mount testing of a Kistler transducer and almost any other flush diaphragm transducer used in rocket motor testing. A shock tube was constructed which was capable of mounting two transducers directly opposite each other for side mount testing (See Figure 10). Results of these shock tube runs may be seen in Figures 24 and 26.

During the course of this program it was found that ground shock, which may be seen prior to the incident wave hitting the diaphragm, was considerably decreased if a rubber or plastic "O" ring seal were used in preference to a copper or brass gasket type seal.

This effect may be seen in Figure 34.

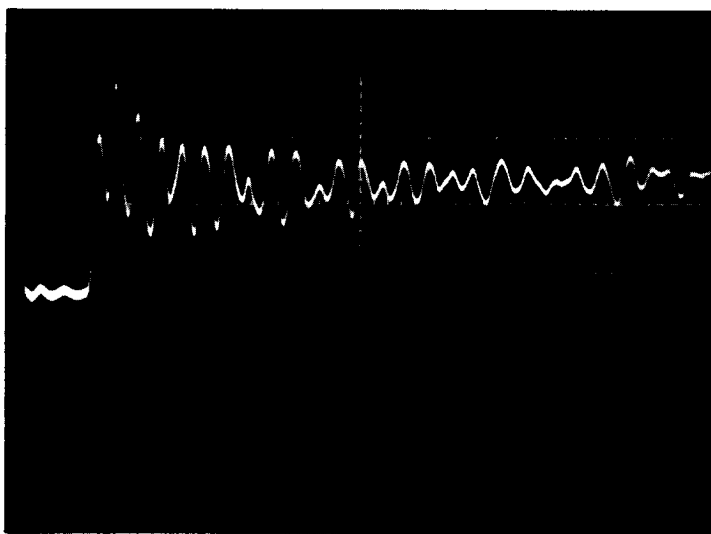
A Kistler 601A was mounted in such a way that it could be extended into the side of the shock tube or recessed within the side wall. A survey varying the transducer position from protruding $1/16"$ from the sidewall in increments of $1/32"$ to recessed $1/16"$ within the side wall showed no noticeable difference in ground shock, natural frequency, damping, and rise time.

KISTLER 601A SIDE MOUNT TESTS
COMPARISON OF COPPER AND PLASTIC SEALS



Kistler 601A installed in side using copper gasket side between adaptor and shock tube (sweep 20 μ sec/cm, sensitivity 500 mv/cm, 566 charge amplifier at 10 mv/pcb)

FIGURE 34a



Kistler 601A installed in side using plastic "O" ring seal between adaptor and shock tube (sweep 20 μ sec/cm, sensitivity 500 mv/cm, 566 charge amplifier at 10 mv/pcb)

FIGURE 34b

IV. THE PRINCETON SINUSOIDAL PRESSURE GENERATOR

A. Purpose and Objectives

The purpose of this work was to investigate the Princeton Sinusoidal Pressure Generator (SPG), its methods of operation, and to demonstrate its practical value as a rapid, relatively simple, and accurate test device for various types of transient pressure measuring transducers.

In order to accomplish this and to understand more completely the principles of the SPG, it was necessary to develop a theoretical model. From this model the relationship of some of the geometric features and operating conditions could be determined. Further relationships between these and average and peak-to-peak pressure fluctuations in the chamber could also be derived. These relationships could be useful in determining the results of changes in operating conditions or geometry, and similarly, they could indicate what changes to make in order to achieve desired conditions in the chamber.

Another objective was to investigate chamber resonant conditions and chamber response. Much of this work would be an extension of the work reported by Carwile in Princeton University Aeronautical Engineering Report No. 595-d, although the approach would be somewhat different.

The last major objective was to test various types of transient pressure measuring transducers on the SPG in order to determine the practicality of the SPG as a test device for these transducers.

During the course of the testing, it was expected that operating techniques would be improved, and that the SPG itself would be improved. Improvements would be desirable in the following

areas:

1. Higher average chamber pressures.
2. Higher peak-to-peak pressure fluctuations especially at the higher end of the frequency range.
3. More accurate results.
4. More economical operation.

B. Theory

1. Resonant Modes of the Chamber

The standing waves in a cylindrical chamber, such as that found on the SPG, may be determined from the wave equation written in cylindrical coordinates (Ref. 6,37):

$$\frac{1}{c^2} \frac{\partial^2 p}{\partial t^2} = \frac{1}{r} \frac{\partial}{\partial r} \left(r \frac{\partial p}{\partial r} \right) + \frac{1}{r^2} \frac{\partial^2 p}{\partial \theta^2} + \frac{\partial^2 p}{\partial z^2} \quad (1)$$

The solution to this equation, with appropriate boundary conditions, yields an expression for the frequency of standing waves in a cylinder (Ref. 6)

$$\nu = \frac{c}{2} \sqrt{\left(\frac{n_z}{L}\right)^2 + \left(\frac{\alpha_{mn}}{a}\right)^2} \quad (2)$$

Thus, for a given resonant mode in a given chamber, the frequency will depend on the velocity of sound in the medium filling the chamber. Values for n_z and α_{mn} for various resonant modes are given in Ref. 6 and 38.

Therefore, if the chamber dimensions are known, and the speed of sound in the chamber medium is known, the theoretical frequency for any resonant mode is easily calculated. Resonant modes are identified as "radial," "tangential," or "longitudinal," depending on their

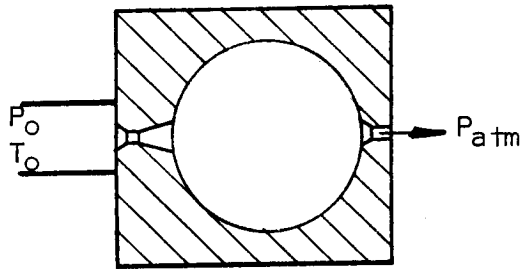
relationship to the cylindrical axis. For a flat chamber the longitudinal mode cannot be excited. The pressure patterns of various transverse modes are shown on Figure 35.

A more detailed development of the above theory can be found in Reference 6.

2. Chamber Pressure

a. Average chamber pressure

In order to develop the ideal theory for average chamber pressure, a simple model of the SPG chamber will be constructed. Consider a cylindrical chamber with inlet and outlet as shown below.



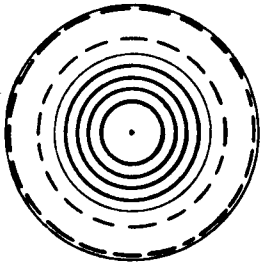
The following assumptions are made:

- (1) Perfect gas laws apply
- (2) Flow up to the inlet throat is isentropic
- (3) Flow from the chamber to the outlet throat is isentropic
- (4) The flow is adiabatic throughout
- (5) The flow is choked at the inlet and outlet

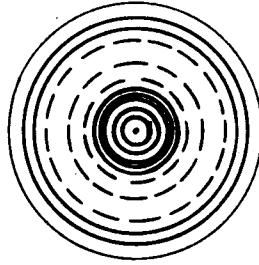
With these assumptions, mass flow rate into the chamber may be conveniently expressed as the mass flow at the inlet throat, and will be a function of reservoir conditions and inlet throat area only (Ref. 29).

$$\dot{m}_{in} = \sqrt{\frac{\gamma g}{R}} \sqrt{\frac{P_o}{T_o}} \left(\frac{2}{\gamma+1} \right)^{\frac{\gamma+1}{2(\gamma-1)}} A_{in} \quad (3)$$

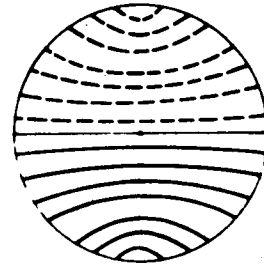
---NEGATIVE PRESSURE — POSITIVE PRESSURE



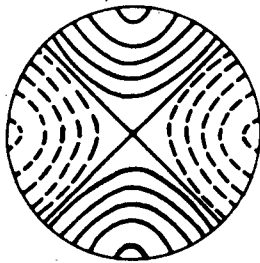
$\alpha_{01} = 1.2197$
FIRST RADIAL



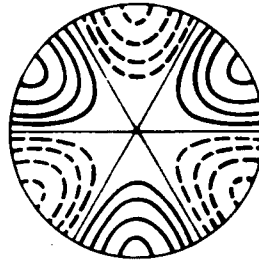
$\alpha_{02} = 2.2331$
SECOND RADIAL



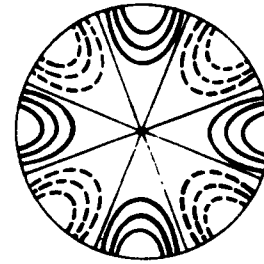
$\alpha_{10} = 0.5861$
FIRST TANGENTIAL



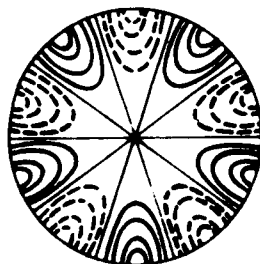
$\alpha_{20} = 0.9722$
SECOND TANGENTIAL



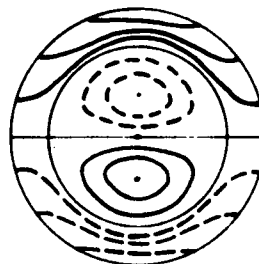
$\alpha_{30} = 1.3373$
THIRD TANGENTIAL



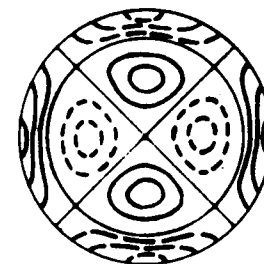
$\alpha_{40} = 1.6926$
FOURTH TANGENTIAL



$\alpha_{50} = 2.0421$
FIFTH TANGENTIAL



$\alpha_{11} = 1.6970$
FIRST COMBINED



$\alpha_{21} = 2.1346$
SECOND COMBINED

TRANSVERSE MODES OF PRESSURE OSCILLATION IN A CYLINDRICAL CHAMBER

The flow rate out of the chamber will be a function of chamber conditions and outlet throat area.

$$\dot{m}_{out} = \sqrt{\frac{\gamma g}{R}} \frac{P_c}{\sqrt{T_o}} \left(\frac{2}{\gamma+1} \right)^{\frac{\gamma+1}{2(\gamma-1)}} A_{out} \quad (4)$$

When considering average conditions, the flow rate into the chamber and the flow rate out of the chamber must be equal. Since the chamber cross section is very large compared to inlet area, the velocity in the chamber is very small and the chamber temperature therefore may be assumed equal to the stagnation temperature. Setting Equations (3) and (4) equal results in the following:

$$P_o A_{in} = P_{avg} A_{out} \quad (5)$$

In the above relationship, A_{out} must be an average outlet area. Since the theoretical outlet area varies from zero to maximum A_{max} , it will be most convenient to express this average area in terms of the maximum area. To find this relationship, it is assumed that the outlet area varies sinusoidally.

Average area is defined as follows:

$$A_{avg} = \frac{\int_0^+ A dt}{\int_0^+ dt} \quad (6)$$

where A is the sinusoidally varying outlet area defined as follows:

$$A = \frac{A_{max}}{2} (\cos \omega t + 1) \quad (7)$$

Considering n cycles, where n is any integer, t will vary from $t = 0$ to $t = n2\pi/\omega$. Average area is then calculated

$$A_{avg} = \frac{\int_0^{n2\pi/\omega} \frac{A_{max}}{2} (\cos \omega t + 1) dt}{\int_0^{n2\pi/\omega} dt} = \frac{A_{max}}{2} \quad (8)$$

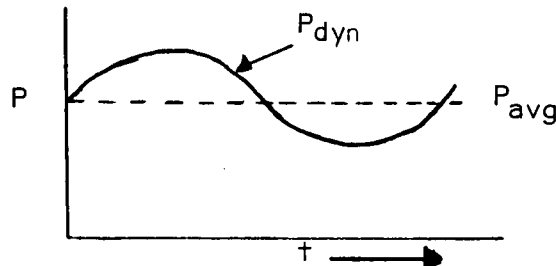
Thus, average outlet area is equal to one-half the maximum area, the final ideal relationship between reservoir pressure, inlet throat area, chamber pressure, and outlet area may be rewritten as follows:

$$P_o A_{in} = P_{avg} \frac{A_{max}}{2} \quad (9)$$

b. Peak-to-Peak Pressure Fluctuations

To develop the theory of pressure fluctuations in the SPG the simple SPG model is again used as before but outlet area variation is now considered.

The chamber pressure may now be considered to have two components - an average pressure and a dynamic pressure component. The dynamic component varies about the average as shown below.



Similarly, other intensive properties of the gas in the chamber may be considered to have an average and a dynamic component.

If it is assumed that perfect gas laws apply, the chamber pressure may be expressed as follows:

$$P = \rho RT \quad (10)$$

The density, ρ , may be expressed as mass in the chamber divided by chamber volume.

$$\rho = \frac{M}{V} \quad (11)$$

where M is the mass in the chamber and V is the chamber volume in

appropriate units. If constant temperature is assumed, the pressure is found to be directly proportional to the mass of the gas in the chamber. Combining Equations (10) and (11):

$$P = K_1 M ; \quad K_1 = \left(\frac{RT}{V} \right)_{\text{chamber}} = \text{constant} \quad (12)$$

The mass of gas in the chamber will depend on the mass flux into the chamber and the flux out of the chamber. If time $t = 0$ is defined as that time when the dynamic pressure component is zero, the mass in the chamber at any time t is:

$$M_t = M_o + \int_0^t \dot{m}_{in} dt - \int_0^t \dot{m}_{out} dt \quad (13)$$

where M_o is the mass in the chamber at $t = 0$. Since the dynamic pressure component is zero at this time, M_o is also the average component of the mass by definition.

If the reservoir conditions are constant, the mass flux into the chamber \dot{m}_{in} , will also be constant since mass flow through a choked inlet is a function of upstream conditions and throat area only. Therefore, the integral of mass flux into the chamber in the interval from $t = 0$ to t may be integrated directly.

$$\int_0^t \dot{m}_{in} dt = \dot{m}_{in} t \quad (14)$$

The mass flux out of the chamber may be written as follows:

$$\dot{m}_{out} = (\rho AV)_{out} \quad (15)$$

This may be expanded further under the assumption made earlier.

$$\dot{m}_{out} = \left[\frac{P}{RT} \sqrt{\gamma g RT} \right]_{out} A_{out} \quad (16)$$

Since the flow is choked, and is assumed to be isentropic from the chamber to the outlet throat, the pressure at the outlet may be expressed in terms of chamber pressure (Ref. 29).

$$P_{out} = P \left(\frac{2}{\gamma+1} \right)^{\frac{\gamma}{\gamma-1}} \quad (17)$$

However, since the average pressure is generally of greater magnitude than the dynamic pressure component, very little error will be introduced if it is assumed that the outlet pressure is a function of average pressure rather than chamber pressure which is the sum of the average and the dynamic components. The mass flux out of the chamber may now be rewritten.

$$\dot{m}_{out} = P_{avg} \left(\frac{2}{\gamma+1} \right)^{\frac{\gamma}{\gamma-1}} \left(\sqrt{\frac{\gamma g}{RT}} \right)_{out} A_{out} = K_2 A_{out} \quad (18)$$

The outlet area, assumed to vary sinusoidally between zero and A_{max} is written as before.

$$A_{out} = A_{avg} (\cos \omega t + 1) \quad (19)$$

Equations (18) and (19) may now be combined.

$$\dot{m}_{out} = K_2 A_{avg} (\cos \omega t + 1) = K_3 (\cos \omega t + 1) \quad (20)$$

This shows that the mass flux out of the chamber follows outlet area variation. This is the rate at which mass is discharged. The expression for instantaneous mass at time t may now be written in integrated form.

$$M_t = M_o + (\dot{m}_{in} - K_3)t - \frac{K_3}{\omega} \sin \omega t \quad (21)$$

Note, however, that K_3 can be shown to be the average mass

flow out of the chamber:

$$K_3 = A_{avg} P_{avg} \left(\frac{2}{\gamma+1} \right)^{\frac{\gamma}{\gamma-1}} \left(\sqrt{\frac{\gamma g}{RT}} \right)_{out} = (\dot{m}_{out})_{avg} \quad (22)$$

For constant average pressure, the mass flux in and average mass flux out of the chamber must be equal. Therefore, the quantity $(\dot{m}_{in} - K_3)$ must equal zero. The instantaneous mass in the chamber at time t may be written in terms of average mass component and the dynamic mass component.

$$M_t = M_0 - \frac{K_3}{\omega} \sin \omega t \quad (23)$$

Similarly, the pressure at time t , may be expressed by combining Equations (12) and (13).

$$P = K_1 \left[M_0 - \frac{K_3}{\omega} \sin \omega t \right] = P_{avg} + P_{dy} \quad (24)$$

where the dynamic pressure component is clearly:

$$P_{dy} = \frac{K_1 K_3}{\omega} \sin \omega t \quad (25)$$

The peak-to-peak pressure fluctuation is two times the maximum magnitude of the dynamic pressure component. This maximum occurs when the magnitude of $\sin \omega t = 1$. Let the peak-to-peak pressure fluctuation be designated at P^* . Then from the above definition

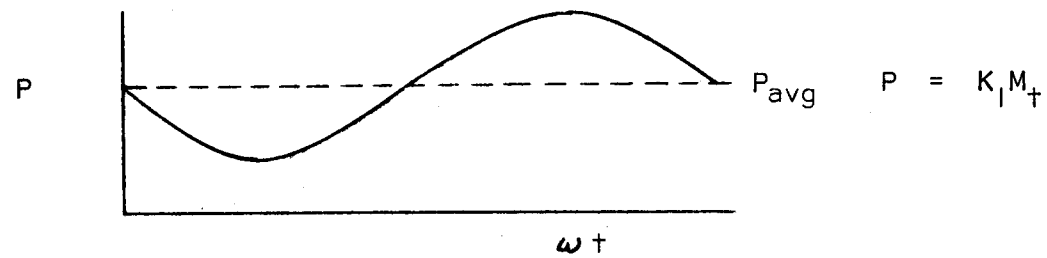
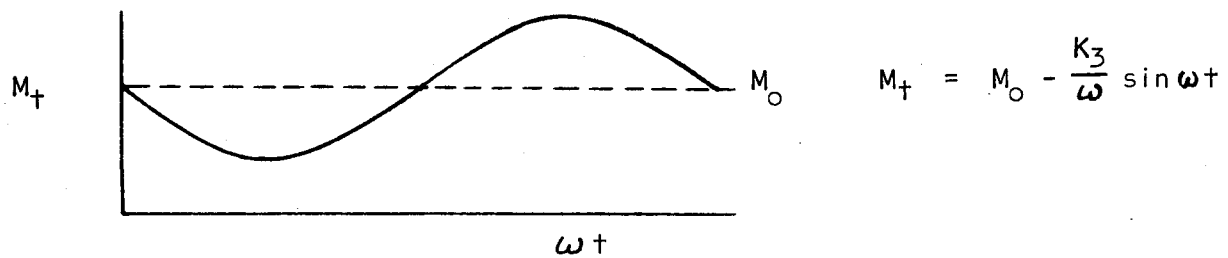
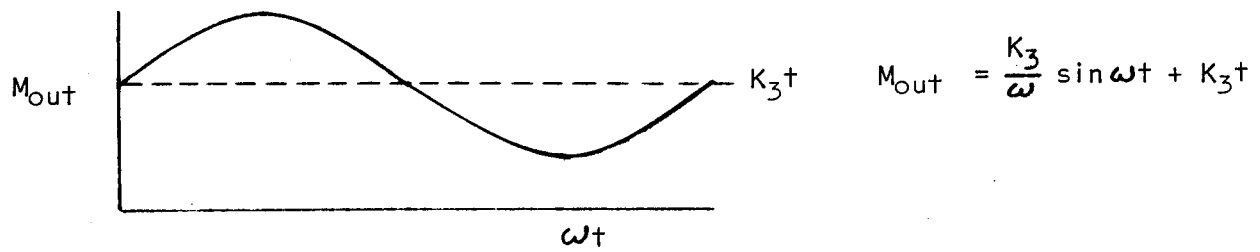
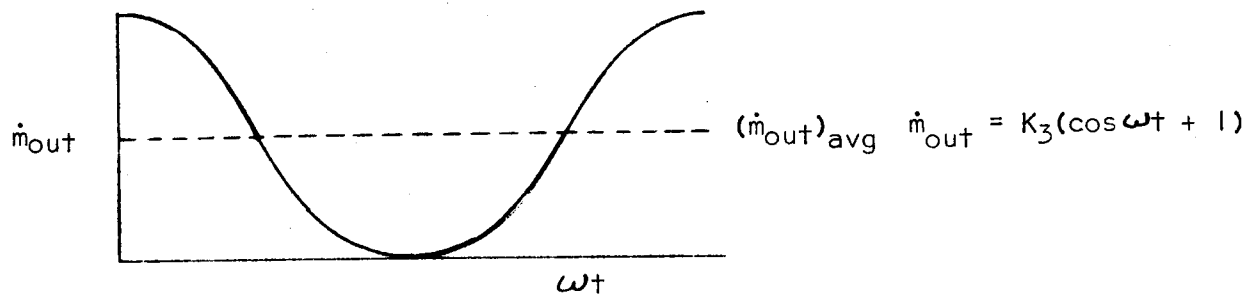
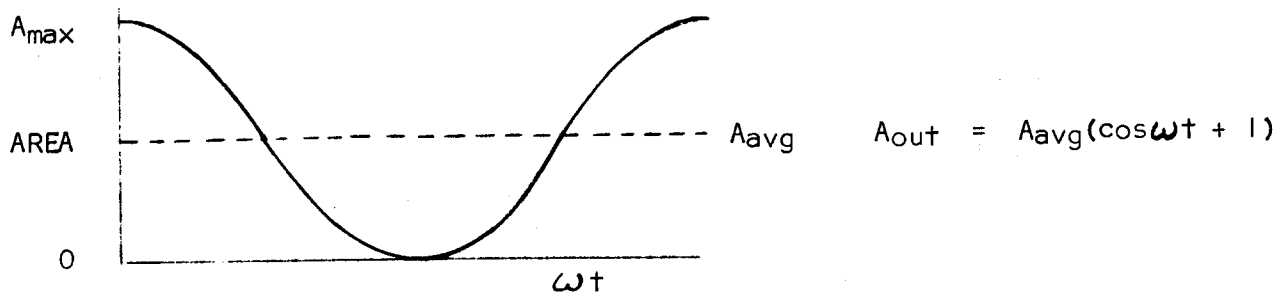
$$P^* = 2 \frac{K_1 K_3}{\omega} = \text{constant} \quad (26)$$

Since it is more convenient to express the frequency in cycles per second, f , rather than radians per second, Equation (26) may be rewritten:

$$P^* f = \frac{K_1 K_3}{\pi} = \text{constant} \quad (27)$$

Thus, a plot of peak-to-peak pressure fluctuations versus frequency should be in the form of an inverse hyperbola.

The phase relationship of area variation, mass flux out of the chamber, the mass discharged, mass in the chamber and pressure is shown in Figure 36.



Phase Relationships

FIGURE 36

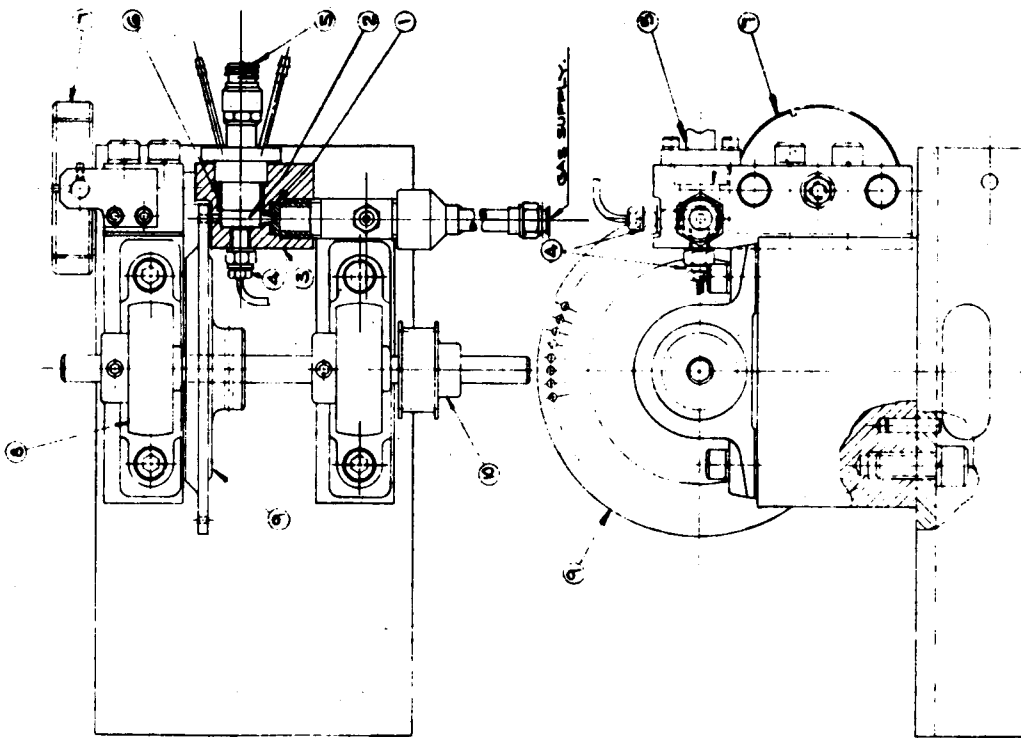
C. Description and Operation of Apparatus

The Princeton Sinusoidal Pressure Generator (SPG) is a gas flow throttling device. The gas flows through a small nozzle inlet, 0.055 inches in diameter at the throat, into a small cylindrical chamber and is discharged through an outlet opposite the inlet. The outlet is a circular port, 0.125 inches in diameter with a beveled entrance and the chamber is 0.70 inches in diameter and 0.275 inches in length. Provision is made for a monitor transducer to be mounted in one end wall of the chamber and for the transducer undergoing evaluation to be mounted in the other end wall. The monitor utilized was a quartz piezoelectric type made by Kistler. The early tests used a Kistler 601 and the later tests used a Kistler 601A. This type of transducer is described more completely later in this section. There is also a fitting provided so that a transducer may be mounted on the curved side wall on top of the chamber.

The flow is modulated by a steel wheel with seventy-two 1/8 inch circular holes near the rim which rotate past the outlet port. The clearance between the wheel and outlet port is adjustable by means of a micrometer adjustment.

See Figure 37 for a detailed drawing and Figure 38 for a photograph of the SPG.

A shunt wound D.C. variable speed motor was used to drive the wheel through a timing belt and gears. This type of drive has proven more satisfactory than the previously used U.S. Varidrive (Ref. 4). Two drive ratios were available, 1:1 and 6:1, although the majority of the testing was done using the 6:1 ratio. Frequencies ranging from 100 cps to 18,000 cps are possible using these gear ratios.



LEGEND.

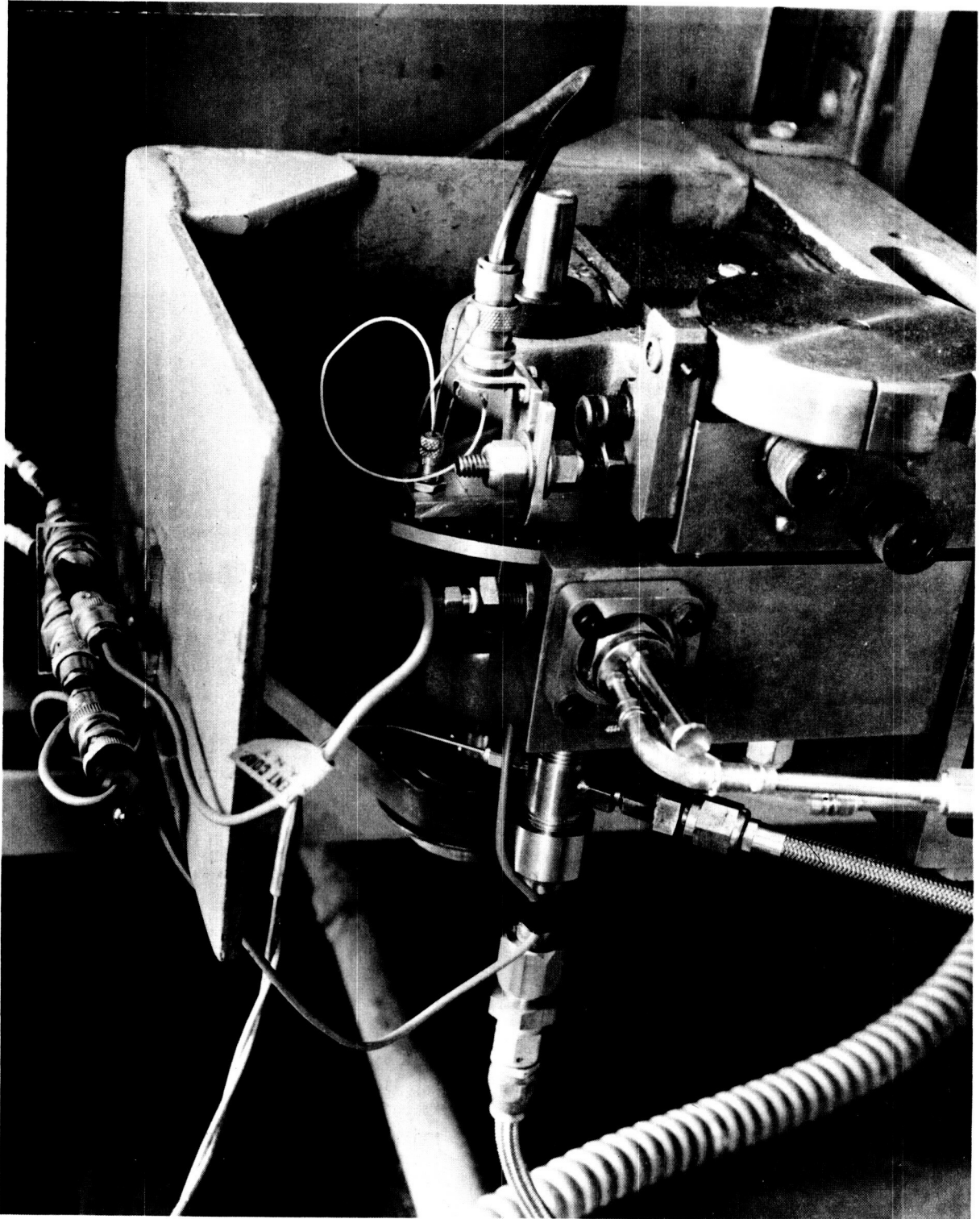
- ① INLET ORIFICE.
- ② CHAMBER.
- ③ BODY.
- ④ REFERENCE TRANSDUCER (KISTLER-601A)
- ⑤ TEST TRANSDUCER
- ⑥ SLEEVE.
- ⑦ MICROMETER ADJUSTMENT NUT.
- ⑧ SELF ALIGNING BEARING.
- ⑨ PERFORATED DISC.
- ⑩ DRIVE BELT PULLEY.

① JPA-1003A

DATE	1/1/74
BY	JPA-1003A
CHKD	JPA-1003A
APPROVED	JPA-1003A
REVISION	1
DESCRIPTION	SINUSOIDAL PRESSURE GENERATOR
TESTER	JPA-1003A
TESTER ASSEMBLY	JPA-1003A
TESTER DISASSEMBLY	JPA-1003A
TESTER REPAIR	JPA-1003A
TESTER MAINTENANCE	JPA-1003A
TESTER STORAGE	JPA-1003A
TESTER DISPOSAL	JPA-1003A

SINUSOIDAL PRESSURE GENERATOR

FIGURE 37



Sinusoidal Pressure Generator

Frequency was adjusted by controlling the D.C. motor speed. The frequency was counted by a Hewlett-Packard Electronic Counter in combination with a variable reluctance detector. The detector was mounted on the SPG so as to sense the passage of each hole in the wheel as it rotated and the electronic counter was utilized to "count" the detector output. Thus, the electronic counter was really a frequency measuring device.

The only gases used in the tests were nitrogen and helium. The gas supply system in both cases is similar. The gas was stored in compressed gas bottles. It passed through two pressure regulators which reduced the pressure in steps to the desired supply pressure. In these tests, supply pressures ranging from 60 to 490 psia were used. The actual reservoir pressure of the gas was measured in a large volume, large cross section settling chamber immediately before the inlet. This settling chamber was also fitted with a thermocouple fitting.

The Kistler 601A is a quartz crystal piezoelectric type pressure transducer. This type of transducer has a very high natural frequency and is assumed to be capable of accurate and precise pressure measurements at all frequencies below 20,000 cps. The vendor reports a natural frequency of 140,000 cps and the shock tube tests described in the previous section also found the natural frequency to be about 140,000 cps. This gives the transducer the capability of faithful reproduction of waveform, amplitude, and phase for frequencies well below the natural frequency. This type transducer had excellent

evaluation in the shock tube tests and makes an excellent monitor for the SPG.

In practice pressure applied to the diaphragm is converted to a force which acts on the transducer crystal. This generates an electric charge which is proportional to the pressure input. The output is expressed in picocoulombs per psi.

A Kistler electrostatic charge amplifier is used with the Kistler type transducer in order to convert the high-impedance charge output of the transducer to a low-impedance voltage. This output can then be read on an indicating meter, or displayed on an oscilloscope. This charge amplifier also eliminates the effect of cable capacitance from the system.

The Dynisco PT-49 AF-IM type transducer has a four arm bonded strain gage as the pressure sensing element. This type of transducer requires an external power supply to excitation of the strain gage. This is usually a ten volt regulated power supply. It is essential that the voltage be precisely ten volts for accurate pressure measurement. The Dynisco PT-49 AF-IM is water cooled and has the coolant flow passage arranged to achieve high coolant velocity and good distribution. It is necessary to use cooling water any time the device is used in an elevated or changing temperature environment to prevent thermal drift.

The diaphragm of the Photocon 755 transducer in conjunction with an insulated electrode forms an electrical capacitor. The pressure applied to the diaphragm produces small changes in capacity

proportional to the pressure. This capacity is connected to an inductance which has been built into the transducer to form a tuned R-F circuit. This circuit is link-coupled by means of low impedance cable to the oscillator detector circuit or Dynagage. The Dynagage consists of an R-F oscillator coupled to a diode detector circuit. Small changes in capacity in the transducer produce relatively large changes in the diode detector impedance. The output of the detector is proportional to the pressure applied to the transducer diaphragm.

A Krohn-hite variable band-pass filter was used in the testing when filtering was required. This type filter has adjustable lower and upper cut-off frequencies which filter from the input frequencies below and above these limits. The filter characteristics are such that slight amplification will occur if the input is filtered close to the driving frequency. However, as the cut-off frequencies are moved closed to the driving signal, the amplification factor decreases and at very close settings, the signal will be attenuated.

The amplification factor was determined by using the signal generator to provide a known input of the desired frequency. This signal was measured before and after filtering. Cut-off frequencies of $2/3$ and $3/2$ of the driving frequency produced an amplification factor of 1.23 in the frequency range of 1000 cps to 10,000 cps. Cut-off frequencies of 100 cps and 20,000 cps or 40,000 cps did not amplify the signal.

Experimentally, it was found that the filter setting of $3/4$ the driving frequency for the lower cut-off and $4/3$ the fundamental for the upper cut-off gave superior filtering characteristics. The

amplification factor was on the order of 1.07 rather than 1.23. It was also decided to increase the lower cut-off to 200 cps rather than 100 cps to eliminate line noise at 180 cps from three-phase power.

A two beam Tektronix Type 551 oscilloscope was used to observe the waveforms of the transducer output and a Polaroid Hewlett-Packard Model 196A oscilloscope camera fitted to the oscilloscope was used to photograph the waveform when desired.

D. Experimental Results

Preliminary tests were conducted in order to determine whether the inlet and outlet were choked over the full operational range of interest, which in this case was from 1 to 10 kcps. The tests were conducted in the same manner as Carwile in Reference 6. The supply pressure of nitrogen was preset at the desired level by pressure regulator adjustment and wheel speed adjusted to give the desired frequency as determined by the electronic counter. All pressures in these tests were measured with the Kistler 601 monitor. The chamber pressure fluctuations were determined from the a.c. output of the monitor which was read on the RMS meter after amplification by the Kistler charge amplifier and filtering through a variable band pass filter, while the average chamber pressure was determined from the d.c. output which was measured on the oscilloscope after amplification. The d.c. output tends to drift towards zero, but it is possible to get good results if reasonable care is exercised. Several different supply pressures were used in these tests. The results indicated that average chamber pressure was never low enough to insure positive choking of the inlet; however, it was high enough to choke the outlet at all times. The average chamber pressure varied slightly over the range of frequencies

tested. The reported average value is the average for all frequencies. Results are listed below in tabular form.

Supply Pressure (psia)	Average Chamber Pressure (psia)
75	55
129	86
150	98
490	335

It is desirable to have the inlet and outlet choked at all times since this provides a constant and known mass flow into the chamber. The constant inlet mass flow also provides the basis for constant average chamber pressure. It was therefore decided to install a new inlet of proper size so that both the inlet and outlet would be choked over the full operational frequency range. The area of the inlet was calculated from the simplified theoretical model. When calculating the inlet area, allowance was made for expected pressure fluctuations above and below desired average chamber pressure so that the inlet would be choked at maximum chamber pressure and the outlet would remain choked at minimum chamber pressure. Calculations indicated that an inlet diameter of 0.055 inches would meet these requirements.

To evaluate the new inlet, tests were conducted as before except that average chamber pressure was now measured with a Dynisco PT-49 AF-IM flush mounted transducer. Again, tests were conducted at more than one supply pressure. As in the case of the larger inlet, average chamber pressure varied slightly over the full range of frequencies and pressures. The results are listed in the table below.

Supply Pressure (psia)	Average Chamber Pressure (psia)
129	40
255	87

It was noted that these pressures are lower than the theoretical pressures.

The response to frequency of the SPG chamber with the new inlet was also checked. Nitrogen was used for these tests since it was necessary to have some of the theoretical chamber resonant frequencies within, or close to, the frequency range of interest. As the frequencies are directly proportional to the speed of wave propagation, they are relatively low in nitrogen which has a wave propagation on the order of 1100 feet per second at room temperature. Since tangential modes are the first to appear in cylinders with a length-to-diameter ratio of less than 1.71 and these tangential modes will not affect an end mounted transducer in the chamber (Ref. 6), an additional transducer was mounted on the curved side wall on top of the chamber (See Figure 38). This transducer, which was also a Kistler 601, made it possible to detect tangential modes since a transducer mounted on the curved side wall will respond to these modes. The output from the monitor and from the side wall mounted transducer was amplified by a Kistler charge amplifier and then filtered by a variable band pass filter. The filtered output was then measured on an RMS AC voltmeter and also fed into the oscilloscope so that waveform could be observed and pictures taken with the Polaroid camera if desired. The average chamber pressure was measured with a Photocon 745. The Photocon output was fed through the Dynagage and was measured with a Simpson 269 Ultra-high Sensitivity

Voltmeter. A schematic of the instrumentation appears as Figure 39.

The output of the three transducers were recorded at various frequencies and filter settings throughout the range of interest. Results are plotted in Figures 40 and 41 for the test with a supply pressure of 131 psia.

The chamber response was also checked with helium. The tests were conducted in the same manner as with nitrogen, except that supply pressure was 121 psia. Results are plotted in Figure 42. Photographs of the monitor and top mounted transducer outputs when using helium in the SPG were taken at various pressures and filter settings. These are included as Figure 43.

In all tests using the new inlet, which was a straight orifice with an 0.055 inch diameter, resulting chamber pressures were found to be lower than theoretical values as predicted by the simplified theoretical model. This indicated that the effective inlet area was less than the actual inlet area. This condition was caused by the formation of an aerodynamic throat in the inlet. In order to eliminate this condition, the inlet was modified from a straight orifice to a nozzle with the throat diameter equal to the diameter of the straight orifice.

The chamber was rechecked with helium using the new nozzle inlet. The instrumentation was the same as previously used except that a Dynisco PT-76 flush mounted transducer was used to measure average pressure in place of the Photocon system. The tests were run at supply pressures of 120, 240 and 360 psia. Results are plotted on Figures 44, 45 and 46, respectively.

A settling chamber with large cross section and large volume was installed immediately before the inlet on the SPG so that accurate

TYPICAL INSTRUMENTATION AND
GAS SUPPLY FOR SPG

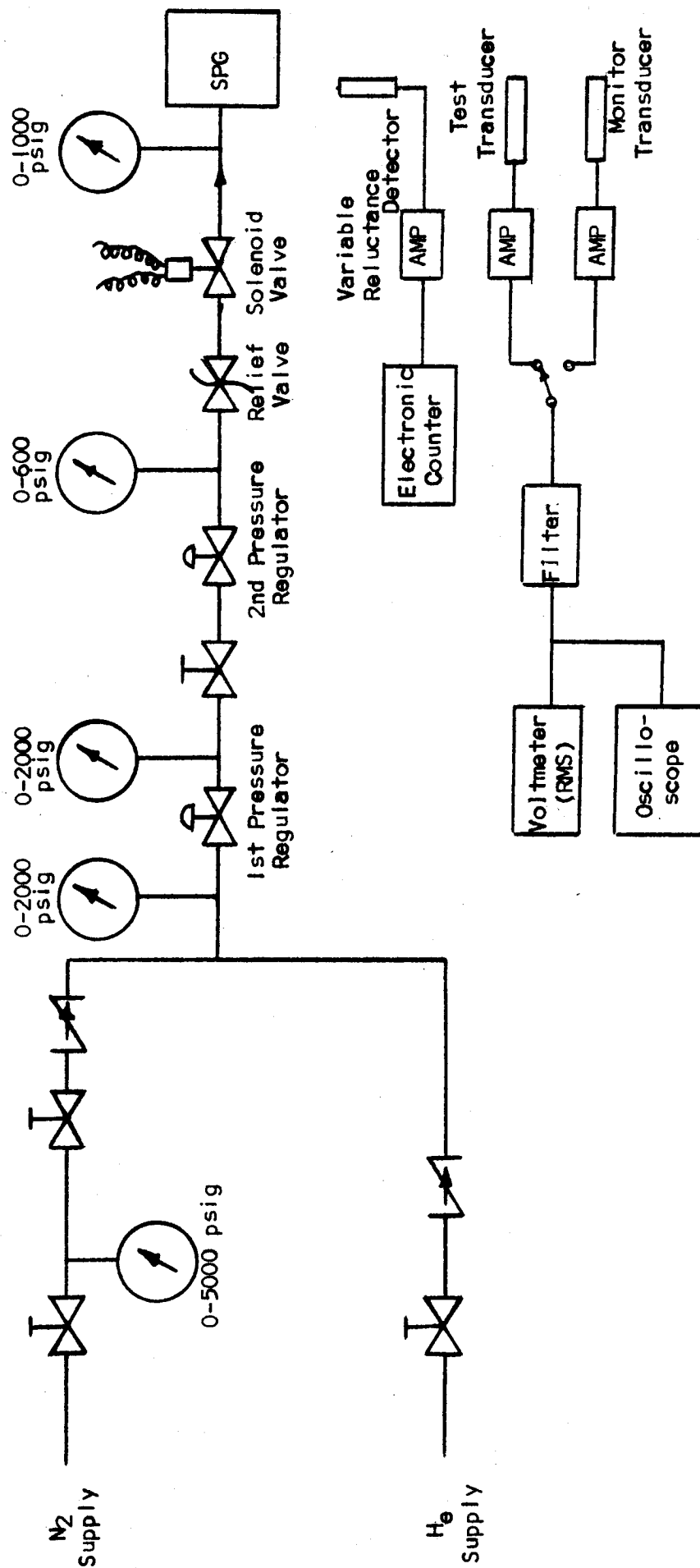


FIGURE 39

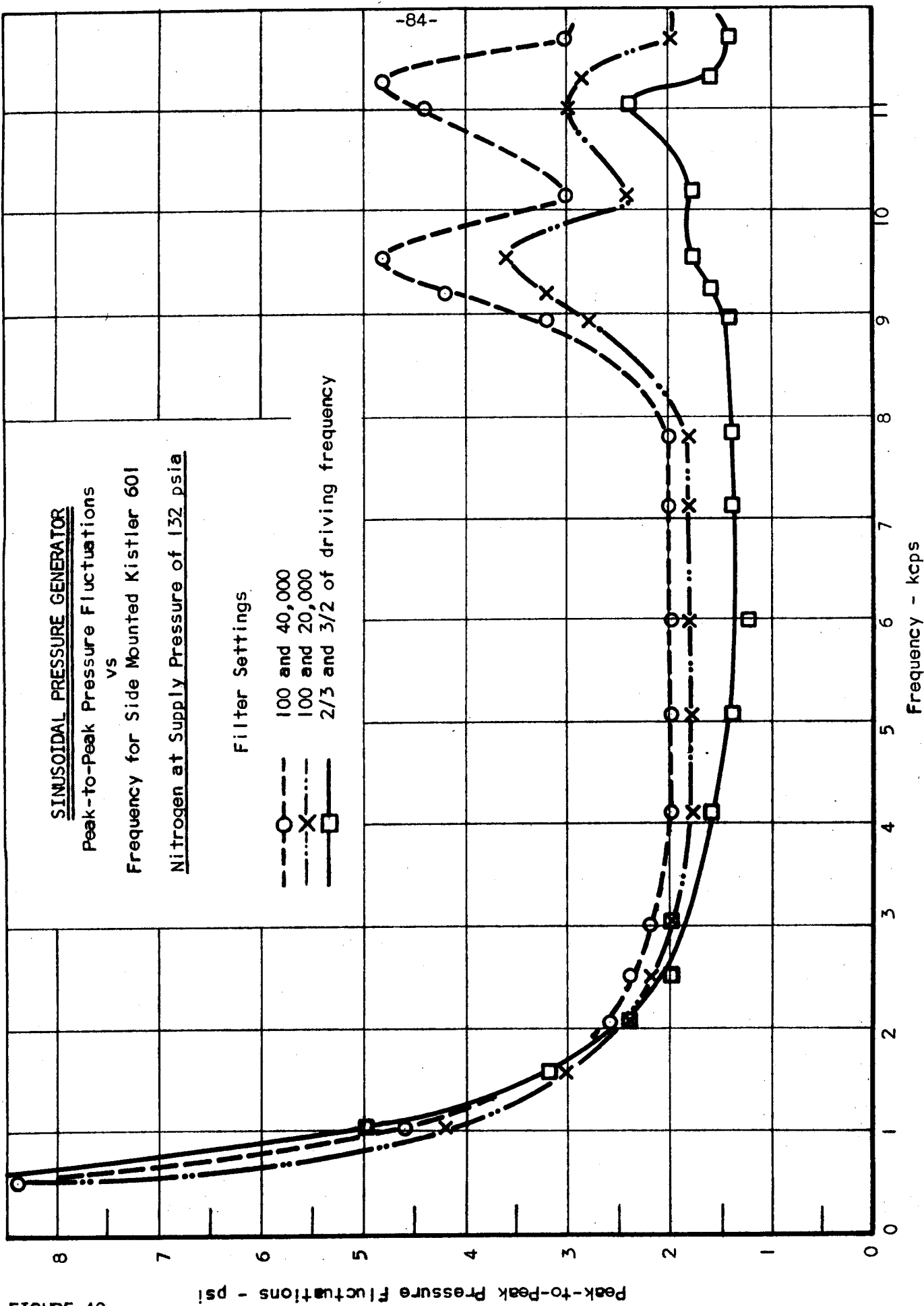


FIGURE 40

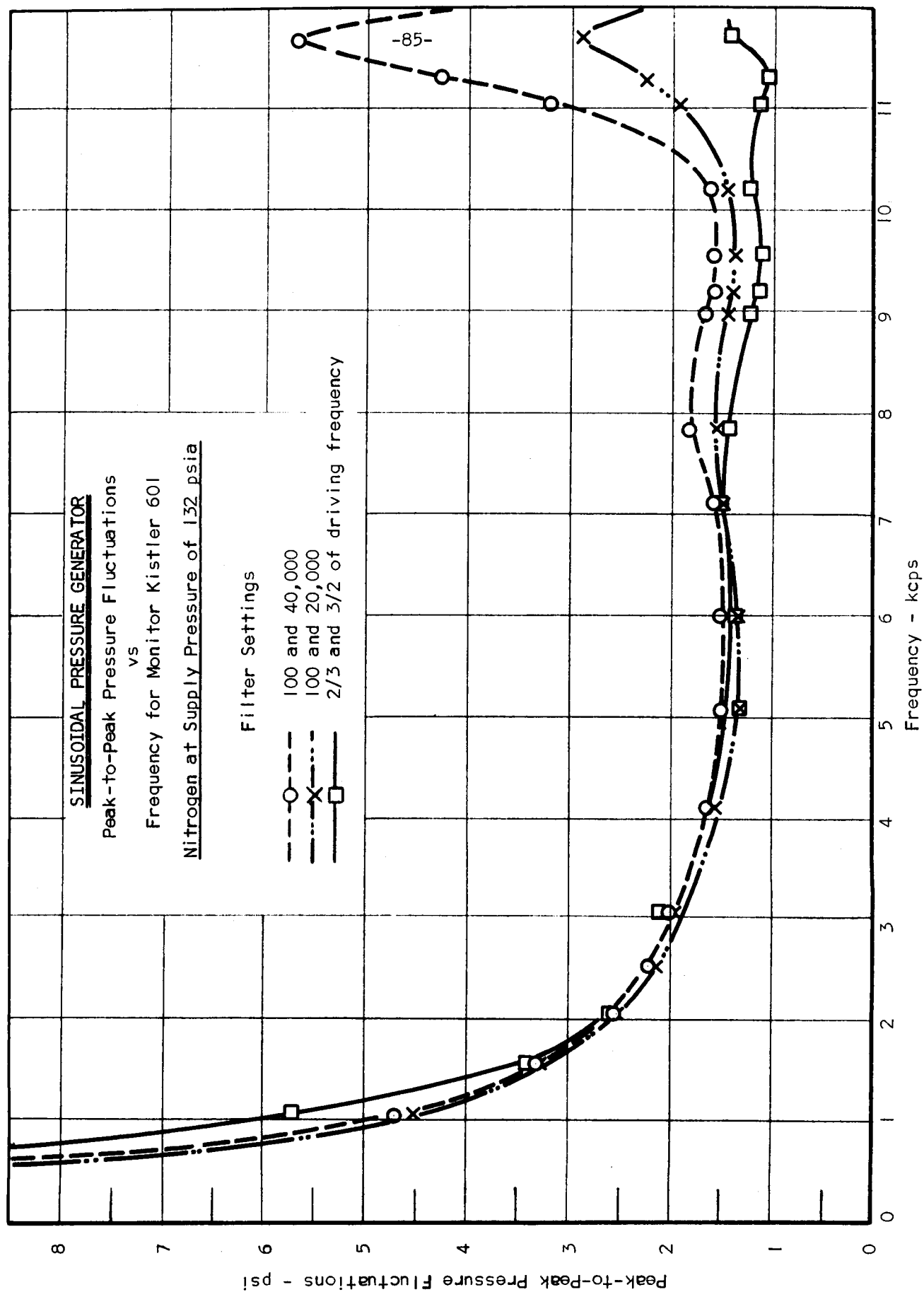


FIGURE 41

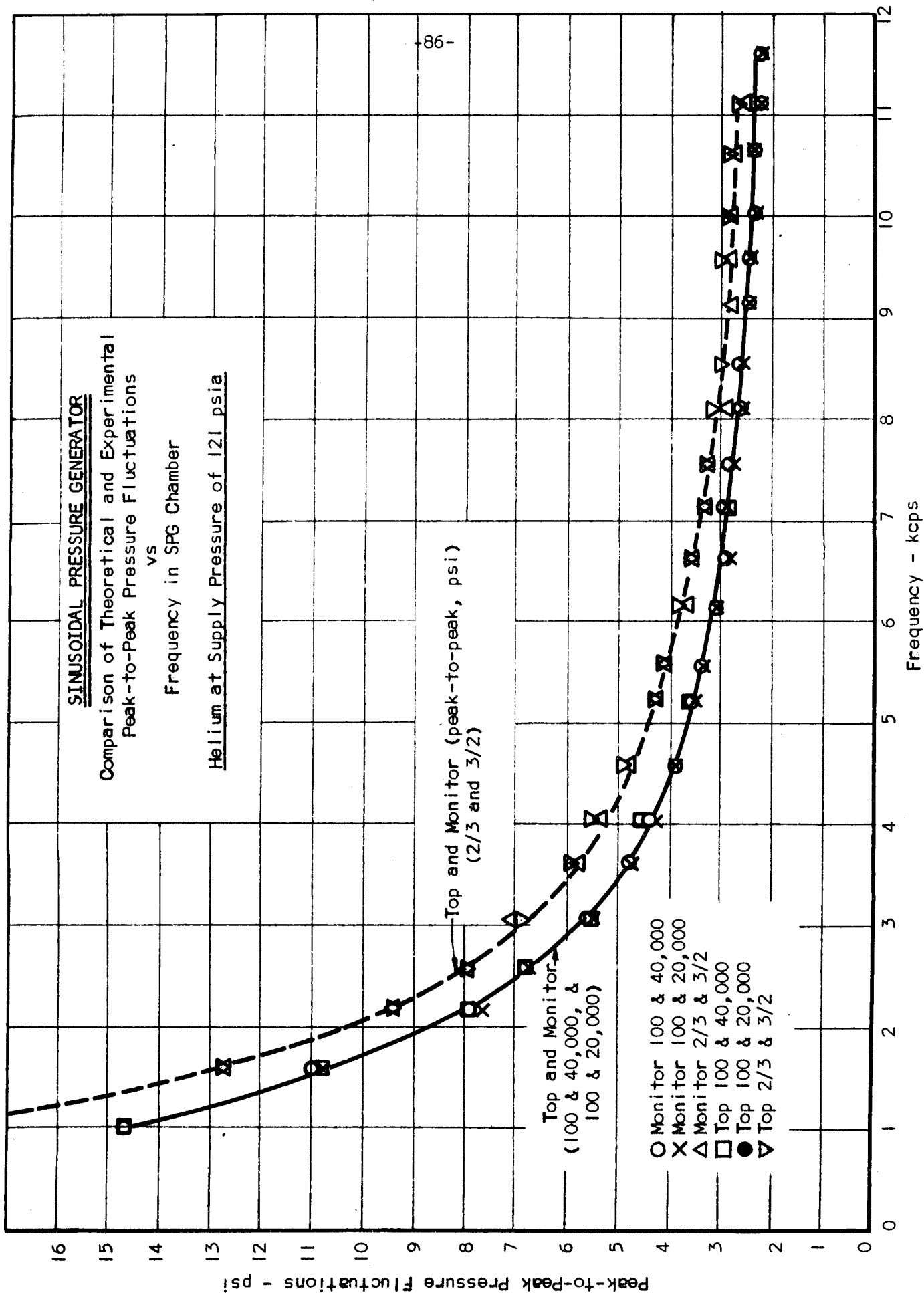
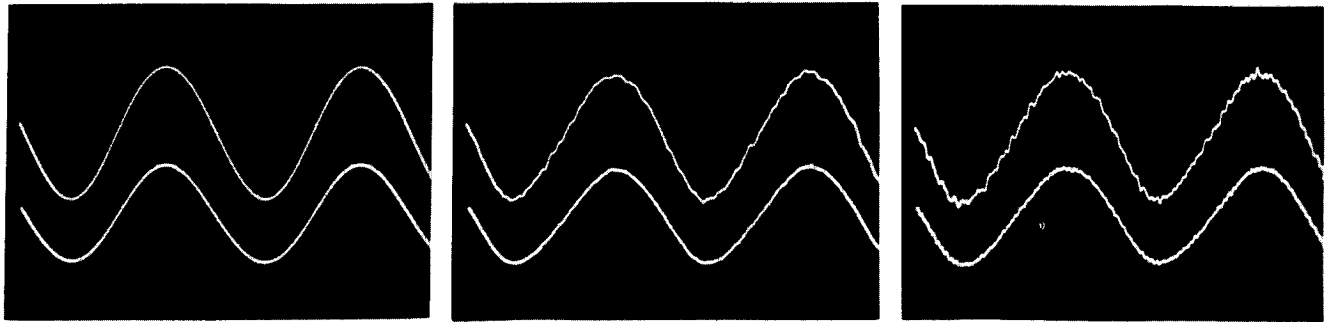


FIGURE 42

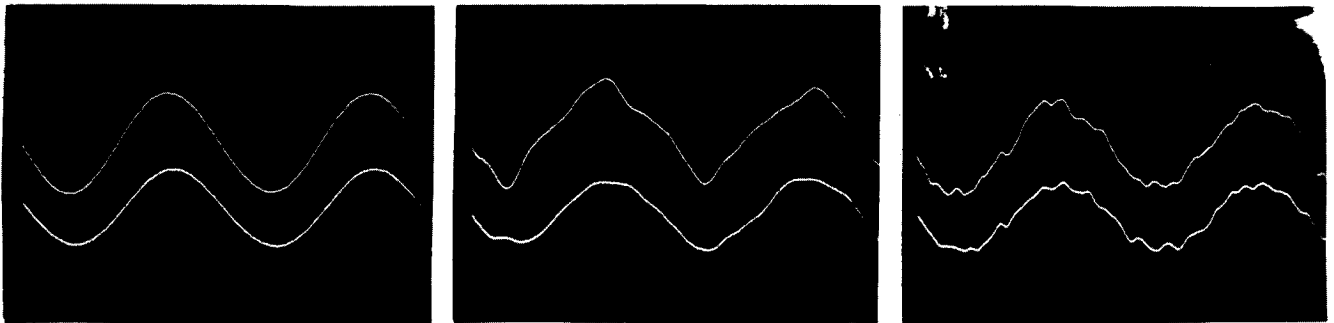
SPG CHAMBER RESPONSE WITH HELIUM AT 120 PSIA SUPPLY PRESSURE
UPPER BEAM MONITOR LOWER BEAM TOP MOUNTED TRANSDUCER



(a)

(b) 1000 cps

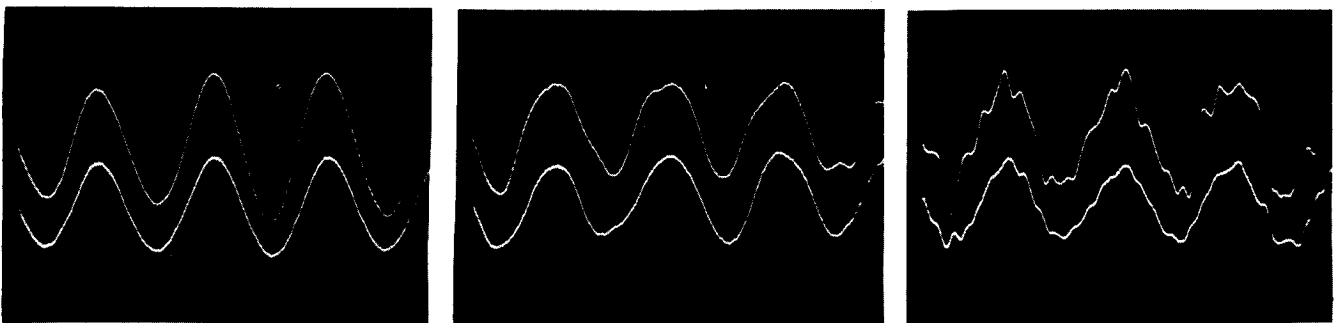
(c)



(a)

(b) 4000 cps

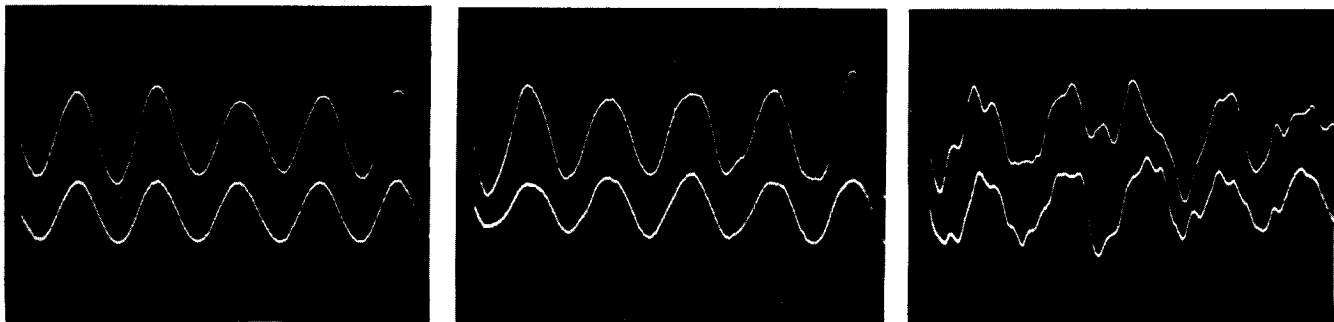
(c)



(a)

(b) 7000 cps

(c)



(a)

(b) 10,000 cps

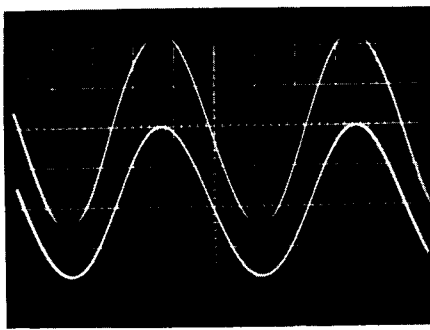
(c)

- (a) Lower filter cut-off $3/4$ driving frequency, upper filter cut-off $4/3$ driving frequency
(b) Lower filter cut-off 200 cps, upper filter cut-off 20,000 cps
(c) Lower filter cut-off 200 cps, upper filter cut-off 40,000 cps

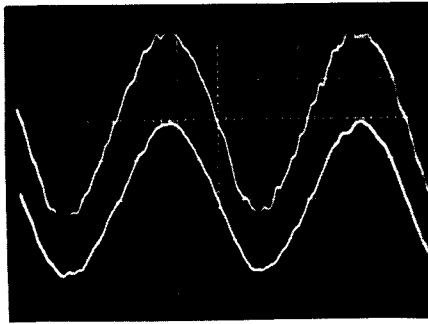
FIGURE 43a

SPG CHAMBER RESPONSE WITH HELIUM AT 360 PSIA SUPPLY PRESSURE

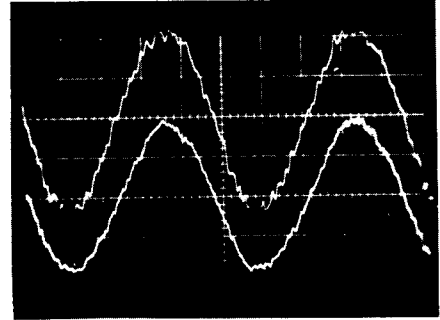
UPPER BEAM MONITOR LOWER BEAM TOP MOUNTED TRANSDUCER



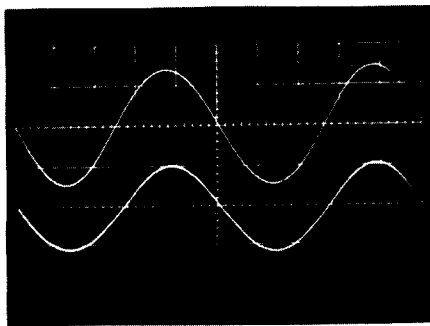
(a)



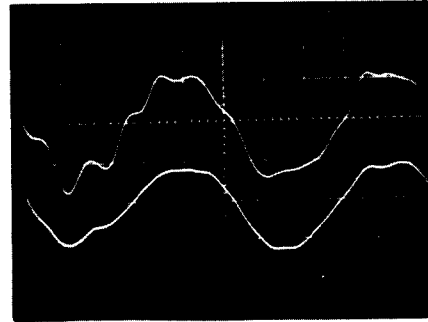
(b) 1000 cps



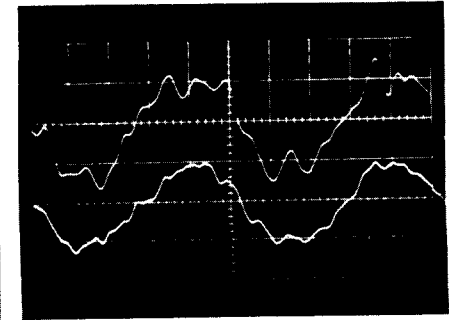
(c)



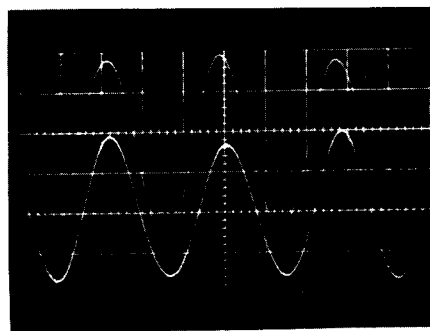
(a)



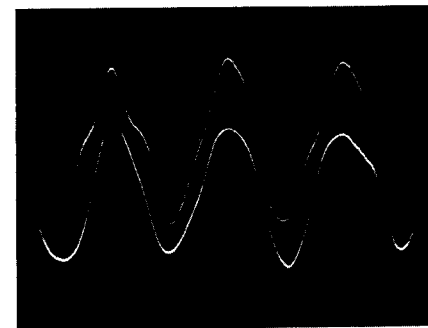
(b) 4000 cps



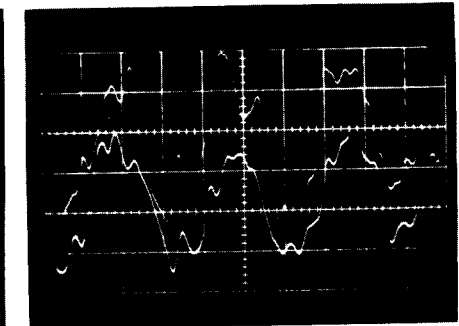
(c)



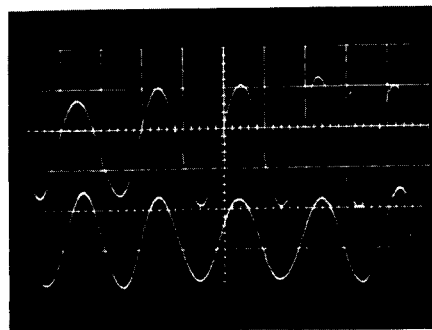
(a)



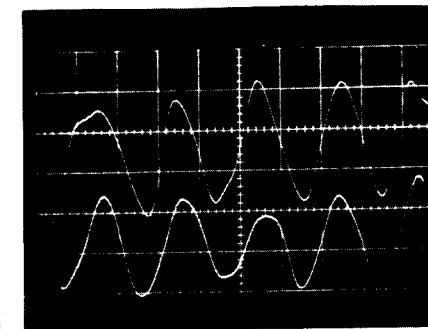
(b) 7000 cps



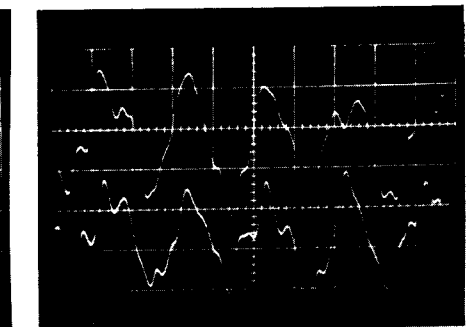
(c)



(a)



(b) 10,000 cps



(c)

- (a) Lower filter cut-off $3/4$ driving frequency, upper filter cut-off $4/3$ driving frequency
 (b) Lower filter cut-off 200 cps, upper filter cut-off 20,000 cps
 (c) Lower filter cut-off 200 cps, upper filter cut-off 40,000 cps

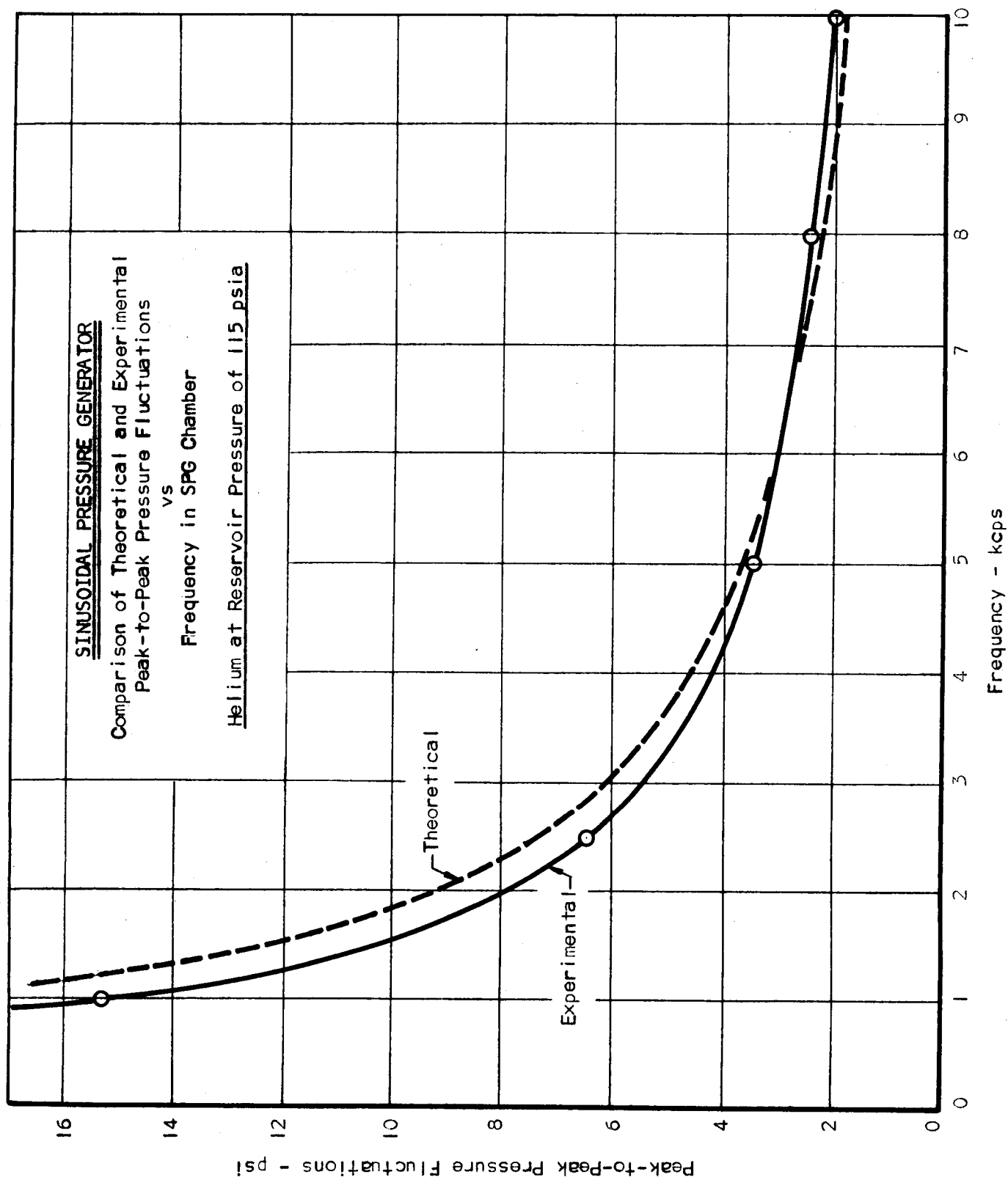


FIGURE 44

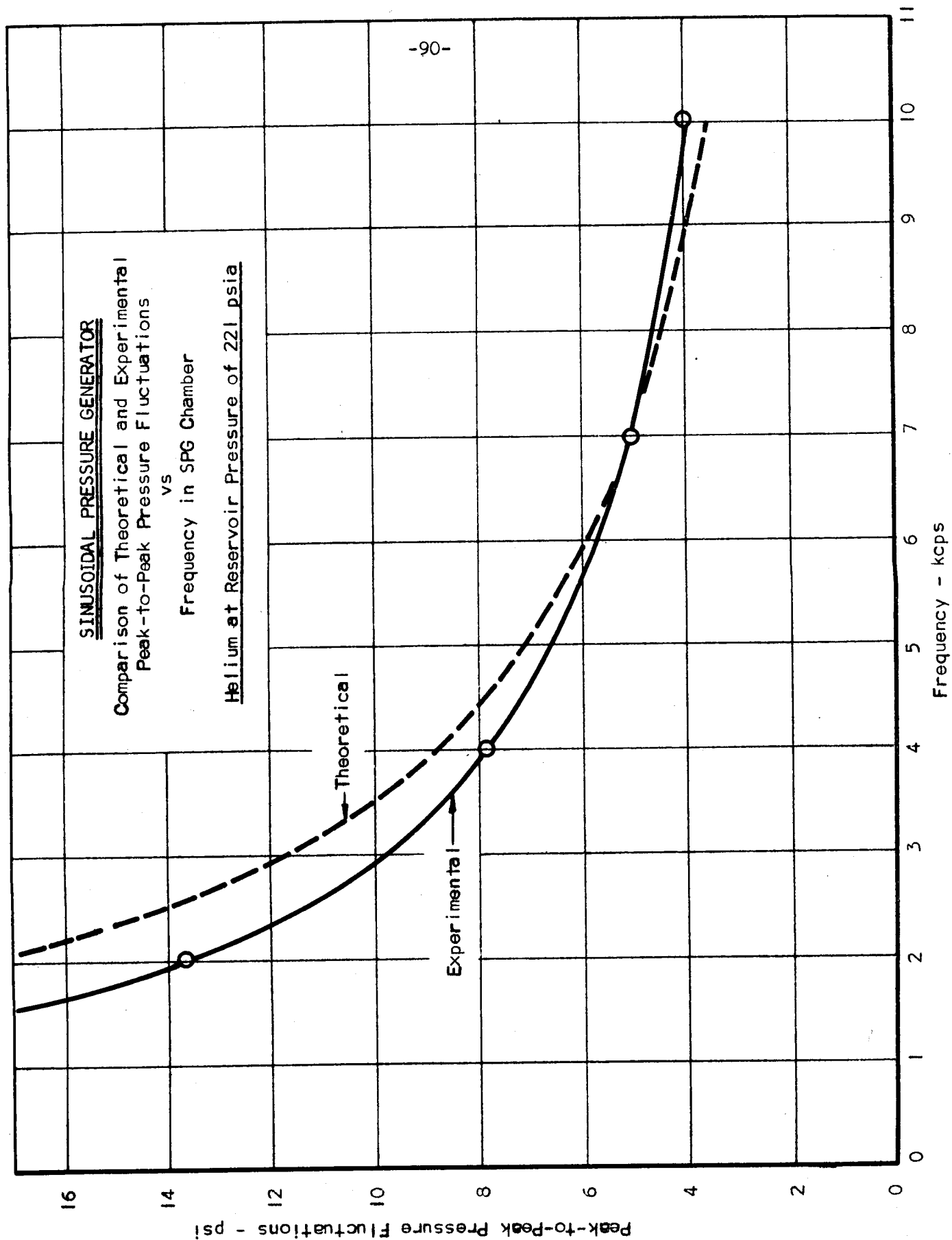


FIGURE 45

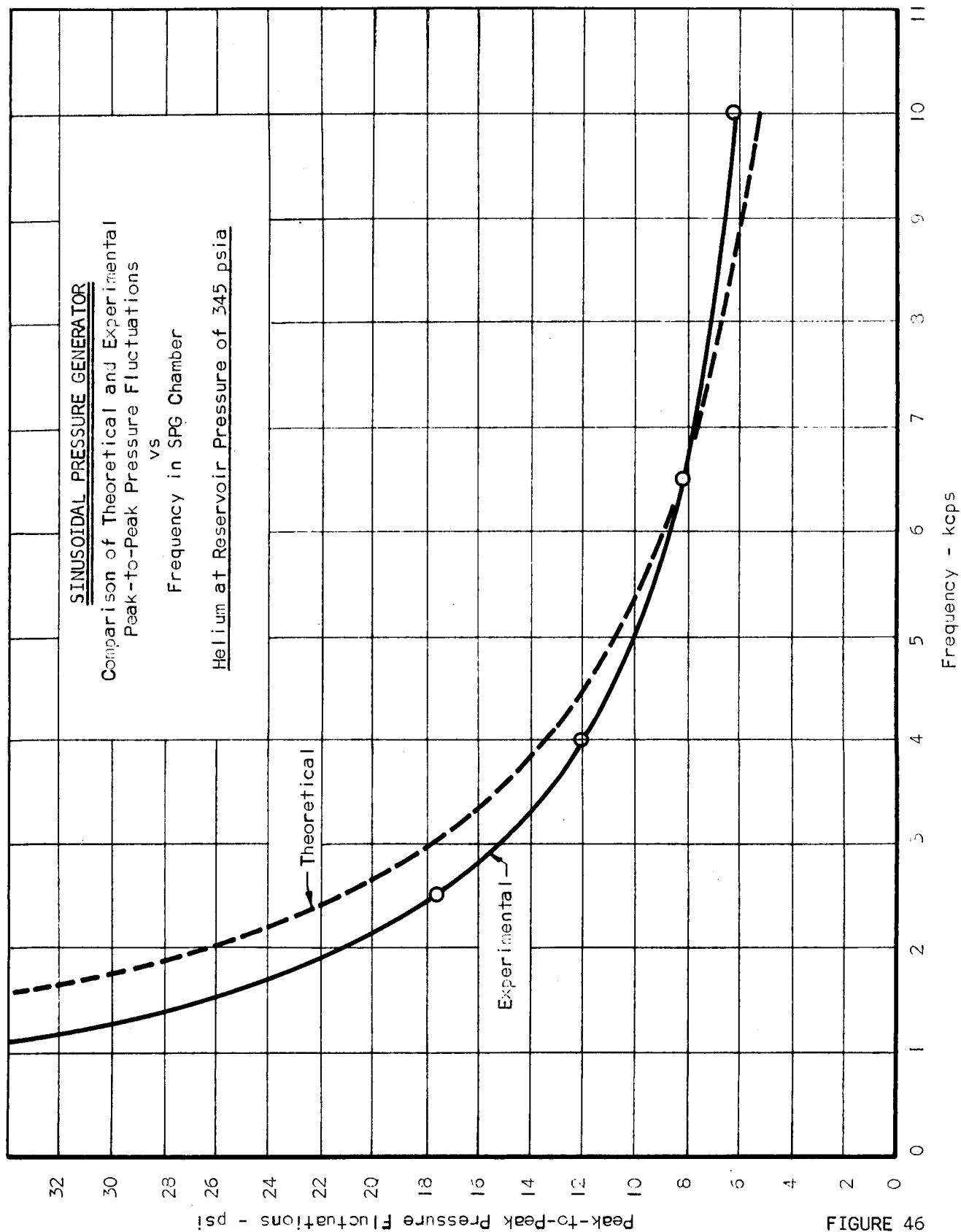


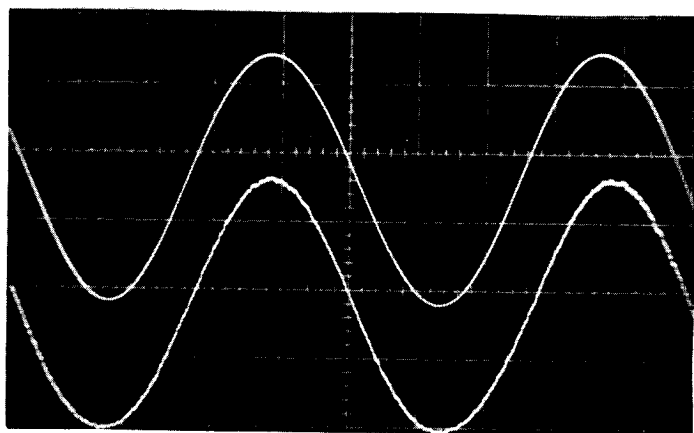
FIGURE 46

measurement could be made of the actual reservoir pressure and temperature of the gas. The tests were run at various supply pressures as indicated at the pressure regulator and at various frequencies. The pressure at the reservoir was measured with an accurate test gauge and recorded. This data was used to correlate supply pressure and reservoir pressure.

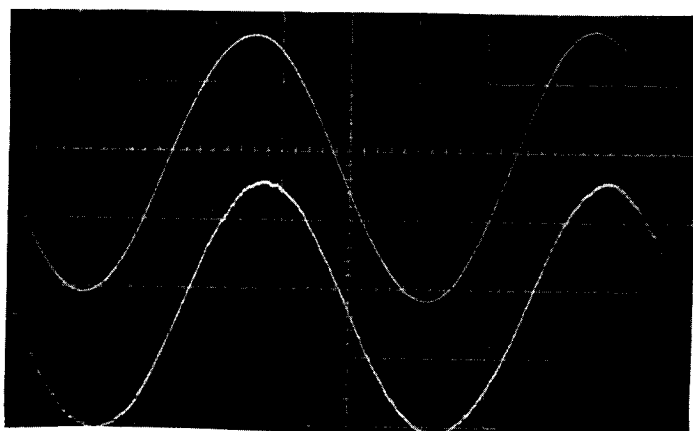
Comparison of the SPG output and a generated sine wave was made by utilizing the oscilloscope. A signal generator was used to generate a sine wave which was fed into the lower beam of the oscilloscope. The output of the SPG monitor filtered at $3/4$ and $4/3$ of the driving frequency was fed into the upper beam, and a photograph was made of the two simultaneously. These photographs are included as Figure 47. Phase angle has no significance in these pictures.

When conducting an evaluation of a transient pressure measuring system with the SPG, the following procedure was used. The transducer was placed in the test transducer position so as to form one end wall of the SPG chamber. The monitor was mounted directly across the chamber in the chamber end wall. Mounting the test transducer usually involved special fittings individually made for each type of transducer, since the SPG was originally designed for the Dynisco PT-49 type of transducer. Necessary instrumentation was then connected so that the output of both monitor and test transducers could be easily read. Again this varied with each type of transducer. The operation of individual pieces of equipment is described in Section IV-C. The complete system was then checked for unusually high noise levels from line sources, ground loops, or any other source.

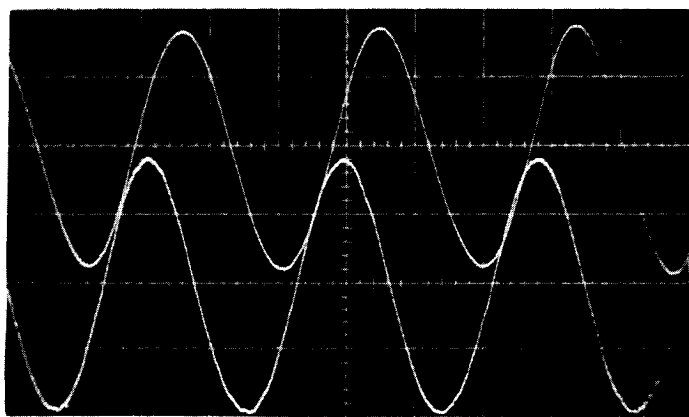
As before, wheel speed was adjusted prior to flowing the gas. This is the most satisfactory procedure from an economical point of



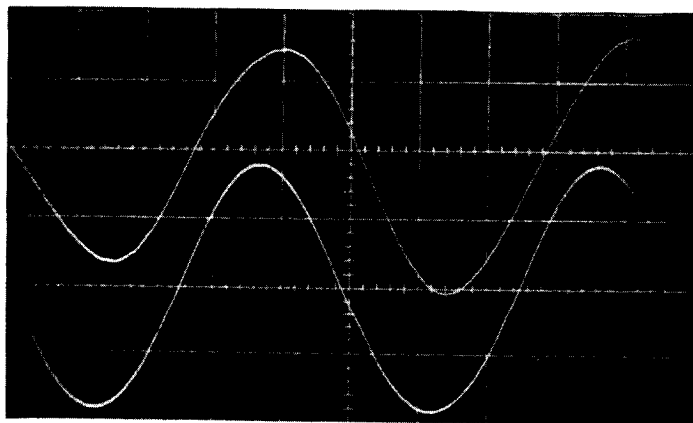
1000 cps



4000 cps



7000 cps



10000 cps

Comparison of SPG Monitor Output (Upper Beam)
With Generated Sine Wave (Lower Beam) at Same Frequency

NOTE: Test gas was helium at 360 psia supply pressure.
Lower filter cut-off frequency was $3/4$ driving frequency,
upper cut-off frequency was $4/3$ driving frequency.

FIGURE 47

view. The outputs of the monitor and the test transducer were recorded as close to simultaneously as possible at 1000 cps, 1500 cps, 2000 cps, and every 1000 cps thereafter up to the desired upper limit. Usually, the readings were continued to 18 kcps, although the primary range of interest is only up to 10 kcps.

At each frequency, a ratio of the test transducer output to the monitor output was calculated. The ratio at 2000 cps was arbitrarily made unity, and all other ratios adjusted accordingly. This gives a response ratio of the test transducer, since it is assumed that the monitor output is a faithful reproduction of the actual chamber conditions. Results of this type of evaluation for typical transducer types are shown as Figures 48 through 51.

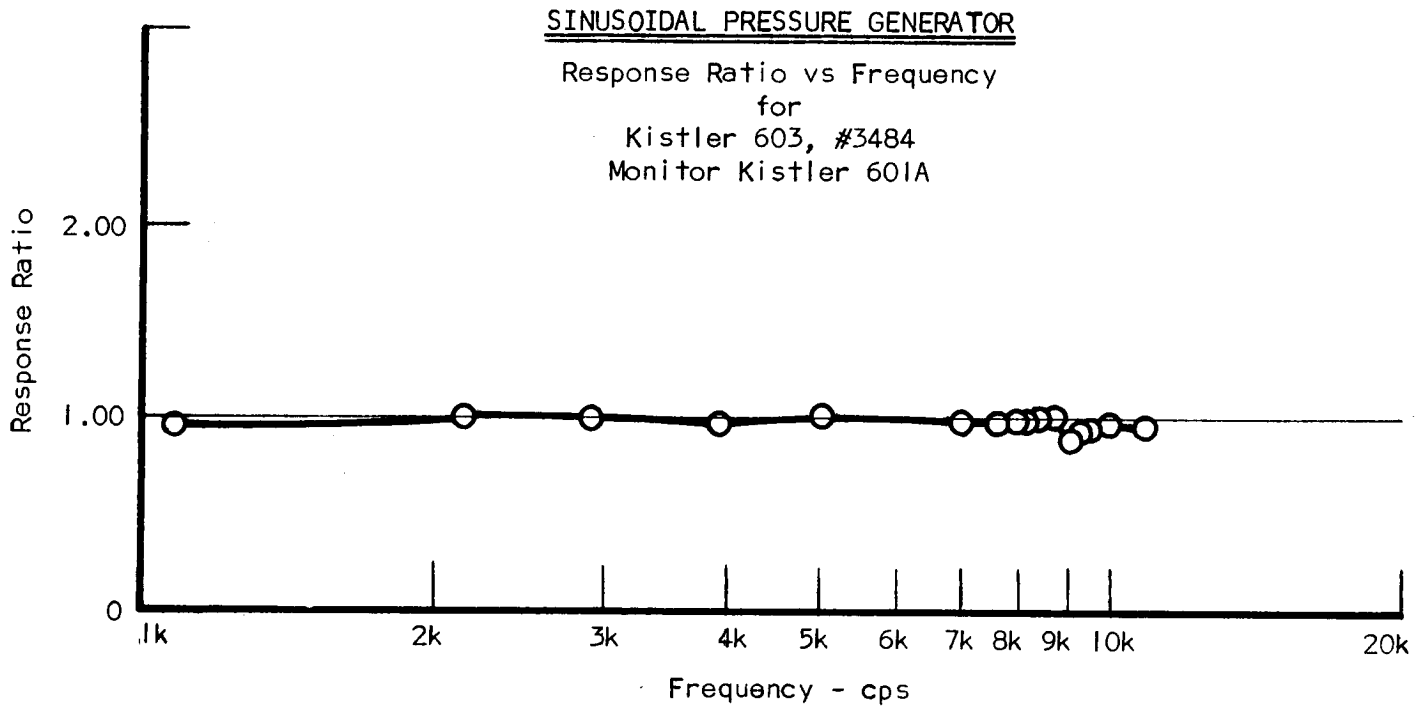


FIGURE 48

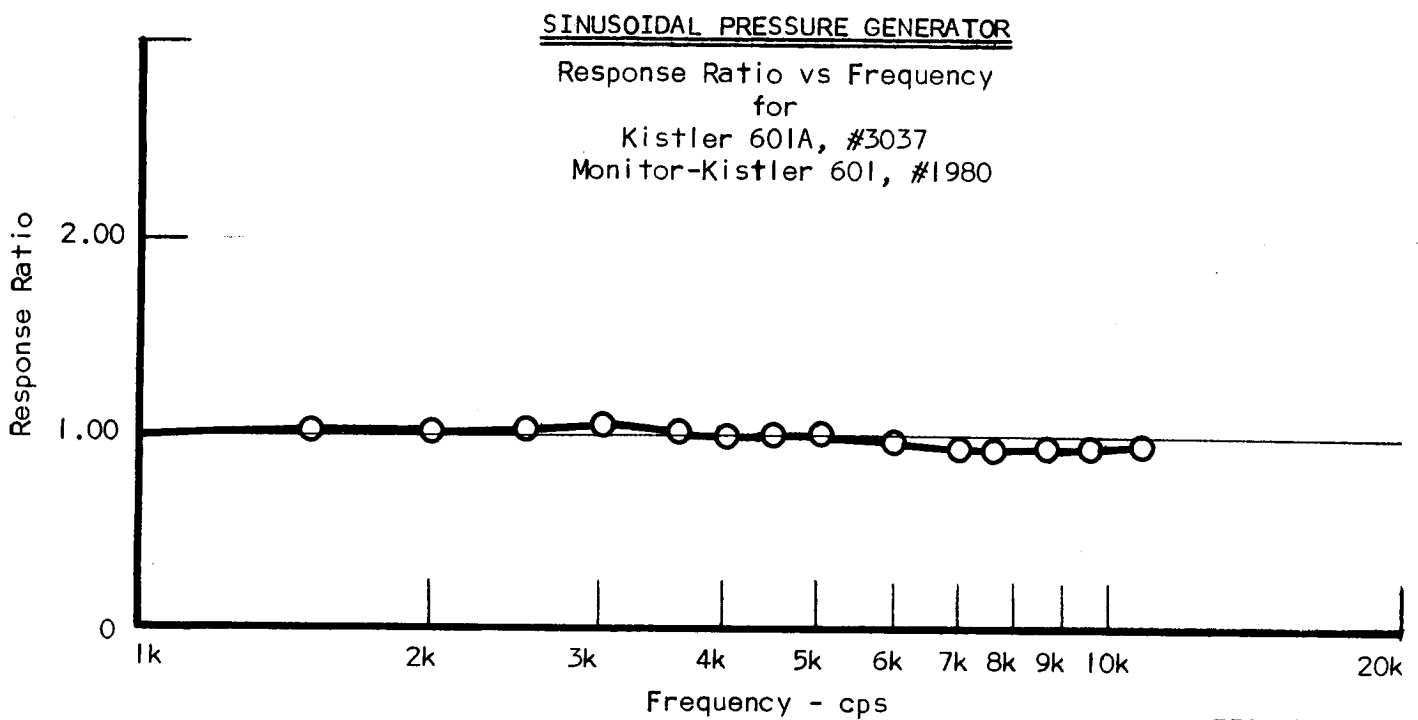


FIGURE 49

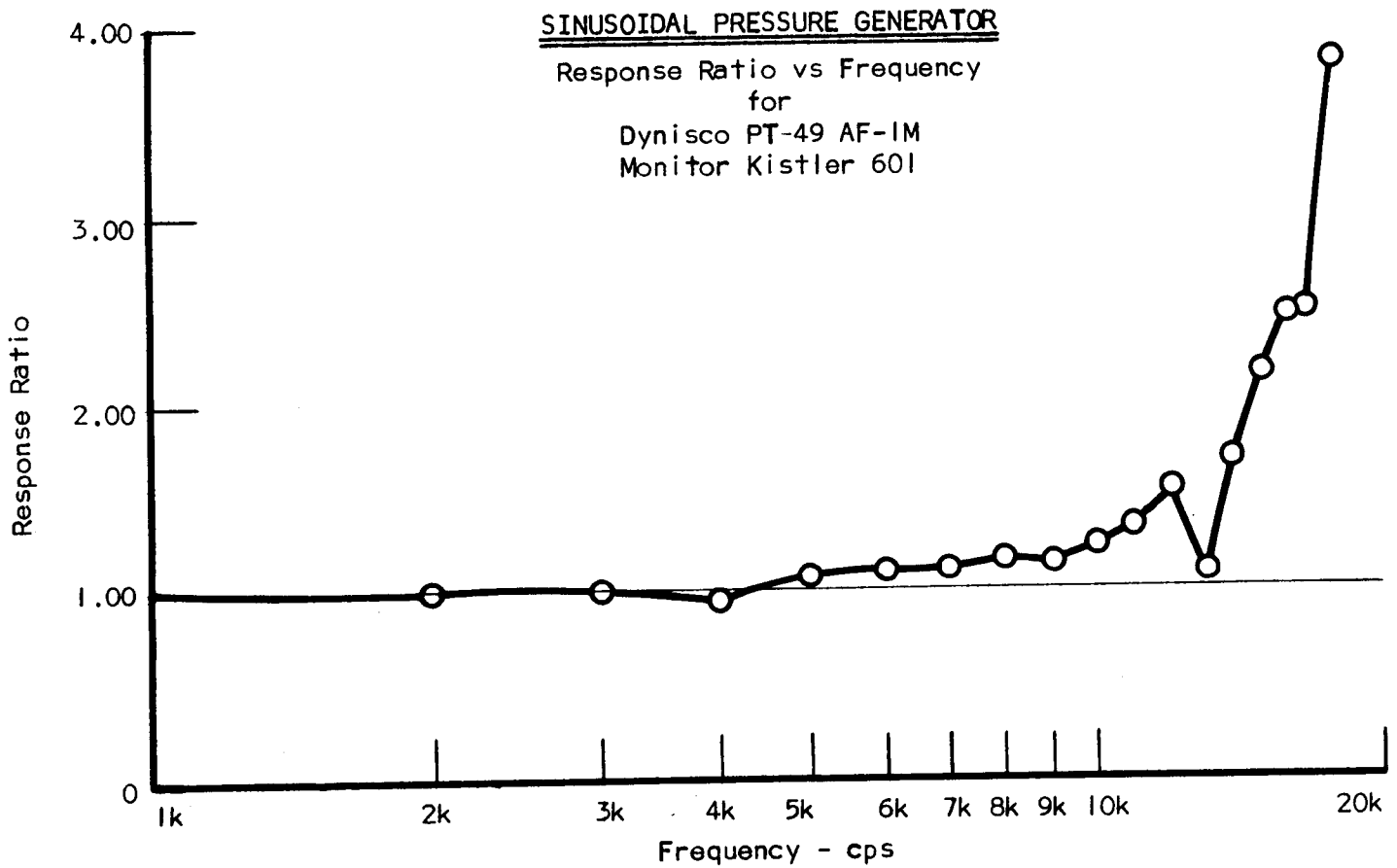


FIGURE 50

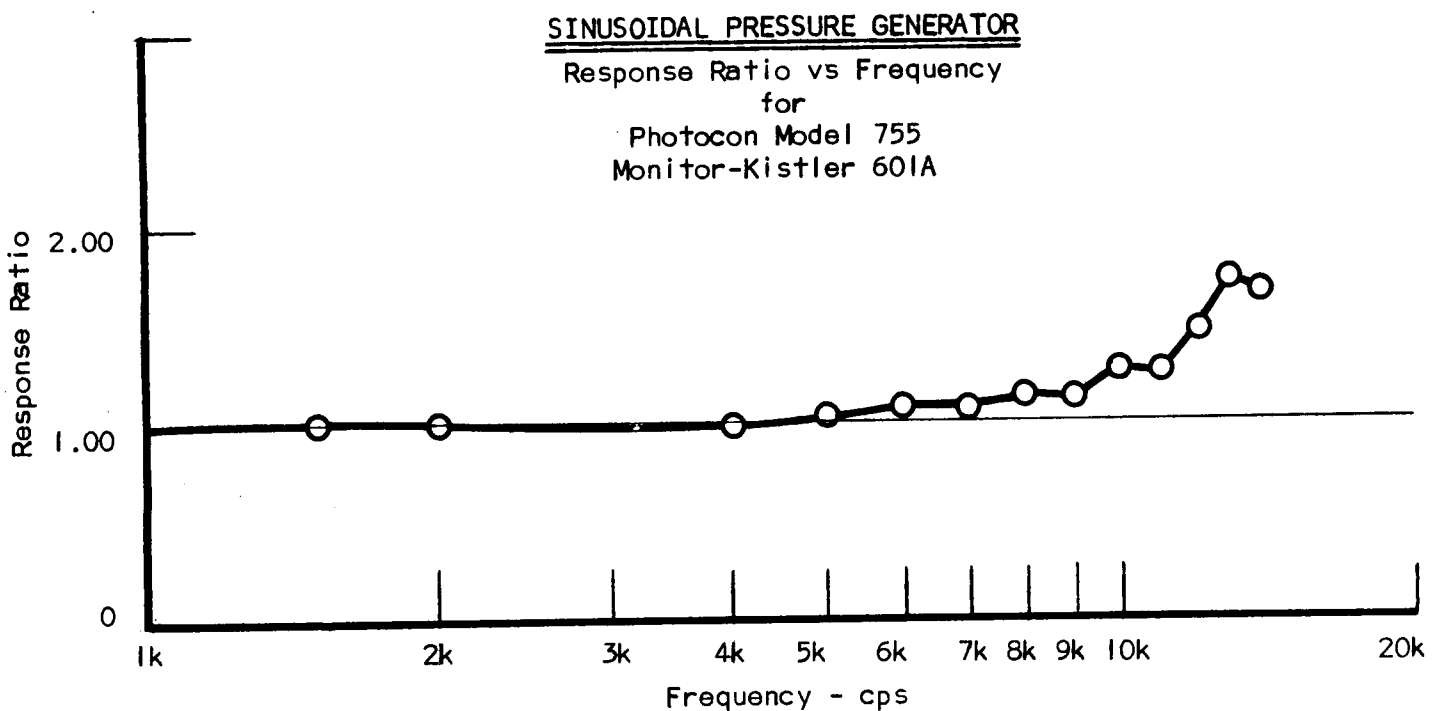


FIGURE 51

V. ROCKET COMBUSTION CHAMBER TESTS

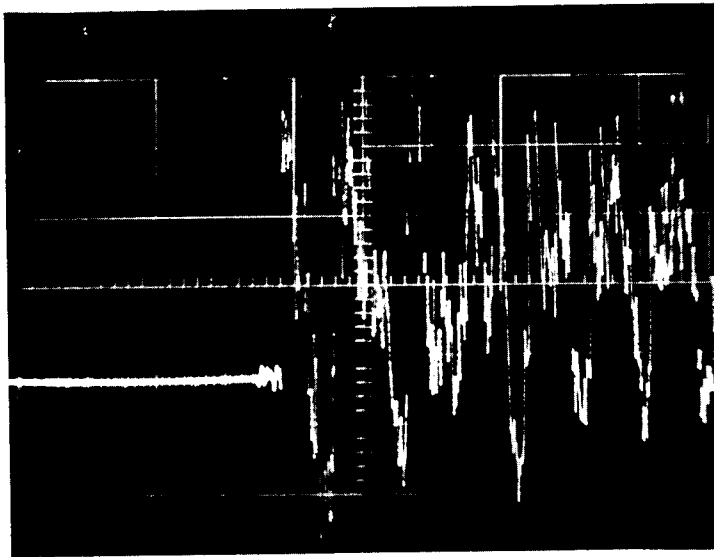
An investigation was conducted in order to confirm that the various transducer characteristics as determined in the laboratory testing would predict actual performance in a liquid propellant rocket engine.

Two experimental liquid propellant rocket motors, the principal one consisting of a 4-inch cylindrical length and 9-inch inner diameter, the other a 2 11/16 inch square chamber of variable length were utilized in the investigation. A pressure pulsing mechanism was incorporated into the side of the combustion chamber to induce various modes of oscillation in the motor. A Mauser action was used to fire a 404 caliber cartridge inside the pulsing mechanism. When the pressure built up to a preselected value, a disc separating the gunpowder charge from the chamber ruptured permitting a high pressure wave to pulse the chamber.

Transient pressure transducers were mounted in the side wall opposite the pressure pulsing mechanism so that the wave induced by the pulse impacted directly on the transducer diaphragm. The pulse mechanism could be used with either a cold rocket run, with the exit nozzle closed off or with the rocket motor in stable operation. Operating conditions could also be adjusted to induce the combustion chamber to become unstable as it was pulsed.

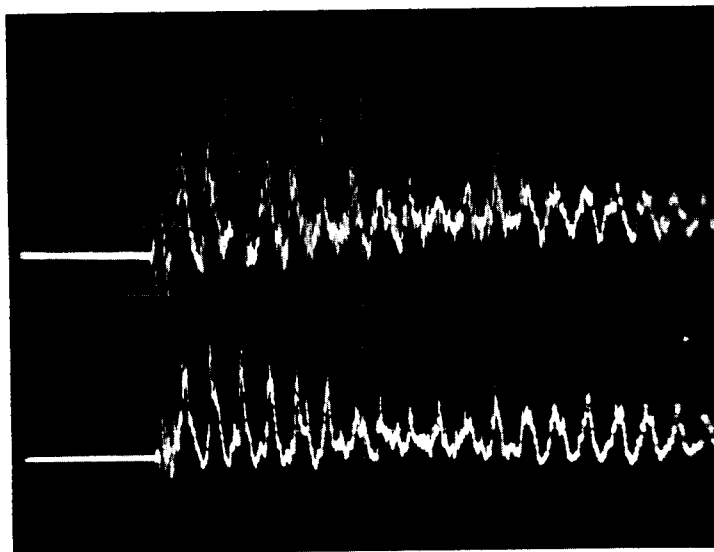
Photographs of oscilloscope records of several different test runs using Dynisco PT-49 and Kistler 601A transducers are shown in Figures 61, 62 and 63.

CYLINDRICAL ROCKET CHAMBER COLD RUNS



The first tangential frequency of 1200 cps is the predominant frequency. Superimposed on the trace is the natural frequency of the Dynisco PT 49. Sweep 1 msec/cm. Run XA-15.

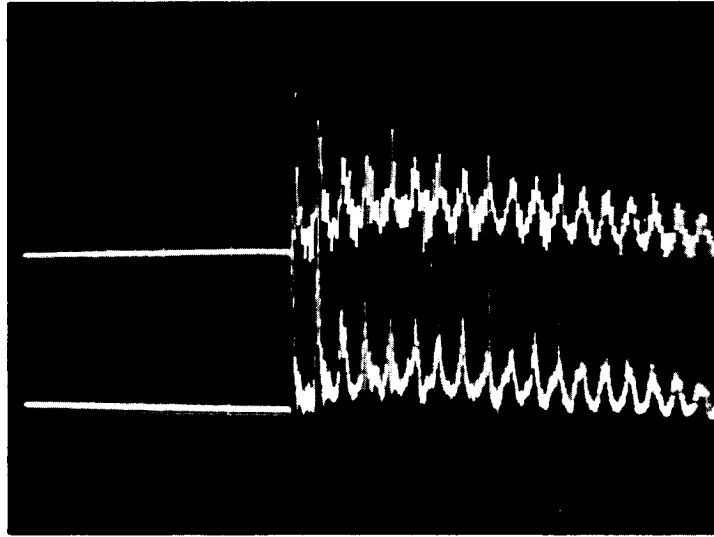
FIGURE 61a



Dynisco PT 49 compared with Kistler 601A transducer, both show the predominant frequency of about 1200 cps. The natural frequency of the transducer plus harmonic frequencies of the chamber are superimposed on each trace. Shows a need to filter out the natural frequency of the transducers. Sweep 2 msec/cm. Run XA-18.

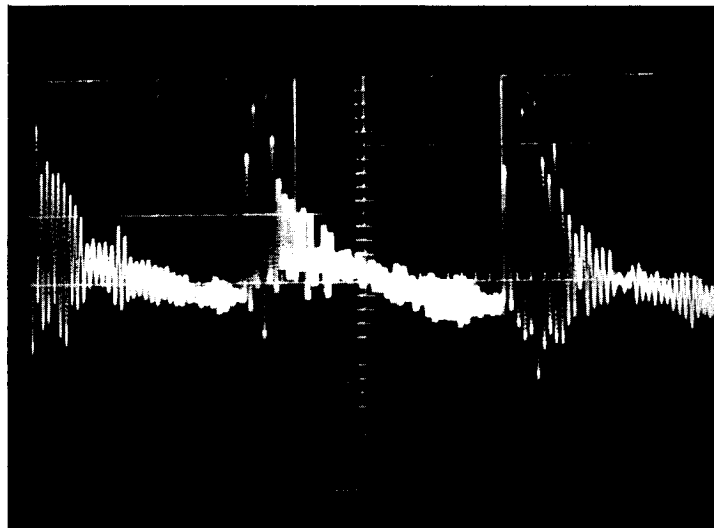
FIGURE 61b

HOT RUNS OF ROCKET COMBUSTION CHAMBERS



Cylindrical motor hot run shows predominant freq. ≈ 3000 cps. Dynisco PT 49 (top) compared with Kistler 601A. Run X-952.

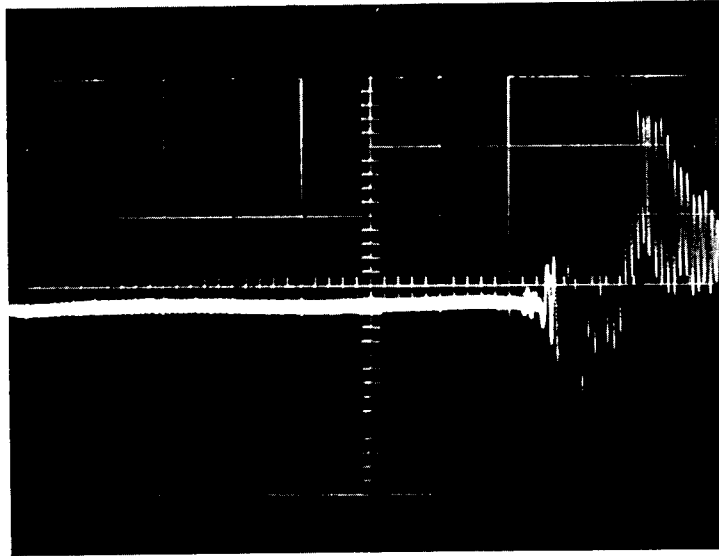
FIGURE 62a



Square motor hot run Dynisco PT 49 predominant freq ≈ 500 cps which is the longitudinal mode of oscillation. The natural frequency of the Dynisco $\approx 22,000$ cps is superimposed on the waveform. Run B-3123.

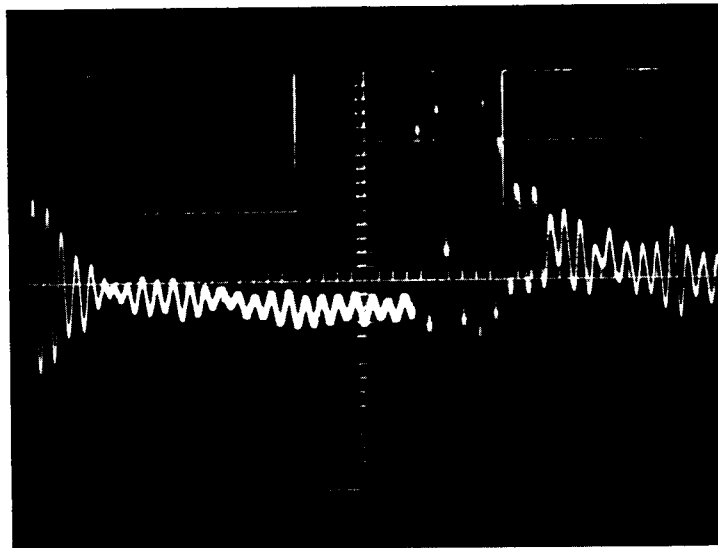
FIGURE 62b

SQUARE MOTOR TEST RUNS



Dynisco PT 49 transducer shows initial steady operation of square motor then pulsed by gunpowder charge. Slow response to pulse shows that shock wave does not form. Sweep 500 μ sec/cm. Run B-3119.

FIGURE 63a



Dynisco PT 49 transducer showing waveform .5 milliseconds after initiation of gunpowder charge to pulse the combustion chamber. Sweep 200 μ sec/cm. Run B-3122.

FIGURE 63b

VI. DISCUSSION OF RESULTS

A. Shock Tube

From the investigation to determine the merits of the helium-to-air shock tube as an appropriate facility for testing transient pressure measuring systems the following items are significant.

From the experimental data and theoretical analysis by others, it has been seen that the shock tube produces a pressure level increase which closely approximates a step function and has a rise time of about 10^{-9} seconds. Such a reproducible input is more than sufficient to shock-excite any transient pressure measuring device suitable for use in rocket motor applications.

Operating the shock tube at the tailored interface condition gives the sharpest step with the least distortion, and most important, it provides a constant pressure level following the passage of the shock wave. This enables a precise high pressure dynamic evaluation of a transducer even though it may be poorly damped and have a low natural frequency. Prior to utilization of the tailored interface condition, only the transducers with high natural frequency that were well damped could be evaluated accurately.

The use of springs to suspend the shock tube in the axial plane considerably reduces the ground shock effect. Using rubber and plastic "O" ring seals in adaptors and transducer mounts whenever possible serves to further isolate the system under test from the unwanted interference from ground shock.

An interesting fact noted during evaluation of a Kistler 601A was the lack of any noticeable noise or interference on the trace of the transducer side mounted and tested while extending 1/16" into the tube,

flush with the tube, and recessed 1/16". All of the traces appeared to be identical except for a small variation in amplitude. This indicated the transducer was not responsive to sidewise acceleration or vibration effects.

The photograph of the oscilloscope trace provides directly the rise time, natural frequency, and damping for the transducer being tested. Unfortunately, the analysis of the waveform of the trace to obtain the frequency response is most complicated and requires either tedious and time-consuming methods or expensive and sophisticated methods such as the Flying Spot Scanner or optical scanner and IBM 7090 computer program. In this respect the sinusoidal pressure generator is extremely useful. The SPG is simple to operate, much cheaper and faster than the complicated shock tube method of obtaining frequency response. Unfortunately, the SPG is limited to frequencies less than 20,000 cps.

The ground shock tests conducted on the Kistler 601A and 603A mounted behind a one-quarter inch steel plate showed that the ground shock is a very small interference factor. The plate prevented the shock wave from impinging directly onto the transducer diaphragm. The transducer therefore was subjected only to the ground shock which is transmitted through the metal of the tube. The limits of the precision with which the photographs of the oscilloscope trace are taken prevents determination of the ground shock effect on any conventionally shock tube tested transducer. The fact that the amplitude of the ground shock is one-fortieth as strong as the amplitude felt when the normal shock wave impinges on the diaphragm of an end mounted transducer permits disregarding the ground shock effect.

Ground shock is particularly more important and becomes a significant factor when conducting side-mounted tests, since then the amplitude differs by a factor of ten.

The ground shock effect in the side is more obvious because only the incident shock is felt by the transducer. This pressure step is only about 80 psi, whereas the pressure step at the end mount at the tailored interface is about 400 psi.

The ball drop testing of transducers appears to provide almost the same photographic results as the shock tube. Natural frequency, damping, and frequency response which are determined show a remarkable similarity to that of shock tube evaluations. Rise time was not obtained. However, through the use of a photocell or triggering device to sense the arrival of the ball just prior to impact on the transducer diaphragm, the rise time could be obtained. The ball drop method is restricted to transducers having a flat, flush-type diaphragm. It is not possible to use the ball drop on a transducer with a catenary type diaphragm or one with spiral cooling passages. The ball drop evaluation of transducers proves to be simple and inexpensive compared to the shock tube method of determining dynamic response. This method can be recommended to users of flat diaphragm transducers who do not have shock tube facilities available for testing.

The sinusoidal pressure generator, since it is a gas flow throttling device, requires a transient pressure measuring transducer for use as a standard to give the true conditions in the chamber. This monitor transducer must be capable of high frequency response and should be linear over the 20,000 cps frequency range of the SPG. The

Kistler series 601, 601A and 603A were investigated for monitor use because of their natural frequency around 150,000 cps, high linearity, and repeatability. The Kistler one-quarter inch diameter diaphragm was also most desirable. From an analysis of the resultant shock tube frequency response curves obtained by end mount, side mount, and ball drop the transducer showing the best linearity to more than 20,000 cps was the Kistler 601A. This transducer was selected for use as monitor in all SPG work.

The Benson-Lehner Optical Scanner and IBM 7090 computer method of analysis of the frequency response of a transient pressure measuring system appears to be quite good. The results of this program were verified by the magnetic drum wave analysis of a Kistler 601 at the National Bureau of Standards. Several comparisons with frequency response curves obtained by the Flying Spot Scanner were also made and found to be quite comparable for a given transducer type. The disadvantage of the method, is, of course, its inherent expense and complicated method of data reduction. Once the computer program is established it becomes a simple procedure to read and punch the coordinates of the waveform, but several errors appear in the reading of the waveform. The least of these is the human error in mispositioning the crosshairs of the optical scanner over the waveform. The biggest error comes from the Polaroid photograph of the oscilloscope trace. It is not possible to avoid an error in the data reduction due to distortion by magnification of the photograph expanded trace width, and the inherent 2-3% error in the optical scanner's print out of the coordinates from the magnified photograph.

Other possible errors arise from the fact that the computer

program presupposes a perfect step function input by the shock tube. This error is deemed insignificant in comparison to the error involved in reducing the data from the photograph. All of these errors of course are compounded and appear as sharp oscillations in the frequency response curves especially at the higher frequencies or those approaching the natural frequency of the transducer.

By using a fast film strip camera to photograph the oscilloscope trace and doing a detailed graphical analysis of the waveform to obtain the coordinates one could obtain better accuracy for the frequency response. This is, however, an expensive and time-consuming process and is not deemed advisable. The magnetic wave drum analyzer and Flying Spot Scanner could also be recommended, however, it is felt that the most economical, convenient and fastest frequency response can be obtained directly from the Princeton Sinusoidal Pressure Generator over the range 200 to 10,000 cps.

Side mount testing in order to more closely approach the conditions occurring in rocket motor research and to investigate the propagation of disturbances along the diaphragm of the transducer is subject to a smaller pressure step than is the end mount testing. Since a transducer cannot be mounted in the side exactly at the end of the shock tube so that the reflected wave and incident wave hit at the same time, the tailored interface condition cannot be used. Only a transducer with an extremely small diaphragm could take optimum advantage of this effect in a side mount.

The side mount therefore has a longer rise time than the end mount, because of the time required for the shock wave to pass along the face of the diaphragm. The problem is further complicated

because the pressure step is not as well-defined a step function as is the end mount. The computer program evaluation of frequency response is therefore less accurate unless a ramp function input is used instead of a step function.

The natural frequency may be accurately ascertained from the side mount, but the rise time and the damping differ considerably from the end mount evaluation.

Of interest is the fact that the rise time was about 50% higher for the side mounted transducers regardless of the diaphragm diameter when tested at $M_5 = 3.6$. A kistler average rise time was found to be 2 μ sec for end mount versus 3 μ sec for side mount. A Dynisco PT-49 average rise time was found to be 10 μ sec for end mount versus 15 μ sec for side mount.

It has been noticed that a wide diaphragm transducer such as the Dynisco PT-49 is subjected to varying pressures as a disturbance or shock wave passes along its diaphragm. In order to better analyze the mechanism of this variation further shock tube testing coupled with a more comprehensive computer analysis should be made.

The miniaturized thin film gauges used to obtain temperature profile in the shock tube and to trigger the oscilloscope sweep were extremely useful in the shock tube work. The gauges as described in Appendix B are easy to manufacture, have an extremely fast response, and are very convenient to use. The miniaturized version has a small profile, can be contoured to fit the curve of the tube wall, and will fit in any standard Kistler 601A installation or adaptor.

Dual end and dual side mount operations were useful in

providing a monitor transducer trace on each photograph of a shock tube test run. This proved advantageous in checking the operation of peripheral equipment such as charge amplifiers and cables. The dual mount served as a basis for comparing previous test runs for shock strength and velocity and for verifying the consistency of shock tube procedure and operation.

B. Princeton Sinusoidal Pressure Generator

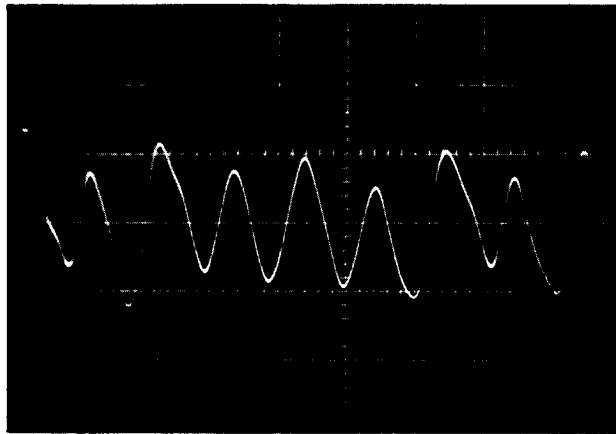
1. Chamber Response

Chamber response of the SPG with nitrogen gas can be seen from Figures 40 and 41. Nitrogen was used as the gas for this test in order to bring some of the chamber resonant frequencies within the range of interest. The resonant frequency of a given mode varies directly as the speed of wave propagation in the flow medium. Since the speed of wave propagation in nitrogen at room temperature is relatively low, the resonant modes are also relatively low. Chamber response can be determined from the pressure fluctuation amplitude in the chamber. Theoretically, the pressure fluctuations will decrease with frequency and when plotted versus frequency, the curve will have the form of an inverse hyperbola. At resonant frequencies, the amplitude of the pressure fluctuations will increase. Figure 40 shows the peak-to-peak pressure fluctuations measured on a transducer mounted along the curved side wall of the chamber. Since in theory as developed by Carwile in Reference 6, an end mounted transducer in the SPG will not respond to tangential modes, but a side mounted transducer will, this transducer should indicate the tangential modes. It can be shown that two distinct peaks at the high frequency end of the plot are caused by tangential modes.

The first peak occurred at 9580 cps. The curve representing the output with the filter set wide, that is, to filter below 100 cps to eliminate 60 cycle noise, and to filter above 40,000 cps to eliminate high frequency noise and the transducer natural frequency, shows the greatest increase in amplitude. The filtered curve representing output of the transducer with the filter cut-off frequencies set at $2/3$ and $3/2$ of the fundamental or driving frequency to eliminate harmonics shows very little increase in amplitude in this region. This indicates that the peak is caused by harmonics. Calculations show that for a gas temperature of 62°F , which represents a typical measured chamber gas temperature, the theoretical second tangential mode frequency is 18,800 cps. This peak, which appears at 9580 cps, is actually due to the second harmonic of the driving frequency which is 19,160 cps. Reasons for the discrepancy in frequency will be discussed in a later section. This phenomenon occurs in linear systems (39). Further evidence that this peak is due to the second tangential mode is found in the fact that there is no disturbance at this frequency in the monitor output since the monitor is end mounted. See Figure 41. A picture of the waveform at this frequency also points out that the peak is due to the second harmonic of the driving frequency. This picture is found as Figure 54a. Note that the waveform shows evidence of large harmonic content, as it is non-sinusoidal, and that the frequency is 19,100 cps, which is the second harmonic of the driving frequency.

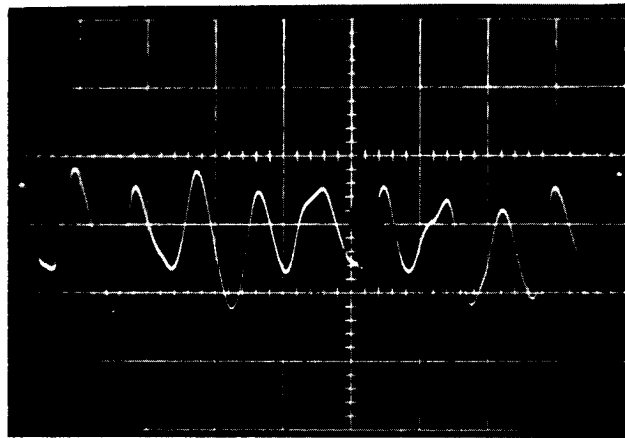
The second peak of the output occurs with the filter set wide at the frequency of 11,300 cps. This peak is due to the second harmonic of the driving frequency. The theoretical first radial mode

CHAMBER RESPONSE WITH NITROGEN



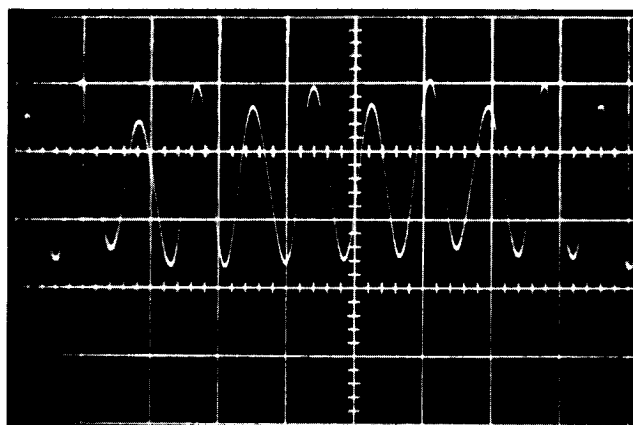
Top mounted Kistler 601
9580 cps
Sweep - 50 μ sec/cm

(a)



Top mounted Kistler 601
11300 cps
Sweep - 50 μ sec/cm

(b)



Monitor Kistler 601
11700 cps
Sweep - 50 μ sec/cm

(c)

is approximately two times this frequency at a frequency of 23,600 cps. Again evidence that this peak is due to harmonics is shown from the outputs which are more closely filtered and have very little if any increase in amplitude at this frequency. The waveform picture, Figure 54b shows high harmonic content and a frequency of approximately 23,550 cps. In this case the monitor shows an increase in amplitude in this region. This would be correct for a radial mode which will affect an end mounted transducer if the transducer radius is less than the chamber radius.

The peak in output with filter set to pass the fundamental and to filter harmonics shows an increase at 11,050 cps. This is evidently from the first tangential mode which has a theoretical frequency of 11,310 cps.

The monitor output as shown on Figure 41 shows one relatively large region of greatly increased amplitude. Since there are no resonant frequencies in this region that will cause an end mounted transducer to respond, this must also be from a harmonic. As pointed out previously, the first radial mode has a theoretical frequency of 23,600 cps. The center of the peak occurs at a frequency of 11,700 cps and the second harmonic of this frequency evidently excites the first radial mode. The waveform picture as shown in Figure 54c verifies the fact that the second harmonic is the dominant frequency. The frequency indicated by the picture is approximately 24,000 cps.

It is of interest at this time to compare the experimental and theoretical values.

Mode	Theoretical Frequency	Experimental (from top mounted transducer)	Experimental (from monitor)
1st Tangential	11,310	11,050	N.A.
2nd Tangential	18,800	19,160	N.A.
1st Radial	23,600	22,600	23,400

In general, the experimental values are lower than the theoretical values. The only direct comparison is found in the case of the first tangential mode. All others were found from harmonics of the driving frequency. Any error made in measuring the driving frequency would then be carried through and multiplied by a factor of two or three depending on which harmonic excited the resonant mode. There are several possible reasons for the difference between the theoretical and the experimental values.

The first possible reason is a direct error in frequency measurement. The frequency is measured by an electronic counter which counts cycles for a set period of time and then displays this number. If the short time interval is used, which is 0.1 second, the frequency displayed is only accurate to 10 cycles per second. If a longer time interval is used, 1.0 second, the frequency displayed is only an average value for the 1.0 second interval. These errors are normally not very large.

Another problem arises because of changing frequency. Because of economical reasons, it is desirable to keep gas flow time to a minimum. The usual method of obtaining data is to adjust frequency without flowing gas. When the frequency has stabilized to the desired value, the gas is allowed to flow and the instruments are read. The difficulty is that the frequency will decrease when the gas is allowed to flow because the gas causes the wheel to slow down a slight amount. The technique employed is to adjust the frequency initially to a level slightly higher than desired. This allows for the decrease which occurs when the gas is turned on. Since it is impractical to allow the frequency to completely stabilize before taking the readings, the frequency

must be read while it is changing, although this rate of change may be rather low. Since the electronic counter gives an average value, another small error may be introduced, although the effect of this small error may be large at low frequencies.

When searching for the frequency at which a maximum amplitude occurs, another technique must be used. In this case, the gas must be turned on and the frequency changed while observing the output of the transducer. When the maximum occurs, the frequency and the output must be recorded. Since this method requires that the frequency be changed to search for the point of maximum amplitude, it will most likely be changing as it is recorded. Again, a small error may be introduced.

Another possible source of error is in the theoretical speed of sound. As the theoretical resonant frequency is directly proportional to the speed of sound, any error here would cause a corresponding error in the theoretical frequency. Experimental values from the National Bureau of Standards were used when available.

An error in temperature could also cause an error in the speed of sound. It was found experimentally that the gas temperature decreases as the gas flows. This is due to the fact that the gas expands from a high pressure source to a relatively low pressure and is cool from the expansion process. Initially, the tubing through which the gas flows will tend to warm the flow to room temperature, but as the flow continues, the gas and tubing tend to reach an equilibrium temperature. Therefore, the temperature, speed of sound, and resonant frequencies are all decreasing as the gas flows. This effect tends to make the actual resonant frequency different from the theoretical. However, it takes a large error in temperature to make a

significant difference in frequency since the frequency is proportional to the square root of absolute temperature.

In Maslin and Moore it is shown that a strong transverse wave has a lower frequency than the corresponding acoustic frequency (40). Calculations to the first order were made for the case of the first tangential mode and a difference of only 14 cps was found. At very large amplitudes of pressure fluctuations, this difference may become more significant.

The chamber response to frequency was also checked using helium as the gas. The results of this test are included as Figure 42. When using helium, the lowest resonant mode is about 33,000 cps for room temperature (6). It would be expected that there would be no major amplitude increases from resonant frequencies or from harmonic effects in the frequency range at 1000 to 10,000 cps since the harmonics greater than the third are very weak. The experimental data verified this conclusion. The plot of peak-to-peak pressure fluctuations versus frequency is smooth throughout this range. It can be seen that the monitor and the side mounted transducer were at the same pressure throughout this range which demonstrates that the chamber is at uniform pressure throughout this range when using helium.

Figure 43 shows a series of waveform pictures taken at various frequencies with helium in the chamber. The pictures were taken at supply pressures of 120 psia and 360 psia. The upper trace is the monitor output and the lower trace is the output from the side mounted transducer. Comparison of the two traces indicates that there are no resonant modes due to driving frequency or harmonics of the driving frequency in this frequency range. Since the lowest mode is the first

tangential mode, it would appear as a major amplitude difference between the monitor and the side mounted transducer. The two outputs are in the same proportion throughout. This also indicates that the chamber is at uniform pressure throughout this frequency range.

The pictures also demonstrate that the ratio of noise to signal increases with frequency. However, most of this noise can be filtered out when the upper cut-off frequency of the variable band pass filter is set at 20,000 cps. The output when filtered to pass only the driving frequency is very close to sinusoidal form.

In order to compare the waveform of the SPG output to a sinusoidal waveform, a picture of the output when filtered to pass the driving frequency only and a generated sinusoidal waveform from a signal generator was taken simultaneously on the oscilloscope. These pictures are shown as Figure 47. It can be seen that the filtered output may be considered to be sinusoidal for all practical purposes. The phase relationship of the two waveforms has no significance.

2. Chamber Pressure

The original inlet installed on the SPG was 0.083 inches in diameter. It was found that this inlet was too large to choke in combination with the fixed outlet geometry. In the theoretical model of the SPG, the inlet and outlet areas are related to reservoir pressure and average chamber pressure. In order to have positive choking of the inlet and outlet the maximum chamber pressure must have the following relationship to the supply pressure which is assumed equal to the reservoir pressure (29):

$$(P_{\text{chamber}})_{\text{max}} = P_o \left(\frac{2}{\gamma+1} \right)^{\frac{\gamma}{\gamma-1}}$$

A similar relationship between the minimum chamber pressure and atmospheric pressure must hold if the outlet is to be choked:

$$P_{atm} = (P_{chamber})_{min} \left(\frac{2}{\gamma+1} \right)^{\frac{\gamma}{\gamma-1}}$$

The average chamber pressure must therefore lie some where between these two extremes since the chamber pressure will fluctuate above and below the average value. Maximum chamber pressure variation based on previous data and the theoretical model was used as a guide to determine the design chamber pressure for a given supply pressure. This pressure was then used to calculate the required inlet area. The calculated area represents a satisfactory figure for any anticipated supply pressure. The area calculated was equal to a circular area with a diameter of 0.055 inches.

When testing the new inlet, it was found that the pressures in the chamber were less than the theoretical. As the simplified model assumed isentropic flow in part, it would be expected that the actual pressure would be somewhat less than theoretical, but these pressures seemed excessively low. In the case of the test at 129 psia supply pressure, the measured average chamber pressure was 40 psia, and for a supply pressure of 255 psia, it was measured at 87 psia. The theoretical values for these two cases are 50.5 psia and 99.5 psia, respectively.

When a straight edged orifice is choked, an aerodynamic throat will be formed (41). This throat will be smaller in area than the actual cross-sectional area of the orifice, and in the case of the SPG, this reduction of inlet area would serve to reduce the average chamber pressure as can be seen from the theoretical relationship:

$$P_{avg} = P_o \frac{A_{in}}{A_{avg}}$$

According to the work of Weir, York, and Morrison in Reference 41, the ratio of effective area to actual area for a sonic orifice can be calculated from the following empirical relationship:

$$\frac{A_{\text{eff}}}{A_{\text{act}}} = 1 - 0.656 (D)$$

For this orifice, the ratio was calculated to be 0.963. Experimentally, the ratio was found to be 0.875. Some of the possible reasons for this discrepancy are: (a) the geometry of the inlet actually lies between that of an orifice and throat of a duct, and (b) the edge of the inlet was not a true square edge. However, the theory of the aerodynamic throat was proven to be at least qualitatively true, and approximately quantitatively true.

In order to eliminate this aerodynamic throat, the inlet was modified to a nozzle shape with a throat area equal to the previously calculated area corresponding to a diameter of 0.055 inches. The nozzle also has the additional advantage of being able to keep any shock structure in the divergent portion and out of the chamber where it might add to the noise level of the chamber. This can be done, at least in theory, by forcing the flow to shock well within the divergent section by proper selection of nozzle geometry.

The design of the inlet nozzle, which was to replace the constant area inlet duct, was governed by the following factors:

1. The throat area was given. It was to be the same area as the constant area duct inlet.
2. The total length was dictated by the length of the inlet plug.

3. The exit area of the nozzle was limited by the diameter of the inlet plug.

With these limitations in mind, the nozzle was designed to have a divergent section half angle of 11 degrees. This made the divergent section fairly long, about seventy five per cent of the nozzle length, which kept the theoretical shock well within the nozzle and well clear of the chamber. A convergent section half angle of 30 degrees was selected arbitrarily.

The design was checked to see if it would work properly under the expected chamber conditions. The criterion was theoretical shock position for expected chamber pressures. The maximum pressure would be average pressure plus one-half maximum peak-to-peak pressure fluctuation which occurs at the lowest frequency in the range of interest.

The theoretical check was performed by arbitrarily selecting an area ratio in the divergent section and assuming a shock at this station. Tables of compressible flow functions calculated for $\gamma = 1.667$ were used to calculate the conditions at the shock and the resulting conditions at the exit plane of the nozzle. The calculated conditions at the exit plane were assumed equal to the necessary chamber conditions required to cause the flow to shock at the selected area ratio and station. The results indicated that the theoretical shock structure would be well back in the divergent section of the nozzle.

The nozzle was rechecked in the same manner for flow with nitrogen by using tables for $\gamma = 1.40$. It was found to be satisfactory for nitrogen as well as helium. Other pressures were also considered and the nozzle was found to have essentially the same shock position

for the extreme chamber pressures.

Tests conducted with the nozzle inlet showed closer agreement to the theoretical values. Typical experimental values of average chamber pressure are as follows: for a supply pressure of 120 psia, 47 psia; for supply pressure of 240 psia, 84 psia; and for a supply pressure of 360 psia, 122 psia. Theoretical values calculated under the assumption that supply pressure is equal to reservoir pressure are 47 psia, 93 psia, and 140 psia, respectively.

One reason for this difference lies in the calculation of average outlet area. It was assumed that the outlet area varied sinusoidally which is not actually so. The actual variation approaches a sinusoidal variation but deviates from this in part of the cycle. The true variation has been calculated and can be found in Appendix D. Another factor complicating the outlet area variation is that the clearance between the body block and the rotating wheel was neglected in the calculations. This clearance can be measured when the wheel is not rotating, but cannot be accurately measured when the wheel is in motion. The clearance may vary with chamber pressure as the gas pressure on the wheel from the discharging gases increases with increasing chamber pressure. This pressure tends to force the wheel away from the body block increasing the clearance. Any increase in average outlet area will decrease the average chamber pressure. This can be seen from the theoretical relationship:

$$P_{avg} = P_o \frac{A_{in}}{A_{avg}}$$

Another reason for the difference between the theoretical and the experimental is that the supply pressure is not actually equal to the reservoir pressure of the gas. The supply pressure is adjusted

by a pressure regulator from which the gas flows through a fairly long length of tubing before reaching the SPG inlet. Pressure regulator error, pressure regulator gauge error, and losses in the tubing between the regulator and the SPG inlet could cause the actual reservoir pressure to be lower than indicated supply pressure. This would cause the average chamber pressure to be less than the calculated value using supply pressure for reservoir pressure.

In order to determine the relationship between pressure regulator supply pressure and actual reservoir pressure, a large cross section, large volume settling chamber was installed on the SPG immediately before the inlet. The cross section and volume of this settling chamber are very large compared to inlet throat area so that conditions in the chamber are in effect equal to the reservoir condition of the gas. The calculated Mach number in the reservoir was less than 0.01. The difference between indicated supply pressure and measured reservoir pressure would be a combination of regulator and regulator gauge error, and losses in the lines. Tests were run at several pressures and frequencies. Frequency had no effect as would be expected since the inlet was choked and the reservoir could not be influenced by downstream conditions. Pressure results are listed below.

Indicated Supply Pressure (psig)	Measured Reservoir Pressure (psig)
350	318
230	206
105	100

Using this data to recalculate the theoretical average chamber pressures resulted in much closer agreement between theoretical and experimental. Calculated theoretical values are now as follows: For

a supply pressure of 120 psia, 46 psia; for a supply pressure of 240 psia, 86 psia; and for a supply pressure of 360 psia, 129 psia.

Theoretically, the magnitude of peak-to-peak pressure fluctuation will decrease with pressure at such a rate that the plot of the magnitude versus frequency will be in the form of an inverse hyperbola. This can be seen from the theoretical equation developed previously.

$$P^*_{ff} = \frac{K_1 K_2}{\pi}$$

With the constants expanded fully, the expression is useful to determine the effects of changes of SPG characteristics, and to calculate the theoretical magnitude of peak-to-peak pressure fluctuations for a given set of operating conditions.

$$P^*_{ff} = \frac{1}{\pi} \left[\left(\frac{RT}{V} \right)_{\text{chamber}} \right] \left[P_{\text{avg}} \left(\frac{2}{\gamma+1} \right)^{\frac{\gamma}{\gamma-1}} \left(\sqrt{\frac{\gamma g}{RT}} \right)_{\text{outlet}} \right] A_{\text{avg}}$$

The constant was evaluated for three experimental tests and the theoretical curve as determined by this constant, and the experimental curve plotted together. Figures 44, 45, and 46 show the comparisons for supply pressure of 120, 240 and 360 psia, respectively.

Chamber volume can have an important effect on the magnitude of the pressure variation. An increase in chamber volume will cause a corresponding decrease in the magnitude of pressure variation. It is therefore very important to keep the chamber volume constant for all tests where the magnitude of the peak-to-peak pressure fluctuations must be accurately known. Chamber volume is determined from chamber length, which is fixed by the depth to which the test transducer is inserted in the SPG body block. This depth may vary from one test

to another unless carefully controlled. The reason that the depth can vary is that rubber O-ring seals or copper spark plug type washers are used between the test transducer and the SPG body block to seal the chamber. Thus the depth is determined in part by the compression of the seal. As the designed chamber length is small, 0.275 inches, a change of only $1/32$ of an inch would cause over 10% change in volume and a similar change in the theoretical magnitude of peak-to-peak pressure fluctuation.

The operating condition changed most easily is the supply pressure. An increase in supply pressure will cause an increase in reservoir pressure which in theory will cause a proportional increase in the magnitude of pressure variation. Experimentally, this was found to be true. In Figures 44, 45, and 46 it can be seen that the magnitudes of peak-to-peak pressure fluctuation at a given frequency are approximately in proportion to the reservoir pressure.

In general, there is good agreement between the theoretical and experimental curves. In each case, however, the theoretical curve has higher values at the low frequency end and slightly lower values at the high frequency end.

One possible reason for this departure from the theoretical is that real gas will have some inertial and viscous effects. The effect of these forces would be to reduce pressure fluctuations. This would make the theoretical curve higher throughout the frequency range.

Losses occurring in the flow process that were not considered in the theoretical model would also make the theoretical curve higher.

Another factor that would cause a departure from the theoretical is that area variation is not actually sinusoidal. The outlet

area is further complicated by the fact that the clearance between the body block and the wheel was not considered in the theoretical analysis, and that this space may vary with pressure. It was also assumed in the theoretical development that the mass flow rate through the outlet depended on the average pressure. In the real case it depends on the instantaneous chamber pressure. This would also cause some departure from the theoretical.

The above facts complicate an exact analysis, but since the general objective was to determine trends and effects of various changes of parameters, no further investigation was made for this report.

3. Transducer Evaluation

The method of evaluating a transducer in the SPG is relatively simple in theory. The output of the test transducer is compared to the output of the monitor both of which are measuring the pressure in the SPG chamber. In order to do this effectively, however, two basic requirements are: (a) the monitor output must accurately reproduce the chamber conditions, and (b) the pressure must be uniform throughout the chamber.

A Kistler type quartz crystal was used for the monitor in all evaluations. Early tests used the Kistler 601, and later tests used the Kistler 601A. The dynamic characteristics of both are essentially the same from 1 to 10 kcps. These transducers have a very high natural frequency. The Kistler 601A was found to have a natural frequency of 140,000 cps by shock tube tests. Static tests indicate that the transducer is linear within the recommended limits. Therefore, the Kistler 601A has the capability of accurately measuring

the chamber conditions. This includes pressure amplitude, phase angle and waveform.

Extensive tests were performed by Carwile (Ref. 6) which indicated that the pressure is uniform throughout the chamber as long as the driving frequency is below the lowest resonant mode. Tests during this investigation have extended this restriction to a frequency whose second harmonic is the lowest resonant mode. All tests indicate that the pressure in the chamber is uniform throughout when using helium and the frequency is in the range between 1 and 10 kcps.

If the pressure were not uniform it would be difficult if not impossible to make a valid comparison of the two outputs since it must be assumed that the transducers respond to the average instantaneous pressure over the diaphragm. With a uniform pressure throughout, the average pressure will be the same for each transducer regardless of size or shape of the diaphragm.

To compare the outputs, a nondimensional, normalized ratio is calculated. This ratio, called response ratio, is the ratio of the output indicated by the test transducer to the input. The ratio is calculated by first calculating the ratio of test transducer output to monitor output, and then normalizing by dividing by the ratio at a selected frequency. In the past the ratio at 1000 cps was selected under the assumption that the response ratio would be unity at this relatively low frequency which is well below both natural frequencies. However, it was often noted that this point did not always seem correct by inspection. The reason for this lies in the method in which data is collected. As noted before, it is not possible to read both outputs simultaneously, since both are read on the same indicating

instrument. Since the gas flow will cause the wheel to decelerate slightly, the frequency is decreasing when the gas flows. There is a short period of time needed to read the indicating instrument, switch to the other output and then read the instrument again. During this time, the frequency will change. It is at the low end of the frequency range that a change of frequency is most significant since the slope of the peak-to-peak pressure fluctuation versus frequency curve is the greatest at the low frequency end. Therefore a small change of frequency will make a large change in transducer output. The ratio of transducer outputs at 1000 cps is therefore subject to the greatest error due to frequency drift.

Because of this, it was decided that the ratio at a higher frequency where the slope is less should be selected as the normalizing ratio. The selected frequency cannot be too high since it must be assumed that the response ratio of the test transducer is unity at this frequency. The frequency decided upon was 2000 cps as this seemed a good compromise between the two criteria.

Typical evaluation curves, showing response ratio versus frequency, are shown as Figures 48 through 51. An error analysis of a typical instrumentation installation shows that the curves are subject to an error of 6%.

When evaluating a water-cooled transducer, it is essential that water be flowed through the system during evaluation. The dynamic characteristics of a transducer will be quite different with and without cooling water since the water adds mass to the system. In addition, the cooling water will affect the average pressure measuring capability of the transducer, by preventing thermal drift.

C. Comparative Testing

The response curves of transducers as evaluated by the shock tube and by the SPG were used as the basis for comparing the two methods. Both curves were plotted together for typical transducers. These curves are shown as Figures 55 through 58.

In general the agreement between the two methods was very good. The frequency range of primary interest was from 1 to 10 kcps, and the comparison should not be extended past this. In a few cases, where data was available and showed good agreement, the curves were extended for information only. The objective of the comparison was to compare the two methods of evaluation, not to pass judgment on any of the transducers as individuals, or as types.

Since the shock tube is generally accepted as providing an accurate means of evaluating the dynamic response of transducers, the SPG evaluations can be compared to these. It must be remembered that both methods have a certain degree of error, and that these may be of opposite sign at any particular point.

Figure 55 shows the comparison of the curves for the Kistler 603.

The two methods show practically identical data for the Kistler 601A, as shown on Figure 56. This is not too surprising since this transducer has such a high natural frequency that it would be expected to have a response ratio of unity below 10 kcps. Both methods verify this characteristic.

Excellent agreement was achieved when the comparison was made of the response curves for the Dynisco PT-49 AF-IM as shown in Figure 57. This data was extended to 18 kcps with good agreement throughout this range. In general, it should not be expected that all results would be

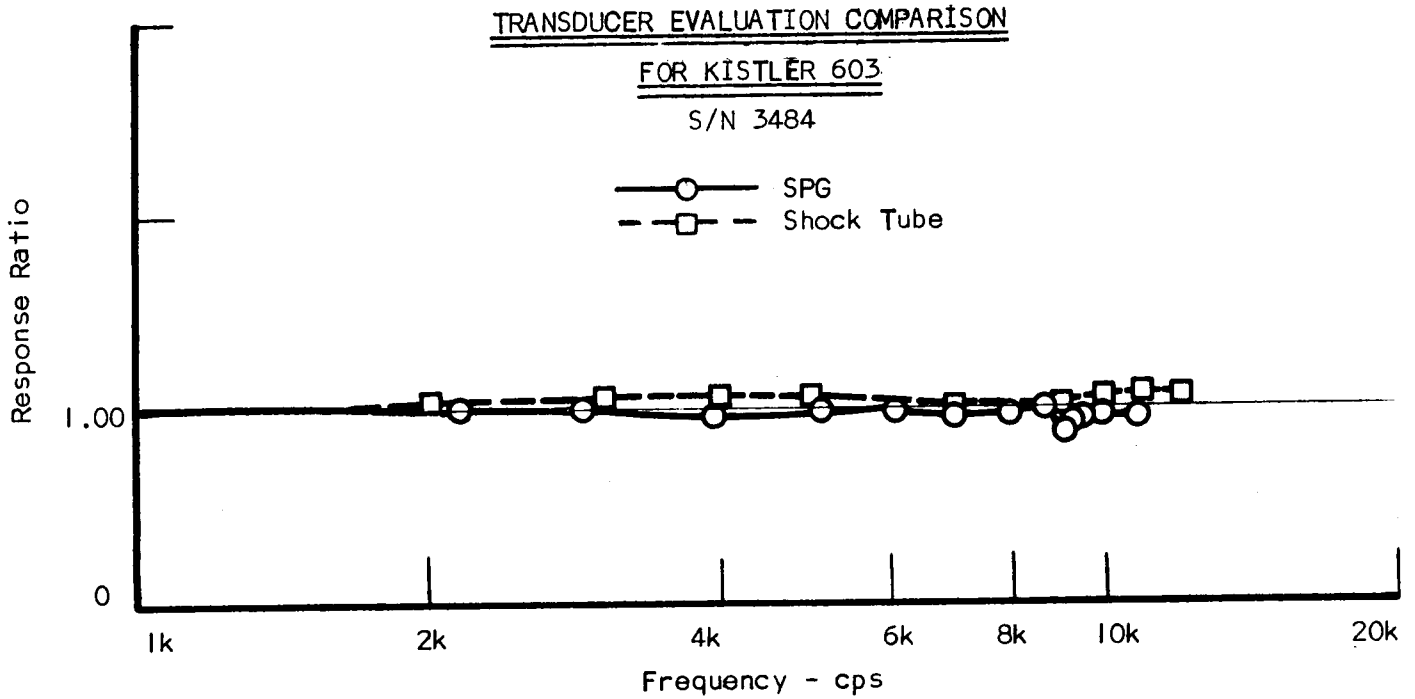


FIGURE 55

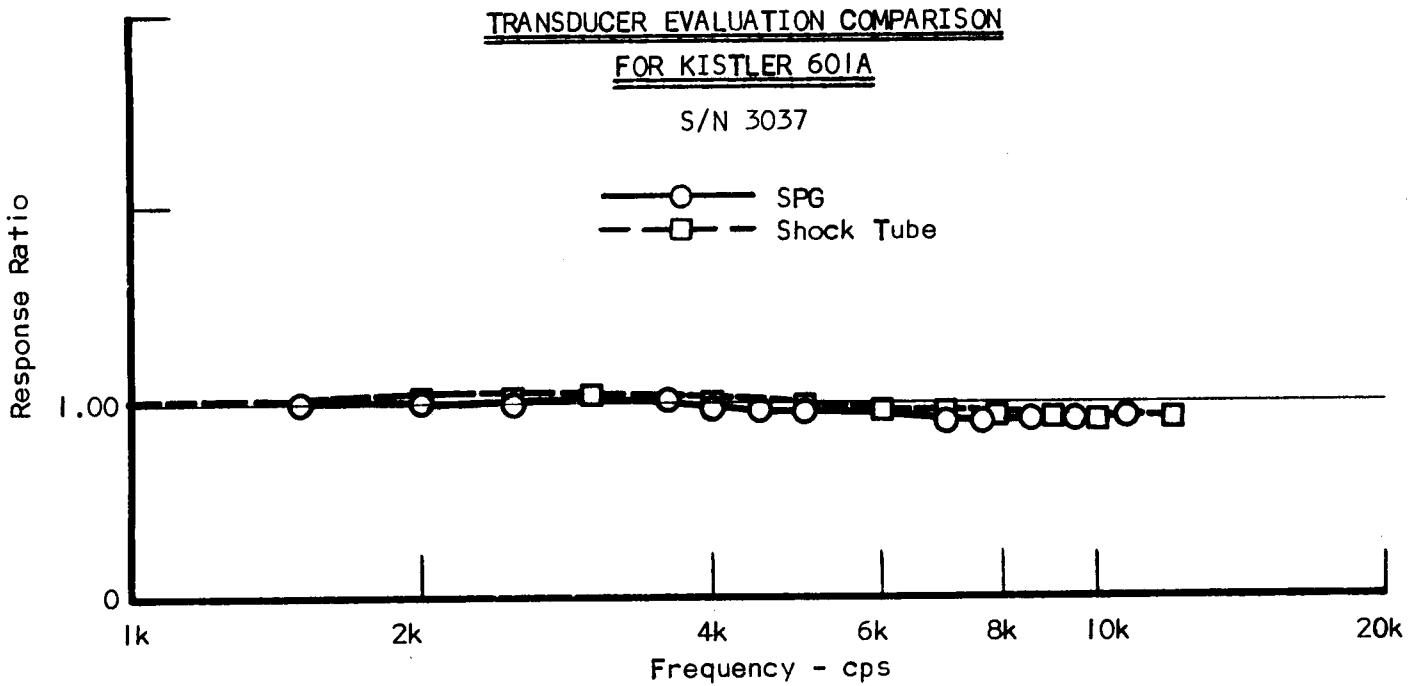


FIGURE 56

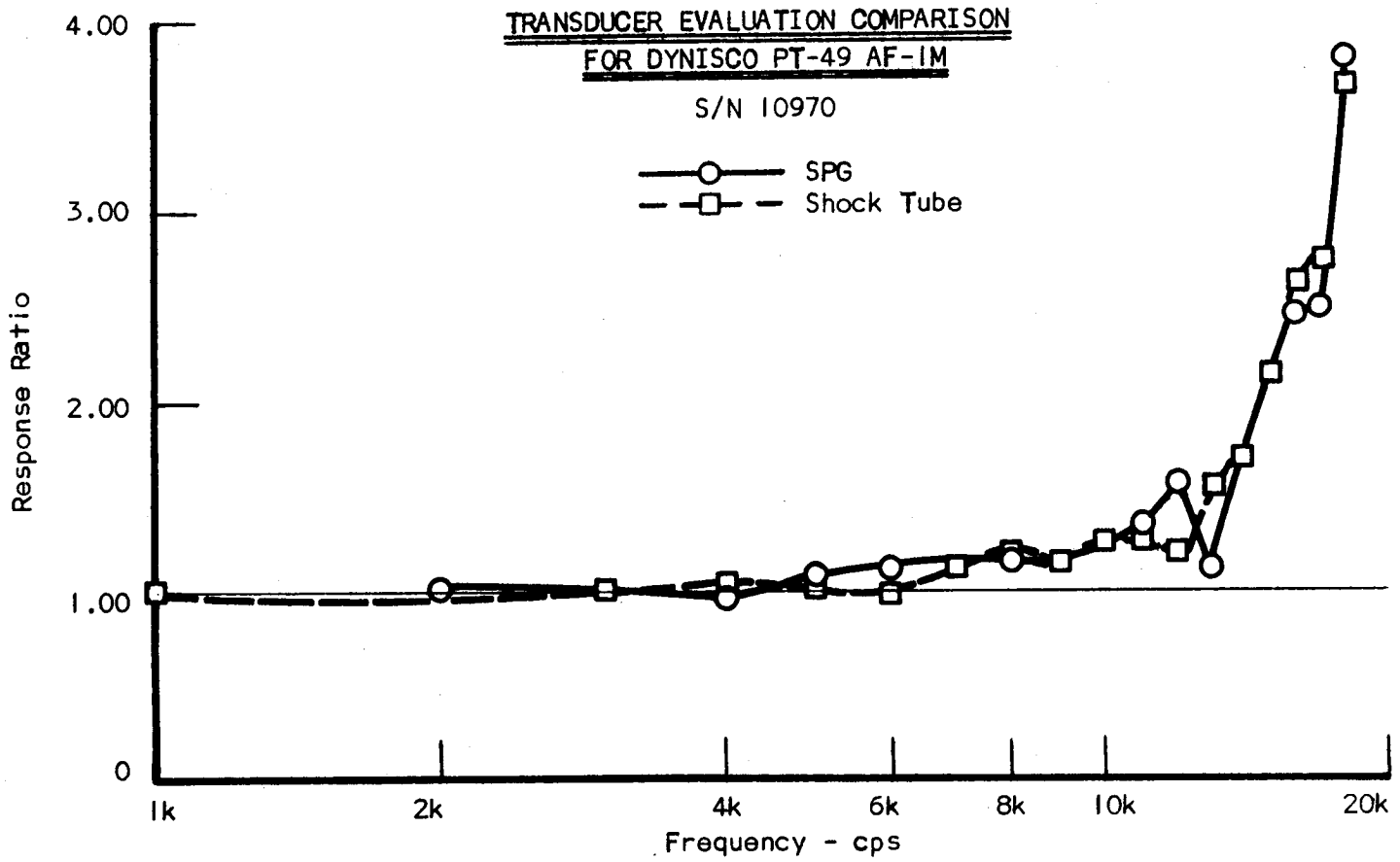


FIGURE 57

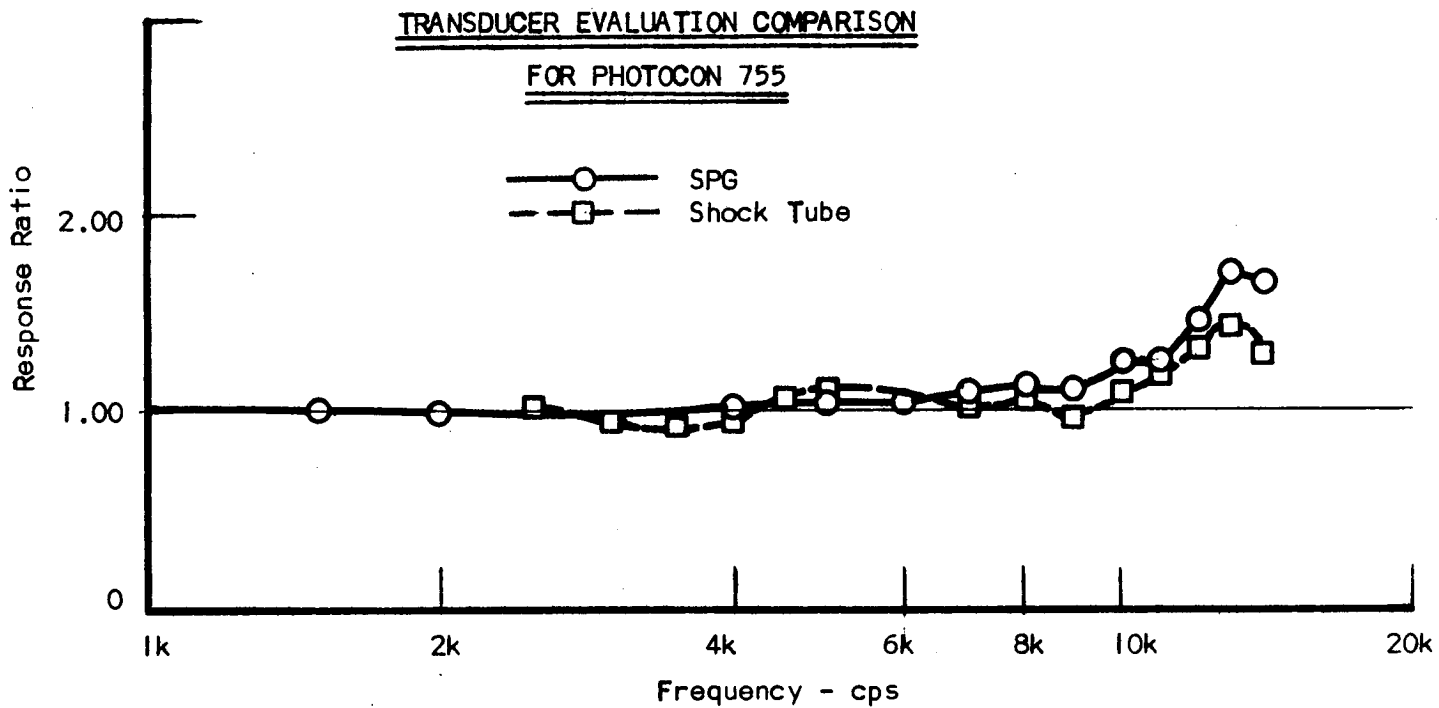


FIGURE 58

JP2 1707

this good, since the SPG is currently of primary use as a test device up to 10 kcps only. The data recorded past this frequency would be expected to show general trends, but could not be expected to give quantitative data.

Figure 58 shows the comparison for the Photocon Model 755. Again the curves show very good agreement especially below 10 kcps. The two methods show some deviation at 14 kcps but the trend is the same in each case. This is beyond the range of interest.

The comparisons indicate that the SPG gives very good results, especially below 10 kcps. The chief virtue of the SPG is, however, that the method offers a simple, convenient, and relatively inexpensive method of evaluating transducer dynamic response. This method gives direct results at least as good as the shock tube without the disadvantage of analytical treatment required in the shock tube method. Considering the tedious transformation of data involved in the shock tube method and the computer time required, the SPG is much faster and no doubt much less expensive. The equipment required is also much simpler and less expensive than that required for the shock tube.

D. Rocket Combustion Chamber Tests

Since the objective of this investigation was to determine the effect of transducer characteristics on performance in a rocket motor, each characteristic will be considered separately. First, however, a few general remarks are in order. The pulse in the experimental liquid propellant rocket engine is not abrupt enough to be a shock wave and hence the rise in pressure which the transducer output record shows is simply the pressure rise in the chamber as it is pulsed. Allen (Ref. 43) in his investigation of transverse waves in

a cylindrical chamber verified experimentally Maslin and Moore's (Ref. 40) thesis that transverse waves cannot steepen into shock waves. Because the waves are not shock waves they do not lend themselves to computer analysis of the frequency response as may be done for the shock tube tests. An attempt was made to obtain a first approximation of the frequency response in the rocket runs using a method similar to that employed in the optical scanner and IBM 7090 computer method, but the results of this analysis were not very satisfactory. Extreme difficulty is incurred in an attempt to analyze any photographic record in which filters have not been used, especially since many harmonics of the fundamental chamber frequency occur. The photographs, Figures 61 and 63, were so cluttered with higher frequencies that the optical scanner could not accurately read the photographs to obtain the necessary waveform coordinates. The only reasonable data obtained from the frequency response curves of the rocket runs merely pointed out the frequencies which could have been read directly from the photograph. The predominant frequencies obtained for the rocket test runs were always those of the chamber such as the first tangential mode for the cylindrical motor and the longitudinal mode for the square motor. The natural frequencies of the transducers are seen to be superimposed over the fundamental frequencies in the photographs and may be obtained directly from the trace.

Damping also is a function of the chamber and of the forces driving the chamber. Damping time to 1/2 amplitude in a hot run in the cylindrical motor was found to be in excess of 75 milliseconds; clearly the damping of the chamber.

Since the conditions within the combustion chamber vary throughout the chamber, transducer location greatly influences the response or the measurements obtained. Because of the variation of conditions inside the rocket chamber, a monitor transducer cannot be used to compare or evaluate the performance of another transducer as is done in the SPG and to a lesser extent in the shock tube.

Rise Time: Rise time is a measure of how quickly the transducer can respond to a driving force. As such it will have no effect on transducer performance unless the driving force oscillates faster than the transducer capability permits. This will occur when the period of the driving force oscillation is on the order of rise time. The measured rise time of the Dynisco PT-49 AF-IM was found to be 10μ seconds. Using conservative figures, the frequency limitation imposed by the rise time was calculated to be about 25,000 cps. For the Kistler 601A, the measured rise time was found to be 2μ seconds, and the frequency limitation was calculated in the same manner to be about 150,000 cps. In both cases the limitations were approximately equal to the transducer natural frequency and were well beyond the useful range of the transducers.

The frequency of the oscillations in the experimental rocket motor was known, from much previous experimental and theoretical work by other experimenters, to be about 1100 cps for the cold runs and about 3000 cps for the hot runs. Since the measured rise times were very small compared to the period of the driving force oscillations, the transducers would be expected to be capable of accurately following the driving force. In all cases, the predominant frequency measured by the transducers was found to be the known frequency, and was the same for both transducers.

Damping: If the transducers were critically damped, and a driving force impressed on the diaphragm, the output would show only the driving force pressure variation. If the transducer were underdamped, the natural frequency would be superimposed on the output waveform. In an extreme case, a transducer with very low damping would oscillate at the natural frequency with very little decay of amplitude. The transducers used in the tests showed fairly low damping factors in laboratory tests. Therefore it would be expected that the natural frequency of the transducers would be superimposed on the output waveform. This can be observed in Figures 61 through 63. Proper filtering will filter out the natural frequency and the resulting waveform is then much less cluttered and easier to interpret.

Phase Angle: Theoretically, a transducer operating well below its natural frequency will have a negligible phase angle between the driving force and output. SPG tests in the laboratory verified this fact. Since these frequencies are well below the transducer natural frequencies, it would be expected that there would be very little if any phase angle between the chamber pressure oscillations and the outputs. Experimentally, in the rocket motor, there was no measureable phase difference.

Waveform: The output waveform of the two transducers appeared to be slightly different. Part of this difference is due to the difference between the transducers natural frequencies. Since this frequency is superimposed on the output, it is quite apparent in the unfiltered records. See Figures 61 through 63. However, when the tape record is played back and recorded on the Visicorder, all frequencies above 10 kcps are filtered out. The resulting waveforms have the

natural frequency filtered out, but are still different in some respects. Minor peaks may occur in one and not the other. Generally, they are the same, but in detail, they are not. This is probably due to the difference in location in the experimental rocket motor. The combustion zone is concentrated within 2 inches of the injector face. Since combustion noise contains numerous frequencies, the transducer in this zone would be expected to have a different output waveform than the transducer outside the zone as is substantiated in Figure 62a in which the Kistler 601A was located 1 inch from the injector face and the Dynisco 3 inches from the face.

Response Ratio: It would be expected that the pressure variations would be accurately reproduced since the chamber frequencies were much less than the natural frequencies. Evaluations showed that both transducers had a response ratio of unity at the frequencies predominant in the chamber. The measured pressures were found to be different. In a typical test run the Kistler 601A output was 315 psi peak-to-peak pressure, and the Dynisco PT-49 AF-IM output was 245 psi peak-to-peak pressure. When the pressures were correlated with transducer location, the magnitudes were found to be correct. Reardon (Ref. 38) found that the oscillating pressures in this motor near the nozzle were smaller than those near the injector. The pressures in this case were in accord with his findings, and were found to be in the same ratio as his reported results. One reason for this difference in pressure oscillations is that there is an outflow through the nozzle which acts as an impedance and tends to reduce the oscillation near the nozzle. Another is that the combustion zone oscillations tend to be greater.

The high temperatures present in the experimental liquid propellant rocket motor were not present in the laboratory tests. It would be expected that these high temperatures would cause a zero shift which would affect the D.C. level of the transducer output, but would not affect the dynamic characteristics of the transducer. There were no changes in performance noted due to thermal effects, although there was no real attempt made to evaluate thermal effects. It is recognized, however, that neither the SPG nor the shock tube can provide the realistically high temperatures and heat flux conditions that are obtained in the experimental rocket thrust chamber. Continued research to evaluate transducer performance adjacent to the intense heat release of the combustion process as found in the experimental rocket motor should be pursued.

The transducers when mounted on the experimental rocket motor are also subject to vibrational disturbances which are not present in the laboratory testing. Again, no major effects were noted although there was no attempt made to measure these disturbances, or their effects.

VII. CONCLUSIONS AND RECOMMENDATIONS

The shock tube when operated at the tailored interface conditions, properly suspended to minimize ground shock and used with a non-frangible diaphragm to prevent damage to transducers under test is a very useful device to dynamically test end mounted transient pressure measuring systems. The shock tube is especially advantageous for testing those high response systems which have a natural frequency in excess of 10,000 cps. The natural frequency, damping, and rise time are readily obtainable from the photographic record of the transducer output when tested in the shock tube. Unfortunately, determination of the frequency-response from this photograph is laborious, time consuming and involves the use of sophisticated computational and electronic systems.

Ground shock becomes a significant factor in side mount testing. This effect can be minimized by judicious use of springs and rubber mountings. Side mount testing is not recommended because of this factor even though it more closely resembles rocket combustion chamber type mounting. End mounting provides a larger pressure step at a constant pressure level, a shorter rise time, and lends itself to more accurate analysis of frequency response by virtue of its more nearly perfect step function.

The ball drop technique gives an accurate natural frequency, damping, and frequency response in close agreement with shock tube results. It is limited to flat, flush diaphragm transducers.

Miniaturized thin film gauges are very effective in detecting passage of the shock wave and can be used to trigger electronic equipment for shock tube operation.

The expressions derived from the simplified model of the SPG are very useful as an aid in calculating correct operating conditions needed to achieve desired chamber conditions. They also make it possible to predict with reasonable accuracy the effect of changes in SPG geometry.

The SPG monitor, the Kistler 601A, has a very high natural frequency and is therefore capable of accurately measuring chamber conditions. The response ratio of this transducer as determined from shock tube and ball drop tests may be considered to be unity for frequencies well in excess of 10 kcps. This characteristic, coupled with the fact that the chamber is at uniform pressure throughout when using helium, up to at least 10 kcps, makes the SPG a most useful test device for testing the dynamic response characteristics of transducers. The SPG is particularly adaptable for testing flush mounted pressure transducers of the type used in liquid propellant rocket combustion chambers.

One of the greatest advantages of the SPG is its simplicity. It gives a direct evaluation with no tedious interpretations, or computer programs and does this with relatively simple instruments. The evaluations are obtained quickly and relative inexpensively.

Transducer characteristics as determined from laboratory testing had predictable effects on transducer performance in the liquid propellant rocket motor, which demonstrated the practicality and usefulness of transducer evaluations in the laboratory.

Recommended suggested areas for further research:

1. Refine data collection and evaluation

- a. Use strip film camera to obtain clearer, sharper

resolution and more cycles than on present photographic technique for shock tube and rocket chamber.

- b. Investigate wave phenomena across side mounted transducer in shock tube and rocket chamber to determine type of function to describe input to transducer for computer analysis.
- c. Develop photographic record reading technique to obtain higher degree of repeatability than with optical scanner.
- d. Modify IBM 7090 computer program to obtain direct print-out of frequency response curve.

2. Improve ball drop technique to obtain rise time measurements.

3. Investigate shock tube testing while subjecting transducer diaphragm to elevated temperatures to more closely simulate rocket combustion chambers.

4. Investigate shock tube operation at lower driver section pressures (but still at tailored interface) to conserve helium. Thinner aluminum diaphragms incorporating a breech type quick diaphragm change device can then be used.

5. Investigate the practicality of incorporating the features of the improved SPG as described in Appendix E in order to increase the frequency range and improve performance of the improved SPG. These would include:

- a. modification of the outlet
- b. use of heated gases
- c. use of a ratio meter or plotter to read the transducer outputs

6. Continue the comparison testing of transducers in rocket motors under varying conditions and relate the results of laboratory testing utilizing improved versions of the shock tube, sinusoidal pressure generator and other special devices designed to evaluate specific transducer characteristics.

APPENDIX A: References

1. Li, Y. T., Class notes MIT (unpublished).
2. Liu, F. F., "Evaluation of a High Frequency Dynamic Pressure Measurement and Analytical System for Rocket and Nuclear Propulsion Research," February (1961).
3. Bibliography & Index on Dynamic Pressure Measurement NBS Circular 558, Washington, D.C., 1955.
4. Jones, H. B., "Transient Pressure Measuring Methods," Aeronautical Engineering Report No. 595b, Princeton University (1962).
5. Inskeep, J., "Dynamic Testing of Pressure Transducers - A Progress Report," Technical Report No. 32-268 JPL CIT, December (1961).
6. Carwile, C. L., "An Analytical and Experimental Study of the Response of a Small Chamber to Forced Oscillations," Aeronautical Engineering Report No. 595d, Princeton University (1962).
7. Lederer, P. S., "A Simple Pneumatic Step-Function Pressure Calibrator," Report No. 6981, National Bureau of Standards, April 1959.
8. Schweppe, J. L., "Calibration of Pressure Transducers with Aperiodic Input-Function Generators," ISA Session Preprint Compilation 46.1.62 (15-18 October 1962).
9. Dykstra, J. D., "Evaluation of a Pressure Transducer Response with a Pressure Step Generator," Eleventh Meeting Bulletin JANAF Solid Propellant Rocket Static Test Panel (October-September 1962) SPIA-SPSTP/11.
10. Glass, I. I., "Shock Tubes - Part I. Theory and Performance of Simple Shock Tubes," Institute of Aerophysics, University of Toronto, UTIA Review No. 12, 1958.
11. Hall, J. G., "Shock Tubes - Part II. Production of Strong Shock Waves; Shock Tube Applications, Design and Instrumentation," Institute of Aerophysics, University of Toronto, UTIA Review No. 12, 1958.
12. Dolder, K. and Hide, R., "Bibliography on Shock Waves, Shock Tubes and Allied Topics," AD-127681 (Great Britain: Atomic Energy Research Establishment, 1956).
13. Glass, I. I., Martin, W. and Patterson, G. N., "A Theoretical and Experimental Study of the Shock Tube," Institute of Aerophysics, University of Toronto, UTIA Report No. 2, November 1953.

14. Smith, R. O. and Lederer, P. S., "The Shock Tube as a Facility for Dynamic Testing of Pressure Pickups," Report No. 4910, National Bureau of Standards, March 1957.
15. Wolfe, A. E., "Shock Tube for Gage-Performance Studies," Report No. 20-87, Jet Propulsion Laboratory, Pasadena, May 2, 1955.
16. Bitondo, D. and Lobb, R. K., "The Design and Construction of a Shock Tube," Report No. 3, Toronto, Institute of Aerophysics, University of Toronto, May 1950.
17. Vielle, P., Comptes Rendus, Acad. Sc. Paris, vol. 129, p. 1228, 1899.
18. Kobes, K. "Die Durchschlagsgeschwindigkeit bei den Luftsaenge- und Druckluft-bremsen," Z. Ost. Ing.-u Arch. Ver., vol. 62, p. 558 (1910).
19. Schardin, H., "Bemerkungen zum Druchausgleichsvorgang in einer Rohrleitung, Phy. Zeits., vol. 33, p. 60 (1932).
20. Payman, W. and Shepherd, F., "Proceedings of the Royal Society," A-186, p. 293, 1946.
21. Courant, R. and Friedrichs, K. O., "Supersonic Flow and Shock Waves," Interscience Publishers (1948).
22. Patterson, G. N., "Theory of the Shock Tube," NOLM 9903 (1948).
23. Fletcher, J. C., "Final Report on Shock Tube, Piezoelectric Gauges and Recording Apparatus," OSRD 6321 (February 1946).
24. Paskusz, G. F., "The Approximation Problem in the Analysis of Pressure Transducers," ISA Session 46.2.62 (15-18 October 1962).
25. Henderson, J. G., "Mechanical Harmonic Analyzer," Engineering, vol. 173, (January 1952).
26. Montgomery, H. C., "An Optical Harmonic Analyzer," The Bell System Technical Journal, vol. 17 (July 1938).
27. Penner, S. S., Harshbarger, F. and Vall, V., "An Introduction to the Use of the Shock Tube for the Determination of Physico-Chemical Parameters," Combustion Researches and Reviews, Butterworths Scientific Publications, London, 1957.
28. Lobb, K., "On the Length of a Shock Tube," Toronto University, Report No. 4, 1950.
29. Shapiro, A. H., "Compressible Fluid Flow," vol. I and II, Ronald Press, N. Y., 1953.
30. Yoler, Y. A., "Hypersonic Shock Tube," Cal. Inst. of Tech., Hypersonic Wind Tunnel Memo No. 18, Pasadena, California, July 1954.

31. Trimpi, R. L. and Cohen, N. B., "A Theory for Predicting the Flow of Real Gases in Shock Tubes with Experimental Verification," NACA Tech. Note 3375, March (1955).
32. Jones, J. J., "Experimental Investigation of Attenuation of Strong Shock Waves in a Shock Tube with Hydrogen and Helium as Driver Gases," NACA Tech. Note 4072, July (1957).
33. McAlevy, R. F. and Summerfield, M., "Research on the Ignition of Solid Propellants," Fourth Quarterly Progress Report, Aeronautical Engineering Report No. 433-d, Princeton University, June 1959.
34. McChesney, M., "Shock Waves and High Temperature," Scientific American (March 1963).
35. Wittliff, C. E., Wilson, M. R., Hertzberg, A., "The Tailored Interface Hypersonic Shock Tunnel," Paper presented at the ASME-ARS Aviation conference, Dallas, Texas, March 16-20, 1958. See also, Journal of the Aero/Space Sciences, vol. 26, no. 4, April 1959.
36. Ford, C. A. and Glass, I. I., "An Experimental Study of Shock Wave Refraction," University of Toronto, Institute of Aerophysics, UTIA Report No. 29.
37. Morse, P. M., "Vibration and Sound," McGraw-Hill Book Company, Inc. New York, 1948.
38. Reardon, F. H., "Combustion Instability in Liquid Rocket Motors - An Investigation of Transverse Mode Combustion Instability in Liquid Propellant Rocket Motors," Princeton University, Aeronautical Engineering Report No. 550, June 1961.
39. Den Hartog, J. P., "Mechanical Vibrations", Third Edition, McGraw-Hill Book Company, Inc., 1947.
40. Maslin, S. H. and Moore, F. K., "On Strong Transverse Waves Without Shocks in a Circular Cylinder", Journal of the Aeronautical Sciences, vol. 23, no. 6, June 1956.
41. Weir, A. Jr., York, J. L. and Morrison, R. B., "Two and Three Dimensional Flow of Air Through Square-Edged Sonic Orifices", Transactions of the ASME, April, 1956.
42. Baer, A. D., "Composite Propellant Ignition," Ph.D. Thesis, University of Utah, (March 1959).
43. Allen, W. D., "Experimental Studies of Transverse Waves in a Cylindrical Chamber," Princeton Aeronautical Engineering Report No. 607, Princeton, N. J.
44. McAlevy, R. F., "The Ignition Mechanism of Solid Propellants," Princeton Aeronautical Engineering Report No. 557, Princeton, June (1961).

45. Schauer, H. M. and Taylor, I. J., "A Dynamic Calibration Method for Piezo-Electric Pressure Gauges," UERD Report No. 4-51, Underwater Explosions Research Division, Norfolk Naval Shipyard (1951).

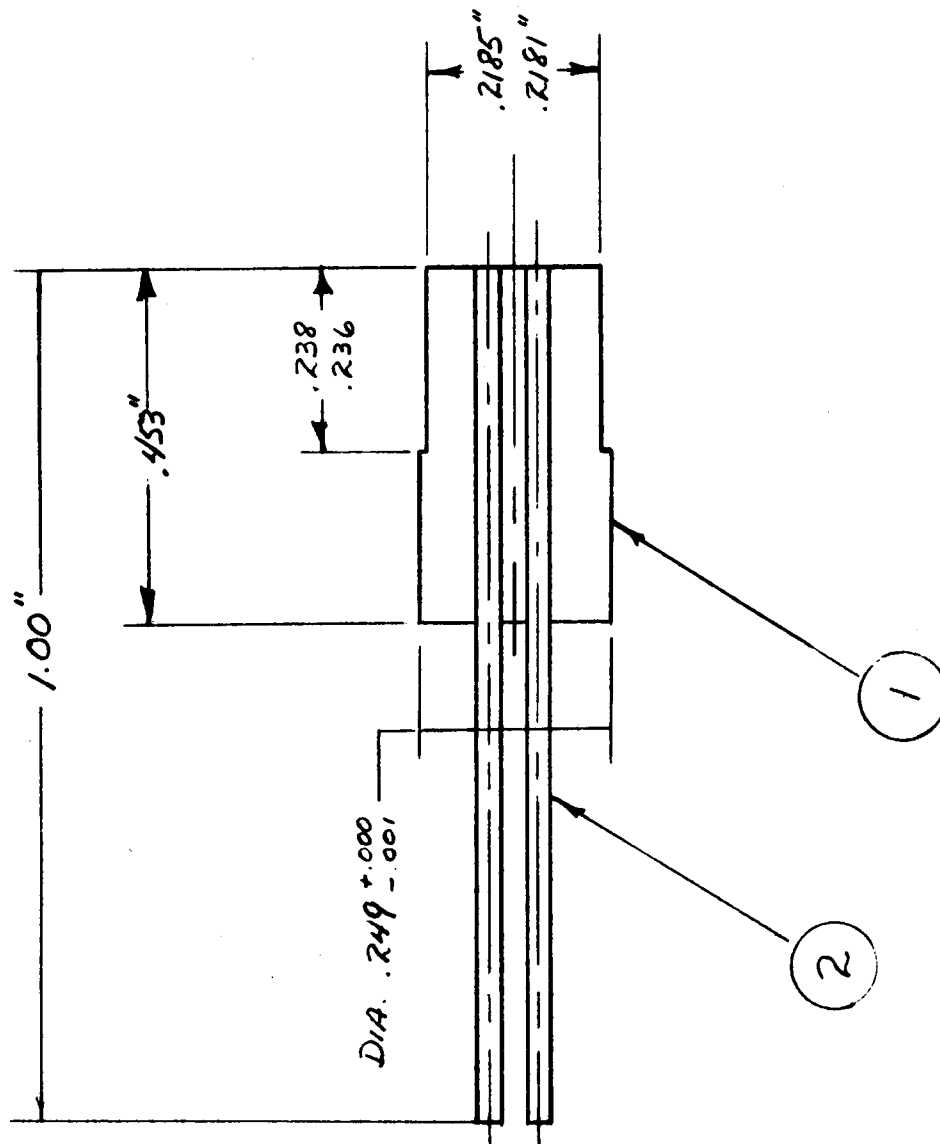
APPENDIX B: Development of Miniaturized Thin Film Gauges

As experimentation with transient pressure measuring systems in the shock tube became more sophisticated, a need arose for a device to sense the instant of shock wave passage. The photographic technique employed and the oscilloscopes and electronic counters used during this program required a simple, reliable triggering device in order to be actuated at the proper moment.

The thin film heat gauge has found wide application in the measurement of transient heating phenomena (Ref. 42, 44). These gauges are formed by painting the surface of pyrex with a suspension of platinum in an organic liquid (Hanovia Liquid Bright Platinum manufactured by the Hanovia Chemical & Manufacturing Company, Newark, New Jersey) and baking the element at a temperature high enough to drive off the organic component and leave behind the metallic film bonded to the pyrex. The pyrex is then cut into thin rectangular shapes, is inserted in a Kel-F plastic housing and soldered to the brass connectors imbedded in the housing. In an effort to develop closer tolerances and a cleaner surface on the inner wall of the shock tube for more accurate testing, the conventional size gauge about 5/16 inches in diameter was discarded because of its large size and because its design offered too much resistance to flow in the tube. A device capable of the same or even better response, yet small enough to fit in a Kistler 601A transducer mounting was highly desirable.

A new miniaturized thin film gauge was designed (See Figure B-1) and may be seen in Figure 33, a photograph, where it is dwarfed by the conventional large size gauge and may be compared to a Kistler 601A transducer. The miniaturized gauge was constructed of boron nitride

MINIATURIZED THIN FILM ASSEMBLY



.062" REAM FOR PRESS FIT
WITH PART NO. 2
2 HOLES

FIGURE B-1

(manufactured by the Carborundum Company of Latrobe, Penna.). Brass rods were press fitted into the boron nitride body and electrical connections soldered to the brass electrodes (See Figure B-1). The gauge was then placed in a type LCI-14B Laboratory Vacuum System (manufactured by Consolidated Vacuum Corporation of New York) which has a mechanical and a three stage diffusion pump and is capable of lowering the pressure from atmospheric to 2×10^{-6} mm of mercury. Several droplets of aluminum were vaporized by heating the tungsten electrodes in the vacuum chamber. Thus an aluminum film less than 1/10 of a micron thick was deposited on the face of the boron nitride element. The face of the element was masked to produce a rectangular film 3/32 by 1/32 inches. The average resistance of the film was about 2 ohms. A specially designed amplifier unit with a variable gain control to adjust the sensitivity of the device to stray electrical transients was used to amplify the signal output and feed a 10 milliamperere current to the thin film gauge. When the shock wave passes the thin gauge mounted in the side of the tube, the thin film gauge senses the impulsive passage of the hot gas in the wave by experiencing a jump in the film resistance. This provides a small, precise, step voltage rise across the circuit of the gauge. The rise time of the thin film gauge is less than one microsecond. Figure 12 shows a typical waveform output of the miniaturized thin film gauge as it is tested in the side and end of the shock tube at $M_s = 3.6$.

APPENDIX C: Step Function Generation by Balldrop Technique

In an effort to investigate and evaluate the usefulness of the shock tube for dynamic response testing of transient pressure measuring systems, a simple method of generating a step-function input was sought. Needed was an input of predictable shape and amplitude in a time sufficiently short to excite the transducer under test in order to obtain a record of transducer response.

The transducer to be tested was mounted in an adaptor which positioned it firmly upright. Dropping a 0.132 gram, 1/8 inch diameter steel ball bearing from a height of 3 inches onto the transducer diaphragm supplied to step input. An oscilloscope with camera attachment was used to obtain a photographic record of the trace of the transducer response.

This concept, although used by researchers during the early phase of liquid rocket engine development, was abandoned in favor of more sophisticated testing techniques. An interesting device employing a similar technique for testing piezoelectric pressure gauges employed in underwater explosion research was developed by Shauer and Taylor in 1950 (Ref. 45). This device subjected the gauges to be tested to pressure pulses produced by a falling weight, which drove a piston into a water-filled chamber. The gauge output was then recorded and compared with the record obtained from a reference gauge.

The balldrop technique employed in this report was considerably less involved than the device of Schauer and Taylor and was limited in application to testing only those transducers with flat, flush design diaphragms as on the Kistler 601A, 603 and the Photocon model 755, etc.

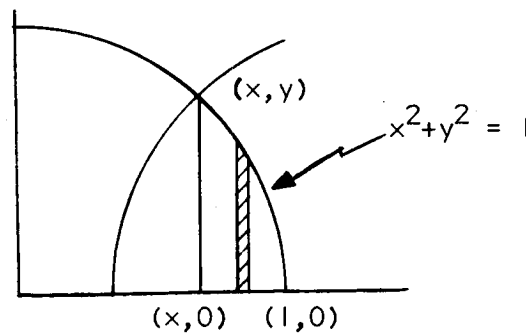
Transducers with corrugated or inconsistent structure of the diaphragm for cooling passages could not be tested by the ball drop technique because the response to the impact of the ball was not uniform across the face of the diaphragm. As an example, the analysis of the photographic trace of a Kistler 601A subjected to ball drop provided much of the same data as that received from shock tube tests. The natural frequency of 150,000 cps obtained directly from the photograph was almost exactly equal to that of the shock tube test. The damping to half amplitude of $\delta = .010$ also compares closely with that of the shock tube of $\delta = .0122$. Unfortunately, the rise time could not be obtained by the impact. An effort to use a photocell to sense the arrival of the ball bearing prior to impact and to act as trigger for the sweep was not successful. Further analysis of the ball drop photographic trace by the optical scanner and IBM 7090 computer program provided a frequency-response curve as seen in Figures 29 to 32. It can be seen that the response is linear far beyond the range of a comparable shock tube test, which lends considerable credence to the belief that the shock tube imposes a certain degree of ground shock and noise interference on the true transducer frequency response. An investigation of shock tube ground shock was conducted by mounting the same Kistler 601A immediately behind a 1/4 inch steel plate and subjecting the transducer to the ground shock which travels through the metal while the shock wave was kept from impacting directly on the transducer diaphragm. The frequency response of these tests as in Figures 27 and 28 substantiates the apparent interference inherent in shock tube testing.

The ball drop technique, by virtue of its simplicity and

convenience is highly recommended for use when shock tubes or other sophisticated testing devices are not available.

APPENDIX D: Sinusoidal Pressure Generator Chamber Outlet Area Variation

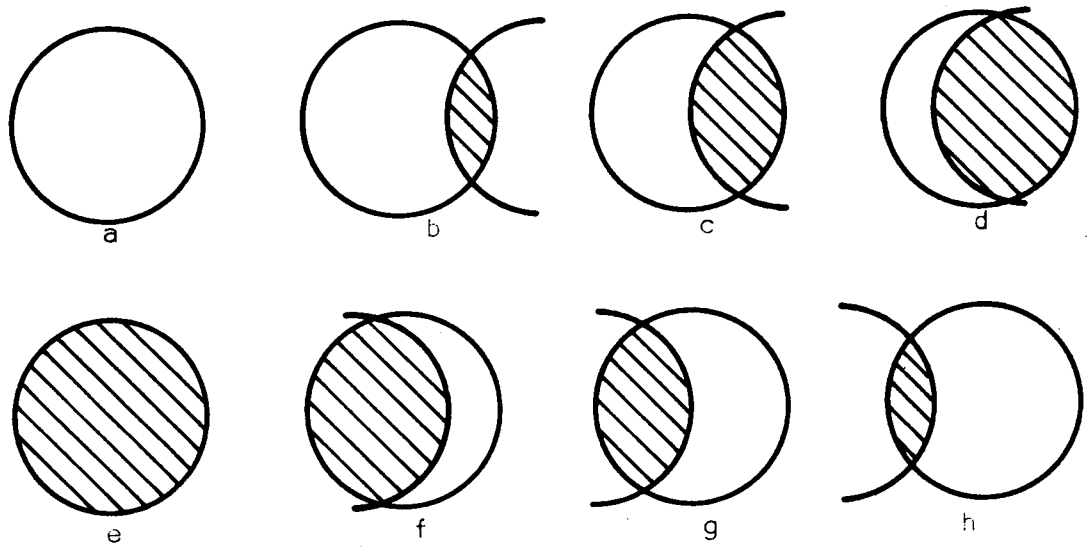
The actual outlet area of the SPG is the area common to two equal radius circles. The circles represent the outlet in the block and the hole in the wheel. The area is varied as the hole in the wheel rotates past the outlet in the block. The sequence is as shown in Figure D-1. The area at any instant may be calculated as shown below.



For convenience, consider two circles of unit radius. The area common to both circles is:

$$\begin{aligned}
 A &= 4 \int_x^1 y dx = 4 \int_x^1 \sqrt{1 - x^2} dx \\
 A &= 4 \left\{ \frac{1}{2} \left[x \sqrt{1 - x^2} + \sin^{-1}(x) \right] \right\} \Big|_x^1 \\
 A &= 2 \left[\frac{\pi}{2} - x \sqrt{1 - x^2} - \sin^{-1}(x) \right]
 \end{aligned}$$

Time variance may be introduced by calculating the area at various values of x , corresponding to the path of one circle past the other (wheel rotation). As x varies from 1 to 0, the area varies from 0 to maximum, A_{\max} , which represents one half cycle. In order to non-dimensionalize, a ratio of instantaneous area to maximum area is used. The variance of



Figures a, b, etc. represent the outlet area variation as the wheel passes the outlet port. Cross-hatched area is outlet area opened by wheel passage. Positions correspond to those similarly marked on plot below.

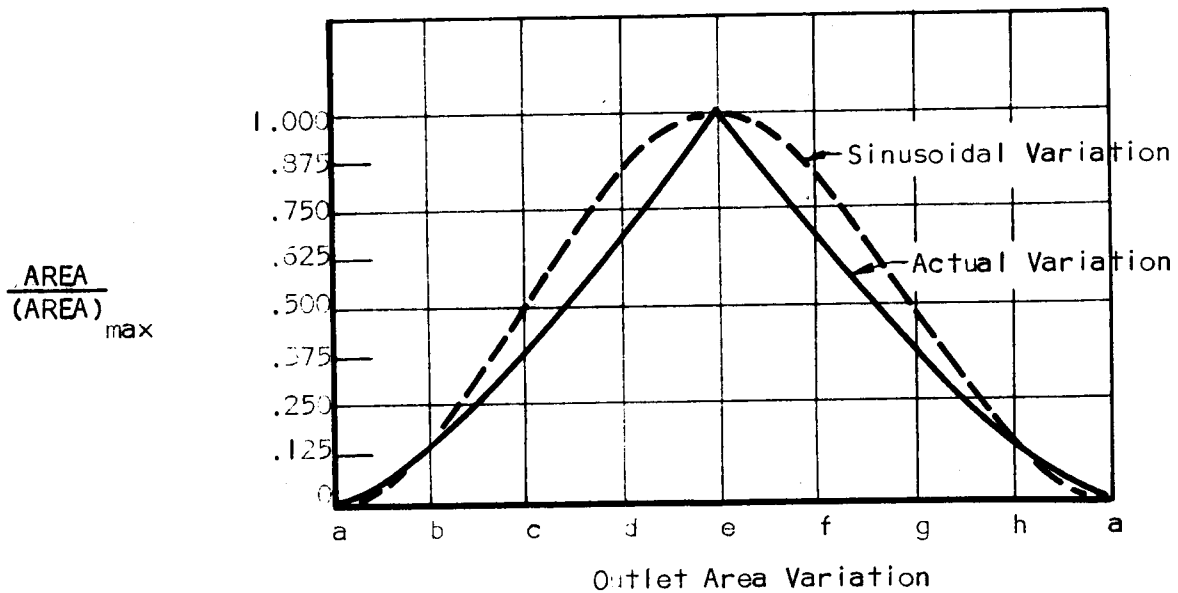


FIGURE D-1

the area with time may then be easily compared to a sinusoidally varying area as shown in Figure D-1. Calculated area ratios are listed below:

x	1	7/8	3/4	5/8	1/2	3/8	1/4	1/8	1/16	0
A/A_{max}	0	.053	.145	.259	.391	.534	.684	.841	.920	1.000

Average area may be calculated by integrating the expression for area from 0 to 1.

$$A_{avg} = \frac{\int_0^1 A dx}{\int_0^1 dx} = \int_0^1 A dx$$

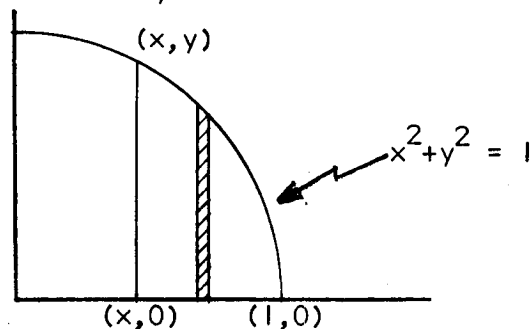
$$A_{avg} = 2 \int_0^1 \left[\frac{\pi}{2} - x \sqrt{1-x^2} - \sin^{-1}(x) \right] dx$$

$$A_{avg} = 2 \left\{ \left[\frac{\pi}{2} x \right] - \left[-\frac{1}{3} \sqrt{(1-x^2)^3} \right] - \left[x \sin^{-1}(x) + \sqrt{1-x^2} \right] \right\}_0^1$$

$$A_{avg} = 2 \left\{ \frac{\pi}{2} + \left[-\frac{1}{3} \right] - \left[\left(\frac{\pi}{2} \right) - (1) \right] \right\} = 2 \left\{ \frac{\pi}{2} - \frac{1}{3} - \frac{\pi}{2} + 1 \right\} = \frac{4}{3} = 1.33$$

Average area for sinusoidal variation is $\frac{\pi}{2} = 1.57$.

A closer approximation to sinusoidal variation can be achieved with a combination of a circular area and a square area. As before, consider one area moving with respect to the other. The area common to both at any instant may be calculated as shown below:



$$A = 2 \int_x^1 y dx = 2 \int_x^1 \sqrt{1-x^2} dx$$

$$A = \left[\frac{\pi}{2} - x \sqrt{1-x^2} - \sin^{-1}(x) \right]$$

As before time variance may be introduced by considering the passage of one area by the other. In this case as x varies from $+1$ to -1 corresponds to area variance from zero to maximum, and therefore will correspond to one half cycle. The sequence is as shown in Figure D-2. Area ratio is introduced to non-dimensionalize. Calculated area ratios are listed below for various values of x :

x	1	3/4	1/2	1/4	0	-1/4	-1/2	-3/4	-1
A/A_{\max}	0	072	195	342	500	658	805	928	1.000

Average area is now calculated as before:

$$A_{\text{avg}} = \frac{\int_{-1}^{+1} A dx}{\int_{-1}^{+1} dx} = \frac{1}{2} \int_{-1}^{+1} A dx$$

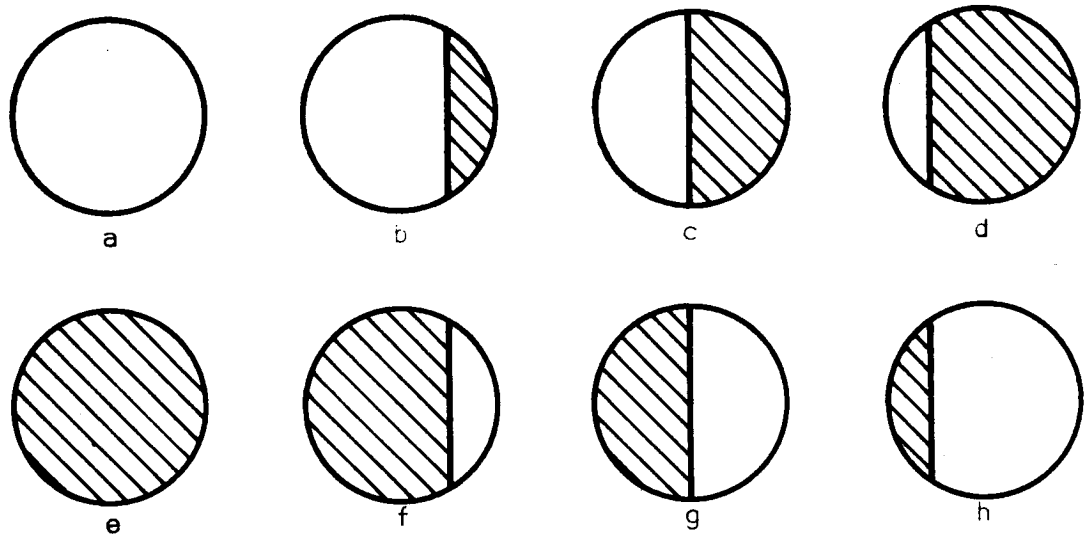
$$A_{\text{avg}} = \frac{1}{2} \int_{-1}^{+1} \left[\frac{\pi}{2} - x \sqrt{1-x^2} - \sin^{-1}(x) \right] dx$$

$$A_{\text{avg}} = \frac{1}{2} \left\{ \left[\frac{\pi}{2} x \right] - \left[-\frac{1}{3} \sqrt{(1-x^2)^3} \right] - \left[x \sin^{-1}(x) + \sqrt{1-x^2} \right] \right\} \Big|_{-1}^{+1}$$

$$A_{\text{avg}} = \frac{1}{2} \left\{ \left[\frac{\pi}{2} (2) \right] + \left[\frac{1}{3} (0) \right] - \left[\frac{\pi}{2} + \left(-\frac{\pi}{2} \right) \right] \right\}$$

$$A_{\text{avg}} = \frac{\pi}{2}$$

Average area for sinusoidal variations is also $\pi/2$.



Figures a, b, etc. represent the outlet area variation as the wheel passes the outlet port. Cross-hatched area is outlet area opened by wheel passage. Positions correspond to those similarly marked on plot below.

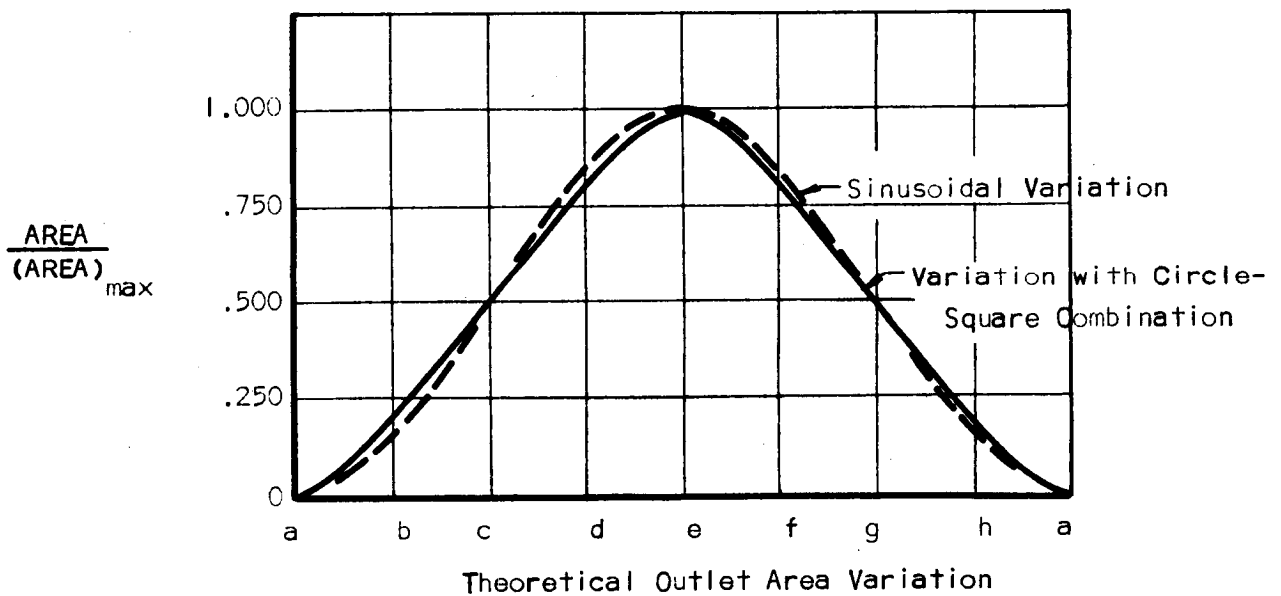


FIGURE D-2

APPENDIX E: Design Recommendations for Improved Sinusoidal Pressure Generator

An improved sinusoidal pressure generator should have a greater frequency range than the present SPG, and should have a cleaner waveform over this range. A cleaner waveform will have lower noise-to-signal ratio. It would also be desirable to extend the capability of the SPG to include heated gases so that thermal effects could be tested. This would not be as rigorous a test as the heat flux testing currently in progress and those planned at Forrestal Research Center at Princeton University, but it would make possible the testing of the dynamic characteristics while in a controlled elevated temperature environment.

In order to extend the frequency range, the highest frequency in the range must be such that its second harmonic is below the lowest chamber resonant frequency. This insures a uniform pressure throughout the chamber. For a given chamber size this can be done only by using a gas with a higher speed of wave propagation.

One solution to this would be to use hydrogen. Hydrogen has a very high speed of wave propagation. It is on the order of 4220 feet per second at room temperature. This increase would result in an approximate 30% extension of the frequency range of the SPG even if no other improvements were made. The percent increase in range is based on the current range using helium. Unfortunately, hydrogen is very hazardous and would require special handling. This would have to include a spark-free atmosphere and an installation with forced ventilation to prevent an accumulation of hydrogen gas.

Another approach to this problem of extending the frequency

range is to use heated helium since this will increase the speed of wave propagation. This also has the additional advantage of providing a controlled elevated temperature. In order to do this, however, the SPG would have to be capable of withstanding elevated temperatures without excessive distortion or warping. This capability could be improved by using stainless steel for all parts that would be exposed to heat. There would also have to be a device to heat the gas and control the temperature within the desired limits. A practical limit for the gas temperature would be on the order of 1000°F. At this temperature, helium has an approximate speed of wave propagation of 5500 feet per second. This would increase the present range by about 65 percent over the present range.

An improved SPG with heated gas capability might also have an economical advantage. In certain types of testing, where the transducer requires testing at low frequencies only, it is possible to test with nitrogen gas. The present useful range with nitrogen is about 3000 cps before the waveform begins to distort badly. This can be extended somewhat by heating the nitrogen. At 1000°F the speed of wave propagation in nitrogen is about 1870 feet per second. Thus, all resonant frequencies and the useful range would be extended by a factor of 65 percent.

Distortion of the waveform for a given frequency, that is deviation from the sinusoidal, also decreases as speed of wave propagation increases. The suggested methods of extending the frequency range will also help clean up the waveform at a given frequency.

Another alteration that should help achieve a more sinusoidal waveform is the incorporation of square "holes" in the rotating wheel

rather than the present circular holes (see Appendix D). The effect of this would be to make the outlet area variation approach more closely a true sinusoidal variation. In theory, the pressure variation will vary as the outlet area variation. Therefore, this change should improve the nonfiltered waveform. In the actual case, the waveform will be influenced by the real gas effects such as inertial and viscous effects and by departures from the assumptions made in deriving the theory, such as neglecting the clearance space between the wheel and the SPG body block.

It is also recommended that the outlet of the SPG be changed to a nozzle shape. There are two possible configurations for this change, each with its own merits. The first to have in the body block only the convergent section and a small constant area section that acts as a throat. The entire divergent section would be cut in the wheel. This should provide smoother and more efficient discharge of the gas. By having the throat at the end of the body, immediately before the wheel, the flow being discharged is at a Mach number of about one as it is "chopped" by the wheel. This keeps any disturbance created by this "chopping" to a minimum since the Mach number will be at least one in any case. The second method would be to have part of the divergent section in the body so that the flow is at a Mach number greater than one when it is discharged and is "chopped." Since the divergent section is between the disturbance and the chamber, and the flow in this section is well above Mach 1, no effects from the wheel will be felt in the chamber. Experiment should prove which method yields the best results.

Improved instrumentation would also be desirable. A ratio meter that would read the outputs from the test and monitor transducers

simultaneously and indicate the ratio would certainly eliminate the problem caused by frequency drift while reading the output. A problem with filters would arise if a ratio meter were used since each output would have to use a separate filter, but this could be eased by filter calibration.

Other suggestions include use of a plotter to plot the outputs at all frequencies. This could be used to advantage by adjusting the frequency from the lowest to the highest frequency smoothly and having the outputs plotted continuously. This may be too sophisticated, however, and might defeat one of the principal advantages of the SPG - relative simplicity and inexpensiveness.